ABSTRACT

Title of dissertation: ROBUSTNESS OF ATTRACTING ORBITS
Madhura Joglekar, Doctor of Philosophy, 2014

Dissertation directed by: Research Professor James A. Yorke
Coadvisors: Professors Ed. Ott and Ulrike Feudel

Understanding the transition to turbulence is a long-lasting problem in fluid dynamics, particularly in the case of simple flows in which the base laminar flow does not become linearly unstable. For flows at a low Reynolds number, all initial conditions decay to the laminar profile. At higher Reynolds numbers, above a critical value, turbulence is observed, often in the form of a chaotic saddle. The magnitude of the perturbation that disrupts the laminar flow into the turbulent region depends on the Reynolds number and on the direction of the perturbation. In Chapter 2, we investigate the robustness of the laminar attractor to perturbations in a 9-dimensional sinusoidal shear flow model. We examine the geometry of the 'edge of chaos', where the edge denotes the boundary of the chaotic saddle, which is embedded in the basin of attraction of the laminar state, and is accessible from that state.

For a smooth dynamical system $x_{n+1} = F(C, x_n)$ (depending on a parameter C), there may be infinitely many periodic windows, that is, intervals in C having a region of stable periodic behavior. However, the smaller of these windows are easily destroyed with tiny perturbations, so that only finitely many of the windows can

be detected for a given level of noise. For a fixed perturbation size ϵ, we consider the system behavior in the presence of noise. In this Chapter, we look at the "ϵ-robust windows", that is, those periodic windows such that for the superstable parameter value C in that window, the general periodic behavior persists despite noise of amplitude $\leq \epsilon$. We focus on the quadratic map, and numerically compute the number of periodic windows that are ϵ-robust. In Chapter 3, we obtain a robustness-exponent $\alpha \approx .51 \pm .03$, which characterizes the robustness of periodic windows in the presence of noise.

The character of the time-asymptotic evolution of physical systems can have complex, singular behavior with variation of a system parameter, particularly when chaos is involved. A perturbation of the parameter by a small amount ϵ can convert an attractor from chaotic to non-chaotic or vice-versa. We call a parameter value where this can happen ϵ-uncertain. The probability that a random choice of the parameter is ϵ-uncertain commonly scales like a power law in ϵ. Surprisingly, two seemingly similar ways of defining this scaling, both of physical interest, yield different numerical values for the scaling exponent. In Chapter 4, we show why this happens and present a quantitative analysis of this phenomenon.

Many dynamical systems reach a level of maximum topological entropy as the system parameter is increased followed by a decrease to zero entropy. In Chapter 5, we give an example such that the number of cascades continues to increase for arbitrarily large values of the parameter. We investigate the map $S_\mu : [0,1] \to [0,1)$ defined by $S_\mu(x) := \mu \sin(2\pi x) \bmod 1$. For this map, the entropy increases without bound as $\mu \to \infty$, and the system has an ever-increasing number of solitary cascades

for $\mu \in [0, m]$ as m is increased to higher and higher integer values. Specifically, we calculate the number of period-k cascades of the map, for $k > 1$, for positive integer values of $\mu \in [0, m]$, where $m \in \mathbb{N}$.

ROBUSTNESS OF ATTRACTING ORBITS

by

Madhura Joglekar

Dissertation submitted to the Faculty of the Graduate School of the
University of Maryland, College Park in partial fulfillment
of the requirements for the degree of
Doctor of Philosophy
2014

Advisory Committee:
Professor James A. Yorke, Chair/Advisor
Professor Edward Ott
Professor Brian Hunt
Professor Rajarshi Roy
Professor Daniel Lathrop

Dedication

To my loving family, for their constant support and encouragement.

Acknowledgments

I owe my gratitude to all the people who have made this thesis possible and because of whom my graduate experience has been one that I will cherish forever.

First and foremost I'd like to express my heartfelt thanks to my advisor and Coach, Professor James Yorke, the best advisor there could ever be, for giving me the opportunity to explore and work on extremely interesting projects over the past five years. In spite of his very busy schedule as the Department Chair, he always made himself available for help, advice and meetings, in person as well as on phone. Interacting with him has been a profound experience. His phenomenal ideas and endless enthusiasm have been a tremendous source of inspiration. It makes me feel proud and humble at the same time to learn from such an exceptional individual.

I would like to express deep thanks to Prof. Edward Ott for his astounding theoretical ideas. There has never been an occasion when I've knocked on his door and he hasn't given me time. Learning from him has been a greatly rewarding experience.

I would like to express deep thanks to Prof. Ulrike Feudel for her excellent ideas and detailed discussions we had, while she was visiting the University of Maryland, and later over Skype.

I would like to express deep thanks to Prof. Brian Hunt for his deeply insightful ideas and intricate analysis during our discussions.

I would also like to thank Professor Rajarshi Roy and Professor Daniel Lathrop for agreeing to serve on my thesis committee and for sparing their invaluable time

reviewing the manuscript.

I have had a remarkable circle of friends at College Park who have enhanced my graduate life in many ways. Ashutosh Gupta has been a truly wonderful friend over the years. My close friend and then roommate Baladitya Suri helped me immensely when I moved to Maryland and was entirely new to the place. I would also like to thank my close friends Umang Agarwal, Shantanu Debnath, Anirban Gangopadhyay, Anirban Ghosh and Sumit Shekhar for countless fond memories and constant support. I would like to express my gratitude to Jayant Kumar, Balachandra Suri, Sidharth Kumar, Anirban Ghosh, Rajibul Islam, Ashwin Kayyoor, Harinii Raghavan, Suriyanarayanan Vaikunthanathan, Varada Shevade, and Souvik Bhattacharjee for their friendship and help. It is impossible to name everyone and I apologize to those I have inadvertently left out.

I would like to thank my professors from IIT Bombay - Prof. K. Sudhakar, Prof. Amiya Pani, Prof. Harish Pillai and Prof. N. Ananthakrishnan for their encouragement and support during my transition from aerospace to applied mathematics. I would like to express gratitude to Pranav Kumar, Ajinkya More, Vaibhav Srivastava and Shreekrishna Rao, my friends from IIT, and to Xuwen Chen from the mathematics department, for their mentoring and advice over the years. I would like to thank my fellow graduate student Suddhasattwa Das for our fruitful discussions.

Guillaume Marcais' immense technical help over the years is highly appreciated. I would like to express gratitude to Alverda McCoy, Prof. Konstantina Trivisa and the entire staff at the mathematics department who were always very helpful, for a truly memorable association over the past five years.

I owe my deepest thanks to my lovely family - my mother and father and my brother who have always stood by me and guided me, and have been indescribably supportive and perpetually encouraging. I would not have been here had it not been for them. My gratitude towards them is beyond words.

Lastly, thank God!

Table of Contents

List of Figures

Chapter 1: Introduction

1.1 Background

Physical systems often have uncertainties in the values of their parameters which can lead to changes in the asymptotic behavior of the system. For a dynamical system $x_{n+1} = f_C(x_n)$, there is often a complex mix of regions (basins) of periodic attractors and regions of chaotic attractors. A small change in x,C can make the difference between being in a chaotic region or in a periodic region. Thus, even if the model and its parameter dependence is precisely known, the accuracy about the prediction of asymptotic behavior becomes an important question.

Chapter 2 addresses this question in the context of a laminar fixed-point attractor in a sinusoidal shear flow. Chapters 3 deals with the stability of periodic windows in general, or period-doubling cascades. Chapter 4 discusses uncertainty exponents, which quantitatively characterize how often a small change in parameter C affects the asymptotic stability of the system. Chapter 5 investigates an *atypical* system we have found, which shows an unbounded increase in the number of period-doubling cascades, as the system parameter is increased. A brief overview of each of the Chapters is as follows.

1.2 Structure of the thesis - Chapters Two to Five

Chapter 2. Chapter 2 deals with the fluid dynamics problem of transition to turbulence in a sinusoidal shear flow. We study a 9 dimensional model, wherein the laminar state is linearly stable for all Reynolds numbers. At a low Reynolds number, all initial conditions decay to the laminar profile. At higher Reynolds numbers, above a critical value, perturbations of the flow can lead to turbulent states. The magnitude of the perturbation that disrupts the laminar flow depends on the Reynolds number as well as on the direction of the perturbation.

In the model that we study, the turbulent state is transient and is a part of a chaotic saddle (a non-attracting chaotic set). On choosing any initial condition lying in the basin of the laminar attractor, and moving along any direction, one almost always encounters turbulent behavior, and this turbulent behavior is preceded by a discontinuity in the lifetimes (where the *lifetime* is the time taken for a given trajectory to reach within a specified distance from the laminar attractor). We say that such a point of discontinuity lies in the 'edge of chaos'. The distance of the edge from the laminar attractor indicates the *minimum perturbation* that would destabilize the laminar attracting state. We examine the geometry of the edge to study the stability of the laminar state as a function of the Reynolds number.

Chapter 3. For a smooth dynamical system $x_{n+1} = F(C, x_n)$ (depending on a parameter C), a periodic window of period k is a region in parameter space that starts with an attracting period-k orbit, and undergoes a sequence of period-doubling bifurcations as the parameter is increased, resulting in a chaotic attractor

with many pieces, which then merge into a k-piece chaotic attractor, and eventually merge into a 1-piece chaotic attractor at a boundary crisis. There may be infinitely many periodic windows. However, the smaller of these windows are destroyed if a tiny disturbance is introduced in the state-space or in the parameter space of the system. In Chapter 3, we consider the quadratic map $x_{n+1} = C - {x_n}^2$, in the presence of a disturbance of magnitude $\leq \epsilon$. We numerically compute the "ϵ-robust windows", that is, those periodic windows such that for the superstable parameter value C in that window, the general periodic behavior persists in the presence of a disturbance of magnitude $\leq \epsilon$. We obtain a corresponding robustness-exponent.

Chapter 4. For a dynamical system $x_{n+1} = f_C(x_n)$ depending on a parameter C, we say that a point (x, C) is **ϵ-uncertain** if the trajectory starting from that point is asymptotic to a periodic attractor, and there exists a point (x', C') whose trajectory is asymptotic to a chaotic attractor, where $|(x, C) - (x', C')| \leq \epsilon$. The fractal-like chaotic/periodic interweaving structure has been quantitatively characterized via scaling exponents. Different studies on the quadratic map have addressed the scaling in different ways and obtained significantly different values of the scaling exponent. In Chapter 4, we establish a relationship between the scaling exponents, by examining the locations of ϵ-uncertain points in terms of the fractal structure of periodic-windows.

Chapter 5. Many dynamical systems, such as the forced damped pendulum or the quadratic map, reach a level of maximum topological entropy, and there are no new period-doubling cascades created beyond a certain parameter value. In this Chapter, we investigate the map $S_\mu : [0, 1] \to [0, 1)$ defined by

$S_\mu(x) := \mu \sin(2\pi x) \bmod 1$. For this system, however, we show that the entropy increases without bound as $\mu \to \infty$ and the map has a progressively increasing number of solitary cascades for $\mu \in [0, m]$ as m is increased to higher and higher integer values. We also enumerate the number of cascades in the system at a given value of μ.

The chapters two to five of this thesis are written as stand-alone articles, intended for publication in peer-reviewed journals. Hence, each of them can be read as an independent work, though their topics are heavily inter-related.

Chapter 2: Basin boundary analysis in a low-dimensional turbulent shear flow model

In this chapter, we investigate the geometry of the edge of chaos for a 9-dimensional sinusoidal shear flow model. We numerically compute the scaling, with respect to Reynolds number, of the minimum perturbation required to drive the laminar attracting state into the turbulent region.

2.1 Introduction

Understanding the transition to turbulence is a long-lasting problem in fluid dynamics, particularly in the case of simple flows in which the base flow does not become linearly unstable. This applies to the Hagen-Poiseuille or pipe flow which is stable for all Reynolds numbers Re or the plane Couette flow [2].

For those flows at a low Reynolds number, all initial conditions decay to the laminar profile. At higher Reynolds numbers, above a critical value, perturbations of the flow obtained by e.g. placing obstacles or making boundaries of the pipe or the plates rough enough can lead to turbulent states, which may last for a long time. As the Reynolds number increases, smaller perturbations are required to destabilize the laminar flow. The magnitude of the perturbation that disrupts the laminar flow

depends not only on the Reynolds number, but also on the direction of the perturbation. Here, direction refers to direction in infinite dimensional state space. Thus, some directions will require a much larger magnitude perturbation to destabilize the laminar flow to turbulent states, as compared to others. Low-dimensional models, based on the Galerkin method, have been used to better understand the turbulent behavior [3–8]. Depending on the model, and on the Reynolds number, when the system exhibits turbulence, the turbulent state can either be transient or sustained.

Models and experiments for Plane Couette flow [8–11] and for pipe flow [9, 12–17] have been studied such that for lower Reynolds numbers, the turbulent state is transient. In the transient turbulence region, the system exhibits an exponential distribution of lifetimes (where the *lifetime* is the time taken for a given trajectory to reach a specified distance from the laminar attractor). This exponential distribution is indicative of a chaotic saddle (non-attracting chaotic invariant set). A transition of turbulence from a chaotic saddle to a chaotic attractor would require a boundary crisis [18], and would result in the average lifetime of a trajectory diverging. Ref. [9–17] show that the median lifetime varies as $1/(Re_c - Re)$ where Re_c denotes the critical Reynolds number, beyond which the system exhibits sustained turbulence, that is, the turbulent state is a chaotic attractor. Other studies ([3, 19, 20]) suggest that the average lifetime of a trajectory increases rapidly with Reynolds number, but does not diverge, and present evidence that it increases exponentially, so that the turbulent state is transient for all Reynolds numbers. Hof et al. [21] have shown that no critical point for the transition exists. More recently, experiments and extensive numerical simulations have revealed that there is a transition between the laminar

and the turbulent state for higher Reynolds numbers ($Re > 2300$) [22,23]. Moreover, the trajectories for high Reynolds numbers possess a memory expressed by a super-exponential scaling with the Reynolds number. The explanation of this transition is based on the existence of spatially localized turbulent structures, so-called puffs, which become more frequent at higher Reynolds numbers. This finding suggests that the transition to turbulence is not only due to a more complex temporal structure of the flow field but that spatial aspects need to be taken into account.

Since the laminar state is linearly stable, irrespective of whether the turbulent state is a chaotic saddle or a chaotic attractor, infinitesimal perturbations will always decay. Evidence of the one or the other scenario can only be obtained using finite size perturbations. While transient turbulent states are related to finite though possibly very long decay times, permanent turbulence will be reached by perturbations which never decay.

For the purpose of our study, we investigate the 9-dimensional sinusoidal shear flow model examined in [1, 3, 24]. For $335 < Re < 515$, the system has a symmetric pair of stable 'non-trivial' attractors associated with sustained turbulence, besides the laminar attractor. For $Re < 335$ and $515 < Re < 1000$, the only attractor in the system is the laminar attractor, and the turbulent state represents a chaotic saddle.

Choosing any initial condition lying in the basin of the laminar attractor, and moving along any direction in the 9-dimensional space, one almost always encounters turbulent behavior, and this turbulent behavior is preceded by a discontinuity in the lifetimes. Such a point of discontinuity is said to lie in the 'edge of chaos' [25]. While the particular notion of the edge is slightly different depending on whether

turbulence is transient or sustained, its procedure of identification is very similar. The edge denotes the accessible part of the boundary, where a path in a basin might terminate. Most points of a fractal boundary are surrounded by infinitely many layers of boundary and these are not in the edge. In case of a transient turbulent state, the edge denotes the "boundary" of the chaotic saddle which is embedded in the basin of attraction of the laminar state and is accessible from that state. In case of bistability with the coexistence of a laminar and a turbulent state, the edge is considered to be the boundary of the basin of attraction. This boundary has been shown to be the stable manifold of a periodic saddle or of a chaotic saddle embedded in the basin boundary [8, 24, 26]. The distance of the edge of chaos from the laminar attractor indicates the *minimum perturbation* that would destabilize the laminar attracting state. This is referred to as the *critical amplitude*.

Several methods have been developed to search for the critical amplitude in the bistable case, where the turbulent state is an attractor [27–30]. This minimal perturbation, corresponding to the minimal distance to the basin boundary, has been computed in terms of the minimal energy needed to perturb the system. This minimal energy has been found to scale with the Reynolds number as $\sim Re^{-2}$ in [28] and $\sim Re^{-2.7}$ in [30]. Different exponents relating the scaling of critical amplitude to the Reynolds number have been computed. Ref. [4] studies a 19-dimensional Galerkin approximation to a parallel shear flow, and suggests that the critical amplitude scales as Re^{-1}. Ref. [31] studies a numerical model of pipe flow and computes an exponent of -1.5. Ref. [32] studies a numerical model of pipe flow and finds a dependence of the critical amplitude on the type of perturbation

with exponents ranging from -1 to -1.5. Ref. [26, 33] compute an exponent of -1. Ref. [34, 35] conduct an experimental investigation of a pipe flow and report that the critical amplitude scales as Re^{-1}. Ref. [36] study experimentally the pipe flow and found an exponent of -1 or -2/3 depending on wavenumbers, to cause transition. Ref. [37] which conducts an experimental investigation of a pipe flow and [38] which conducts numerical simulations of the Hagen-Poiseuille flow show a dependence of the exponent on the type of perturbation, and compute exponents ranging from -1 to -1.5. Ref. [13,17] study experimentally the Hagen-Poiseuille flow and find an exponent of -1. The Hagen-Poiseuille flow is examined numerically by [39] and [40] which compute an exponent of -1 and -1.5 respectively. Ref. [41] studies experimentally the Plane-Poiseuille Flow and computes an exponent of -1.5.

For the 9-dimensional sinusoidal shear flow model in [1, 3, 24], we address the dependence on Reynolds number of the minimum perturbation required to drive the laminar attracting state into the turbulent region.

Our goal is to gain greater understanding of the geometry of the edge of chaos, particularly emphasizing on the edge of chaos points that are closest to the laminar attractor and hence correspond to those directions, which start from the laminar attractor and require relatively small perturbations to create transient chaos. We examine the geometry of the edge of chaos to see how the distance of the edge from the laminar attractor, and consequently 'the stability of the laminar attractor', varies as a function of Reynolds number.

We start with a description of the model, then discuss some basic definitions and elucidate the method to follow the edge of chaos in a high-dimensional phase

space. We then discuss our results related to the dependence of lifetimes and the geometry of the edge on Reynolds number, and compare them with previous findings.

2.2 The model of the Sinusoidal Shear Flow

Recognizing the great difficulty of conducting such studies for the full partial differential equations for the fluid flow, we examine, instead, a 9-dimensional model of sinusoidal shear flow in [1, 3, 24] that is a generalization of the model in [42].

In the model, the fluid between two free-slip walls experiences a sinusoidal body force. The coordinate system is such that x points downstream, y in the direction of the shear, and z in the spanwise direction. d is the distance between the walls and ρ is the fluid density, and ν is the kinematic viscosity. The characteristic velocity U_0 is the laminar velocity that arises due to the forcing at a distance d/4 from the top wall. The Reynolds number is defined as $Re = \frac{U_0 d}{2\nu}$. The lengths are non-dimensionalized in units of d/2, velocities in units of U_0, time in units of $(d/2)/U_0$, and pressure in units of $\rho {U_0}^2$. Then, the evolution equation is

$$\frac{\partial u}{\partial t} = -(u \cdot \nabla)u - \nabla p + \frac{\nabla^2 u}{Re} + F(y)$$

As the fluid is incompressible, $\nabla \cdot u = 0$. There are free-slip boundary conditions at the walls at $y = \pm 1$, hence,

$$u_y|_{y=\pm 1} = 0, \left.\frac{\partial u_x}{\partial y}\right|_{y=\pm 1} = \left.\frac{\partial u_z}{\partial y}\right|_{y=\pm 1} = 0.$$

It is assumed that the flow is periodic in the streamwise and spanwise directions, with lengths L_x and L_z, respectively. Ref. [1, 3, 24] analyze the flow for a domain

with $L_x = 4\pi, L_z = 2\pi$ (which corresponds to the optimal domain size for a plane Couette flow to obtain the formation of stationary coherent structures), as well as for a narrower domain with $L_x = 1.75\pi, L_z = 1.2\pi$ (which corresponds to the minimum domain size that can sustain turbulence for plane Couette flow). We focus on the latter case $L_x = 1.75\pi, L_z = 1.2\pi$.

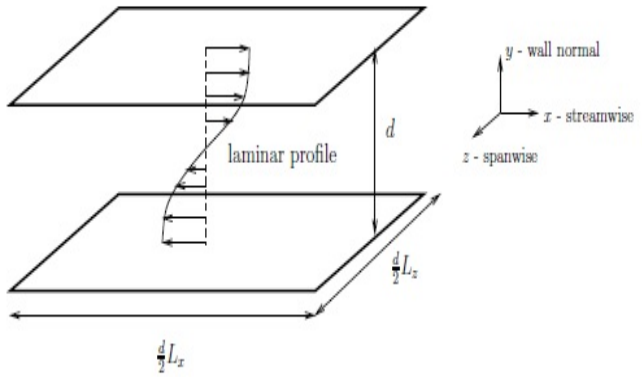

Figure 2.1: The laminar profile for the sinusoidal shear flow is shown. The figure is taken from [1].

The non-dimensionalized volume force is

$$F(y) = \frac{\sqrt{2}\pi^2}{4Re}\sin(\pi y/2)\hat{e}_x$$

This gives the laminar profile,

$$U(y) = \sqrt{2}\sin(\pi y/2)\hat{e}_x$$

The laminar profile is shown in Fig. 2.1, which is taken from [1].

Let $\alpha = 2\pi/L_x, \beta = \pi/2, \gamma = 2\pi/L_z$. The domain is $0 \leq x \leq L_x, -1 \leq y \leq$

$1, 0 \leq z \leq L_z$. The nine modes for the model are, the basic profile,

$$u_1 = \begin{pmatrix} \sqrt{2}\sin(\pi y/2) \\ 0 \\ 0 \end{pmatrix}$$

a streak mode, capturing spanwise variation of the streamwise velocity,

$$u_2 = \begin{pmatrix} \frac{4}{\sqrt{3}}\cos^2(\pi y/2)\cos(\gamma z) \\ 0 \\ 0 \end{pmatrix}$$

a downstream vortex mode,

$$u_3 = \frac{2}{\sqrt{4\gamma^2 + \pi^2}} \begin{pmatrix} 0 \\ 2\gamma\cos(\pi y/2)\cos(\gamma z) \\ \pi\sin(\pi y/2)\sin(\gamma z) \end{pmatrix}$$

modes for spanwise flows,

$$u_4 = \begin{pmatrix} 0 \\ 0 \\ \frac{4}{\sqrt{3}}\cos(\alpha x)\cos^2(\pi y/2) \end{pmatrix}$$

$$u_5 = \begin{pmatrix} 0 \\ 0 \\ 2\sin(\alpha x)\sin(\pi y/2) \end{pmatrix}$$

the normal vortex modes,

$$u_6 = \frac{4\sqrt{2}}{\sqrt{3(\alpha^2 + \gamma^2)}} \begin{pmatrix} -\gamma\cos(\alpha x)\cos^2(\pi y/2)\sin(\gamma z) \\ 0 \\ \alpha\sin(\alpha x)\cos^2(\pi y/2)\cos(\gamma z) \end{pmatrix}$$

$$u_7 = \frac{2\sqrt{2}}{\sqrt{\alpha^2+\gamma^2}} \begin{pmatrix} \gamma \sin(\alpha x)\sin(\pi y/2)\sin(\gamma z) \\ 0 \\ \alpha \cos(\alpha x)\sin(\pi y/2)\cos(\gamma z) \end{pmatrix}$$

the fully three-dimensional mode,

$$u_8 = N_8 \begin{pmatrix} \pi\alpha \sin(\alpha x)\sin(\pi y/2)\sin(\gamma z) \\ 2(\alpha^2+\gamma^2)\cos(\alpha x)\cos(\pi y/2)\sin(\gamma z) \\ -\pi\gamma \cos(\alpha x)\sin(\pi y/2)\cos(\gamma z) \end{pmatrix}$$

where the normalization constant

$$N_8 = \frac{2\sqrt{2}}{\sqrt{(\alpha^2+\gamma^2)(4\alpha^2+4\gamma^2+\pi^2)}}$$

and the modification of the basic profile,

$$u_9 = \begin{pmatrix} \sqrt{2}\sin(3\pi y/2) \\ 0 \\ 0 \end{pmatrix}$$

The domain is denoted by Ω. The 9 modes are orthogonal and normalized so that,

$$\int\int\int_\Omega u_n \cdot u_m d^3x = 2(2\pi/\alpha)(2\pi/\gamma)\delta_{nm}$$

Each mode individually satisfies the incompressibility and free-slip boundary conditions at the walls. Then, the fluid velocity is

$$u(x,y,t) = \sum_{m=1}^{m=9} a_m(t) u_m(x,y)$$

Using Galerkin projection as described in [1, 3], the amplitude equations have the general form

$$\frac{da_i}{dt} = \frac{\beta^2}{Re}\delta_{i,1} - \frac{d_i}{Re}a_i + \sum_{j,k} N_{i,j,k} a_j a_k$$

where $N_{i,j,k}$ are constants for $i, j, k = 1, 2, \ldots, 9$. The Kronecker-delta in the first term reflects the fact that only the first mode is driven. All modes have a viscous damping rate $-d_i/Re$.

Thus, for the given system, the following ordinary differential equations are obtained,

$$\frac{da_1}{dt} = \frac{\beta^2}{Re} - \frac{\beta^2}{Re}a_1 - \sqrt{\frac{3}{2}}\frac{\beta\gamma}{\kappa_{\alpha\beta\gamma}}a_6a_8 + \sqrt{\frac{3}{2}}\frac{\beta\gamma}{\kappa_{\beta\gamma}}a_2a_3$$

$$\frac{da_2}{dt} = -\left(\frac{4\beta^2}{3} + \gamma^2\right)\frac{a_2}{Re} + \frac{5\sqrt{2}\gamma^2}{3\sqrt{3}\kappa_{\alpha\gamma}}a_4a_6 - \frac{\gamma^2}{\sqrt{6}\kappa_{\alpha\gamma}}a_5a_7 - \frac{\alpha\beta\gamma}{\sqrt{6}\kappa_{\alpha\gamma}\kappa_{\alpha\beta\gamma}}a_5a_8 - \sqrt{\frac{3}{2}}\frac{\beta\gamma}{\kappa_{\beta\gamma}}a_1a_3 - \sqrt{\frac{3}{2}}\frac{\beta\gamma}{\kappa_{\beta\gamma}}a_3a_9$$

$$\frac{da_3}{dt} = -\frac{\beta^2+\gamma^2}{Re}a_3 + \frac{2}{\sqrt{6}}\frac{\alpha\beta\gamma}{\kappa_{\alpha\gamma}\kappa_{\beta\gamma}}(a_4a_7 + a_5a_6) + \frac{\beta^2(3\alpha^2+\gamma^2) - 3\gamma^2(\alpha^2+\gamma^2)}{\sqrt{6}\kappa_{\alpha\gamma}\kappa_{\beta\gamma}\kappa_{\alpha\beta\gamma}}a_4a_8$$

$$\frac{da_4}{dt} = -\frac{3\alpha^2+4\beta^2}{3Re}a_4 - \frac{\alpha}{\sqrt{6}}a_1a_5 - \frac{10}{3\sqrt{6}}\frac{\alpha^2}{\kappa_{\alpha\gamma}}a_2a_6 - \sqrt{\frac{3}{2}}\frac{\alpha\beta\gamma}{\kappa_{\alpha\gamma}\kappa_{\beta\gamma}}a_3a_7 - \sqrt{\frac{3}{2}}\frac{\alpha^2\beta^2}{\kappa_{\alpha\gamma}\kappa_{\beta\gamma}\kappa_{\alpha\beta\gamma}}a_3a_8 - \frac{\alpha}{\sqrt{6}}a_5a_9$$

$$\frac{da_5}{dt} = -\frac{\alpha^2+\beta^2}{Re}a_5 + \frac{\alpha}{\sqrt{6}}a_1a_4 + \frac{\alpha^2}{\sqrt{6}\kappa_{\alpha\gamma}}a_2a_7 - \frac{\alpha\beta\gamma}{\sqrt{6}\kappa_{\alpha\gamma}\kappa_{\alpha\beta\gamma}}a_2a_8 + \frac{\alpha}{\sqrt{6}}a_4a_9 + \frac{2}{\sqrt{6}}\frac{\alpha\beta\gamma}{\kappa_{\alpha\gamma}\kappa_{\beta\gamma}}a_3a_6$$

$$\frac{da_6}{dt} = -\frac{3\alpha^2+4\beta^2+3\gamma^2}{3Re}a_6 + \frac{\alpha}{\sqrt{6}}a_1a_7 + \sqrt{\frac{3}{2}}\frac{\beta\gamma}{\kappa_{\alpha\beta\gamma}}a_1a_8 + \frac{10}{3\sqrt{6}}\frac{\alpha^2-\gamma^2}{\kappa_{\alpha\gamma}}a_2a_4 - 2\sqrt{\frac{2}{3}}\frac{\alpha\beta\gamma}{\kappa_{\alpha\gamma}\kappa_{\beta\gamma}}a_3a_5 + \frac{\alpha}{\sqrt{6}}a_7a_9 + \sqrt{\frac{3}{2}}\frac{\beta\gamma}{\kappa_{\alpha\beta\gamma}}a_8a_9$$

$$\frac{da_7}{dt} = -\frac{\alpha^2+\beta^2+\gamma^2}{Re}a_7 - \frac{\alpha}{\sqrt{6}}(a_1a_6 + a_6a_9) + \frac{1}{\sqrt{6}}\frac{\gamma^2-\alpha^2}{\kappa_{\alpha\gamma}}a_2a_5 + \frac{1}{\sqrt{6}}\frac{\alpha\beta\gamma}{\kappa_{\alpha\gamma}\kappa_{\beta\gamma}}a_3a_4$$

$$\frac{da_8}{dt} = -\frac{\alpha^2+\beta^2+\gamma^2}{Re}a_8 + \frac{2}{\sqrt{6}}\frac{\alpha\beta\gamma}{\kappa_{\alpha\gamma}\kappa_{\alpha\beta\gamma}}a_2a_5 + \frac{\gamma^2(3\alpha^2-\beta^2+3\gamma^2)}{\sqrt{6}\kappa_{\alpha\gamma}\kappa_{\beta\gamma}\kappa_{\alpha\beta\gamma}}a_3a_4$$

$$\frac{da_9}{dt} = -\frac{9\beta^2}{Re}a_9 + \sqrt{\frac{3}{2}}\frac{\beta\gamma}{\kappa_{\beta\gamma}}a_2a_3 - \sqrt{\frac{3}{2}}\frac{\beta\gamma}{\kappa_{\alpha\beta\gamma}}a_6a_8$$

where

$$\kappa_{\alpha\gamma} = \sqrt{\alpha^2+\gamma^2}, \kappa_{\beta\gamma} = \sqrt{\beta^2+\gamma^2}, \kappa_{\alpha\beta\gamma} = \sqrt{\alpha^2+\beta^2+\gamma^2}$$

A detailed discussion of the modes and their interaction is given in [3].

The laminar state of the model, which is linearly stable for all Reynolds numbers, corresponds to a fixed point

$$a_1 = 1, a_2 = a_3 = \ldots = a_9 = 0.$$

2.3 The edge of chaos

Let us first give some definitions related to our study.

Lifetime. The lifetime associated to a given point is defined as the time it takes for the trajectory starting from that point to reach a specified distance from the laminar attractor. This specified distance is implemented as a small ball around the fixed point corresponding to the laminar state.

The Edge of Chaos. As one travels along a direction through state space, starting from any point in the basin of the laminar attractor, the edge is the locus of the first point which is encountered where the lifetime goes to infinity.

Although the lifetime approaches infinity along the edge, the turbulent region beyond the edge is unstable, and hence has finite, though possibly very long lifetimes. The edge of chaos is a measure 0 set, and hence it is numerically impossible to encounter the points along the edge, with arbitrarily large lifetimes.

In Fig. 2.2, the histogram plots the distance of the edge from the laminar attractor for 100000 randomly chosen directions in the 9-dimensional state space, at $Re = 400$.

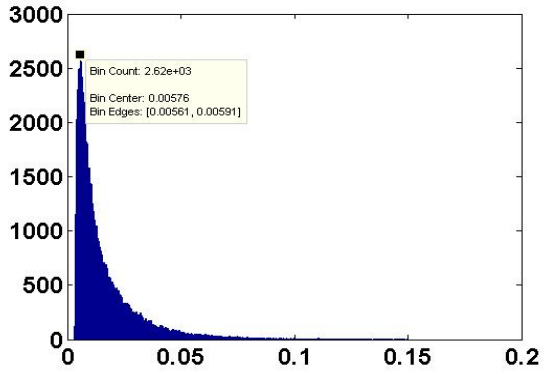

Figure 2.2: The histogram shows the distance of the edge from the laminar attractor for 100000 randomly chosen directions in the 9-dimensional state space, at $Re = 400$. The bin size is 0.0003.

2.4 Following the edge of chaos

To *follow* the edge of chaos we use the technique in [43]. Choosing a direction from the laminar attractor towards the edge, an initial condition on the path before the edge point is reached, has a trajectory, whose amplitude remains small as it

relaxes to the laminar state. However, an initial condition chosen beyond the edge generates a trajectory that would have a chaotic transient that typically contains at least one large amplitude excursion before decaying. A threshold value of amplitude can be chosen based on the maximum amplitude of trajectories starting from initial conditions beyond and before the edge. An initial condition can be classified as being either on the high-side or the low-side based on whether the maximum amplitude of its trajectory is above or below this threshold value. Thus, one can start with a low-side point near the laminar attractor and a high-side point that displays a chaotic transient. A path that connects these two points must intersect the edge. By repeated bisection, the distance between the high-low pair can be reduced to accurately approximate the edge point that lies between them. This distance is reduced within the required tolerance, say ϵ, to get a new high-low pair. As the edge is unstable, a trajectory starting from any point close to the edge diverges away from the edge. Trajectories are started from the 2 initial conditions corresponding to the new high-low pair, and and are followed till time, say T, after which the distance between them exceeds 2ϵ. The edge trajectory is approximated as the pointwise average on the time interval [0, T]. Thereby, the bisection procedure is repeated to reduce the distance between the points to within ϵ. This process can be continued indefinitely, producing a numerical approximation to an edge trajectory to within 2ϵ. We follow the edge trajectory starting from a randomly chosen direction, for Reynolds numbers from 200 to 2000. Our computations indicate that in each case, the trajectory converges to a periodic orbit on the edge. In Fig. 2.3, the distance of the periodic orbit on the edge from the laminar attractor, is plotted as a function of

Reynolds no., for $Re = 200, 300, \ldots, 1000, 1500, 2000$. The distance of the periodic orbit from the laminar attractor scales as $\approx Re^{-1}$. (See Fig. 2.3.)

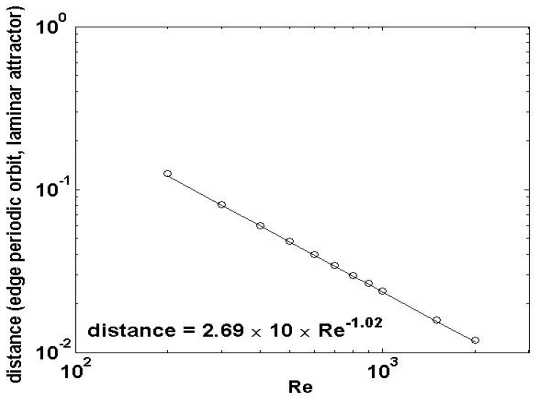

Figure 2.3: The distance of the periodic orbit on the edge from the laminar attractor on the y-axis vs Reynolds number on the x-axis is plotted, for $Re = 200, 300, \ldots, 1000, 1500, 2000$.

2.5 The geometry of the edge of chaos

2.5.1 Contour graphs for three orthogonal vectors.

To examine the edge of chaos, we choose three mutually orthogonal vectors starting from the laminar attractor, namely, $v1 = [1, 1, 1, 1, 1, 1, 1, 1, 1]$, $v2 = [-1, 1, 2, 0, 1, 0, -1, 0, -2]$ and $v3 = [1, -1, 0, 1, 0, -1, -2, 2, 0]$. We look at two different planes: plane 1 formed by vectors $v1$ and $v2$, and plane 2 formed by vectors $v1$ and $v3$. Fig. 2.4a, 2.4c and 2.4e show the contour plots for the lifetimes in plane 1, for Reynolds number 200, 400 and 1000 respectively. Fig. 2.4b, 2.4d and 2.4f show the contour plots for the lifetimes in plane 2, for Reynolds number 200, 400 and 1000 respectively. The figure is shifted so that the origin corresponds to the laminar attractor. In each of the plots, the dark red region indicates those points

with lifetimes exceeding the maximum value indicated by the color bar.

2.5.2 Lifetime distribution.

For $335 < Re < 515$, the system has a symmetric pair of stable 'non-trivial' attractors, besides the laminar attractor. For $Re < 335$ and $515 < Re < 1000$, the laminar state is the only attractor. Ref. [3] observes an exponential distribution of lifetimes for those values of Reynolds number for which the laminar attractor is the only attractor, indicative of the turbulent state being a chaotic saddle. This was also observed by us. This exponential distribution can be used to compute the average lifetime τ of the transients at those Reynolds numbers for which the laminar attractor is the only attracting state. Hence, we use $Re = 200, 300, 600, 700, 800, 900, 1000, 1500, 2000$ to study the distribution of the average lifetimes. In Fig. 2.5, $1/\tau$ is plotted as a function of the Reynolds no., where τ denotes the average lifetime. The figure indicates that $\tau \sim Re^{4.51}$.

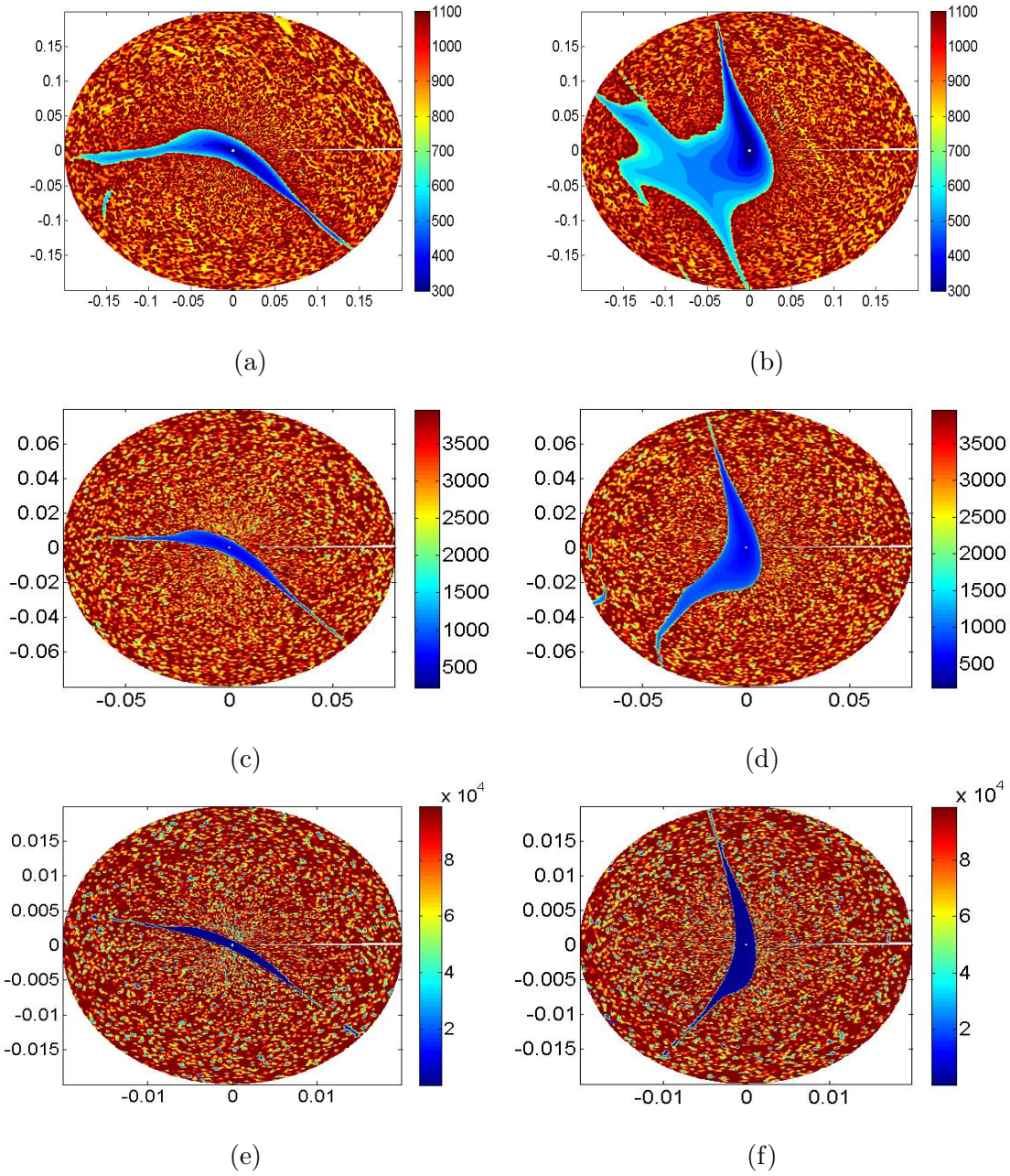

Figure 2.4: Fig. 2.4a, 2.4c and 2.4e show the contour plots for the lifetimes, in the plane 1 formed using orthogonal vectors $v1$ and $v2$, for Reynolds number 200, 400 and 1000 respectively. Fig. 2.4b, 2.4d and 2.4f show the contour plots for the lifetimes, in the plane 2, formed using orthogonal vectors $v1$ and $v3$, for Reynolds number 200, 400 and 1000 respectively. In each of the plots, the dark red region indicates those points with lifetimes exceeding the maximum value indicated by the color bar. The figure is shifted so that the origin corresponds to the laminar attractor.

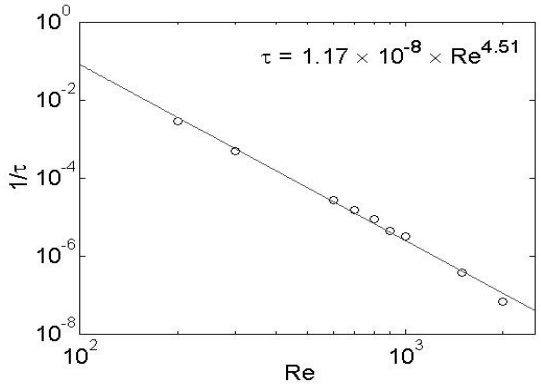

Figure 2.5: $1/\tau$ vs Re is plotted, for $Re = 200, 300, 600, 700, 800, 900, 1000, 1500, 2000$. Here, τ is the average lifetime. Note that we exclude $Re = 400, 500$. Because of the presence of a nontrivial attractor at $Re = 400, 500$ (sustained turbulence instead of a turbulent saddle), the average lifetime for convergence to the laminar attractor is not defined.

For $Re = 600$, we compute the lifetimes for points in Plane 1 starting from the laminar attractor till radius values of 0.05 (similar to Fig. 2.4a, 2.4c, 2.4e). We observe that points that lie within the edge with trajectories converging quickly to the laminar attractor have lifetimes < 2900, and a sudden jump in lifetimes is observed for points lying on the other side of the edge, which exhibit turbulent behavior before reaching the laminar attractor. For points having lifetimes exceeding 2900, Fig. 2.6 plots the radial distance on the x-axis vs lifetime on the y-axis. Observe that in this transient turbulence region, the distribution of lifetimes is largely independent of radial distance.

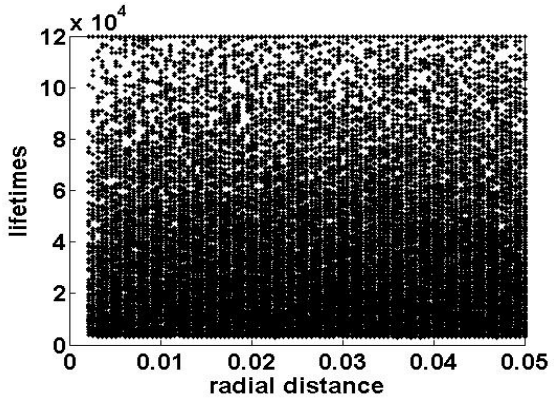

Figure 2.6: For Re 600, we compute the lifetimes for points in Plane 1 starting from the laminar attractor till radius values of 0.05. The figure considers those points lying in the turbulent region, and plots the corresponding radial distance on the x-axis vs lifetime on the y-axis. Observe that in the transient turbulence region, the distribution of lifetimes is largely independent of radial distance.

2.5.3 Non-trivial attracting orbits

The system has a symmetric pair of stable 'non-trivial' attractors associated with sustained turbulence, apart from the laminar attractor, for $335 < Re < 515$. We investigate the symmetric pair of non-trivial attracting orbits at $Re = 425$. For this, we choose a point on one of the non-trivial attracting orbits (we call this point P_{att}) and the corresponding point on the symmetric attracting orbit (we call this point $P_{att,sym}$). We choose P_{att} such that $a_1 = 0.129992, a_2 = -0.0655929, a_3 = 0.0475706, a_4 = 0.0329967, a_5 = 0.0753854, a_6 = -0.00325098, a_7 = -0.042364, a_8 = -0.019685, a_9 = -0.101453$, so that for $P_{att,sym}$, $a_1 = 0.129992, a_2 = 0.0655929, a_3 = -0.0475706, a_4 = -0.0329967, a_5 = -0.0753854, a_6 = -0.00325098, a_7 = -0.042364, a_8 = -0.019685, a_9 = -0.101453$. We look at a plane containing the laminar attractor and the points P_{att} and $P_{att,sym}$. Say the vector directed from the laminar attractor to

P_{att} is called V_{att} and the vector directed from the laminar attractor to $P_{att,sym}$ is called $V_{att,sym}$. Then the vectors $V_{att} + V_{att,sym}$ and $V_{att} - V_{att,sym}$ are orthogonal. In Fig. 2.7 and Fig. 2.8, the x axis is along $V_{att} + V_{att,sym}$ and the y-axis is along $V_{att} - V_{att,sym}$.

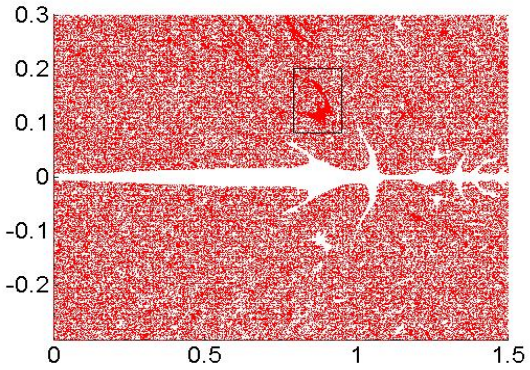

Figure 2.7: The basin of attraction corresponding to P_{att} is plotted in red, where $P_{att} \approx (0.877, 0.115)$. The black rectangle denotes the region zoomed in on, in Fig. 2.8.

The figures are shifted so that the origin corresponds to the laminar attractor. The x and y coordinates corresponding to P_{att} in the x-y plane are $\approx (0.877, 0.115)$ and the coordinates corresponding to $P_{att,sym}$ are $\approx (0.877, -0.115)$. In this plane, Fig. 2.7 shows the basin of attraction corresponding to P_{att} in red, for $x \in [0, 1.5], y \in [-0.3, 0.3]$. For Fig. 2.8a, 2.8b and 2.8c, we zoom in on the region close to P_{att} denoted by the black rectangle in Fig. 2.7. Fig. 2.8a shows the basin of attraction corresponding to P_{att} in red. Fig. 2.8b shows the basin of attraction corresponding to $P_{att,sym}$ in black. Fig. 2.8c shows the basin of attraction corresponding to the laminar attractor in blue. We can see from Fig. 2.8a that the open neighborhood around P_{att} containing points lying in the basin of attraction corresponding to P_{att}

is small. Most of the state space is filled with transient chaos and the basins of attraction of the attractors are well-mixed.

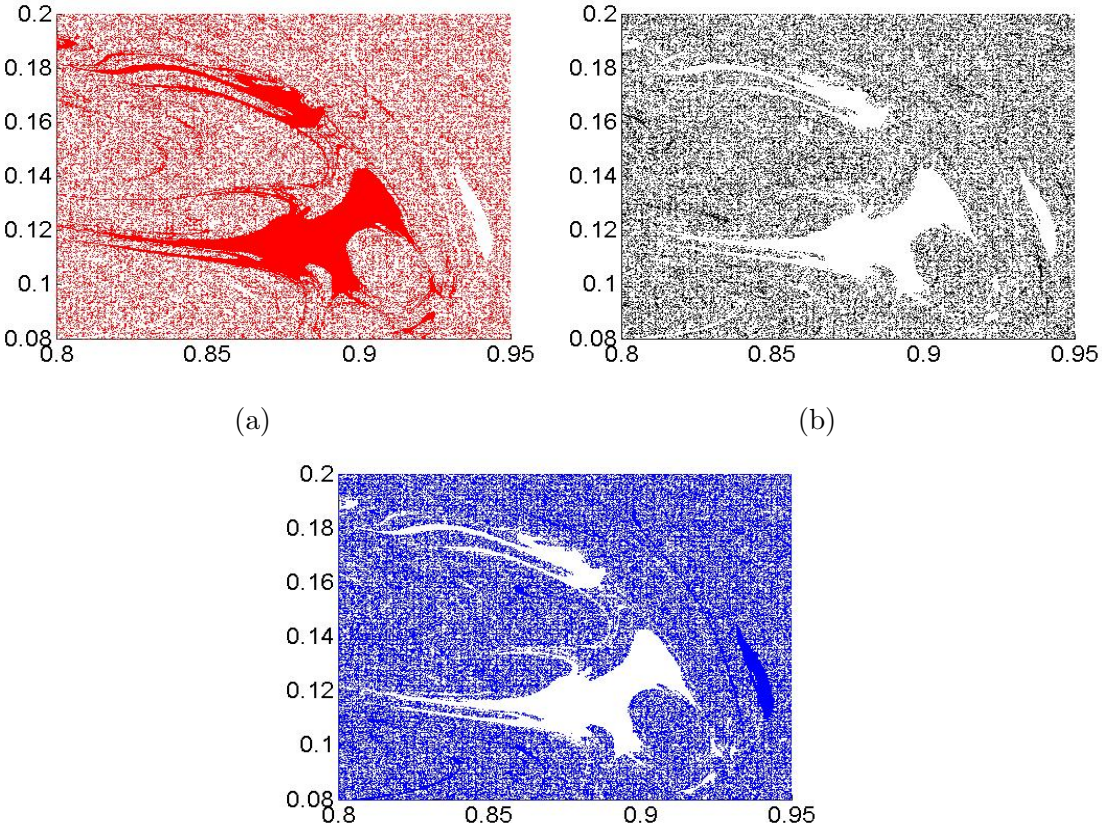

(a) (b)

(c)

Figure 2.8: Figure 2.8a, 2.8b and 2.8c zoom in on the black rectangle shown in Fig. 2.7, close to P_{att}. Figure 2.8a, 2.8b and 2.8c plot the basins of attraction corresponding to P_{att} in red, to P_{attsym} in black and to the laminar attractor in blue respectively.

2.5.4 Properties of the edge as a function of Reynolds number.

To study the properties of the edge, we choose 10000 directions randomly in the 9 dimensional state space, starting from the laminar attractor. For these 10000 directions, we plot various basin properties as a function of Reynolds no., for

$Re = 200, 300, \ldots, 1000, 1500, 2000.$

Fig. 2.9, 2.10 and 2.11 plot the minimum boundary distance, average boundary distance and maximum boundary distance respectively, as a function of Reynolds number.

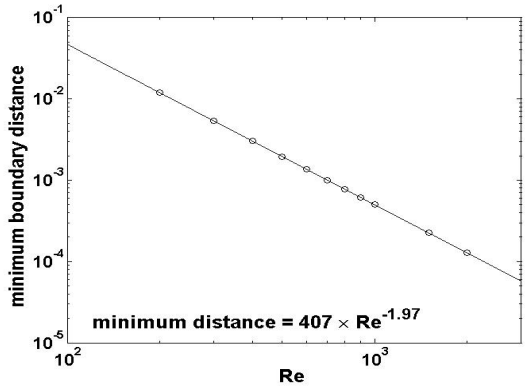

Figure 2.9: For 10000 randomly chosen vectors, the minimum boundary distance vs Reynolds number is plotted, for $Re = 200, 300, \ldots, 1000, 1500, 2000$.

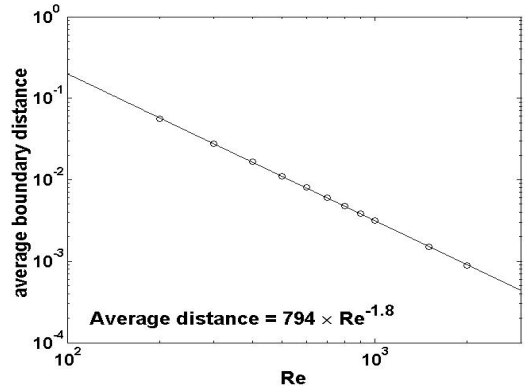

Figure 2.10: For 10000 randomly chosen vectors, the average boundary distance vs Reynolds number is plotted, for $Re = 200, 300, \ldots, 1000, 1500, 2000$.

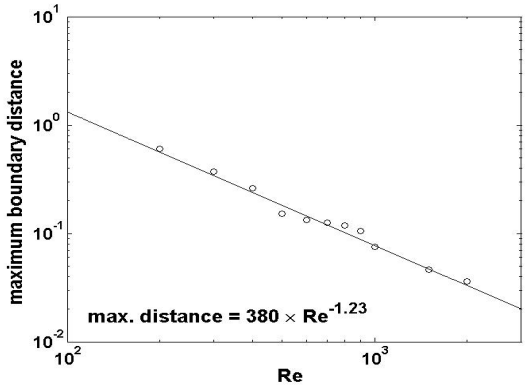

Figure 2.11: For 10000 randomly chosen vectors, the maximum boundary distance vs Reynolds number is plotted, for $Re = 200, 300, \ldots, 1000, 1500, 2000$. We believe that the deviation from the scaling of the maximum boundary distance is caused by the bending of the long tendril-like structures seen in Fig. 2.4a to 2.4f. This deviation from the scaling does not feature in the Fig. 2.10 (which plots the average boundary distance vs Reynolds no.), as there are few points on the edge which have a large distance from the laminar attractor. (See the histogram in Fig. 2.2.)

2.6 Discussion

In all of our investigations, we find that the distance of the periodic orbit on the edge from the laminar attractor scales as $\approx Re^{-1}$ (Fig. 2.3). As per [24], the average energy of the periodic orbit on the edge scales as Re^{-2} where the energy $E = (1 - a_1)^2 + \sum_{j=2}^{9} {a_j}^2$. This implies that the average distance of the periodic orbit on the edge from the laminar attractor would scale as Re^{-1}, which agrees with our computations. We find that the edge of chaos is a stable manifold of a periodic saddle orbit. This is in line with the observation in [24] which study the same system, and also with [8] which studies a 9-dimensional system of Plane-Couette flow. For $Re = 200, 300, 600, 700, 800, 900, 1000, 1500, 2000$, we observe an exponential scaling of lifetimes in agreement with the suggestion that the turbulent

state represents a chaotic saddle [8–11, 25, 44]. On examining Reynolds numbers from 200 to 2000, we find that the nearest point on the edge of chaos to the laminar attractor (and thus the critical amplitude of the perturbation beyond which the laminar attractor becomes unstable), has a distance proportional to $\approx Re^{-2}$ (Fig. 2.9). Thus, the critical amplitude of perturbation A_c that can be added to the laminar attractor beyond which the laminar attractor would fall into the turbulent region scales as $A_c \sim Re^{\alpha}$ with $\alpha = -2$. Ref. [24] calculates the probability that an initial condition with a given energy will lead to chaotic behavior by choosing uniformly distributed initial conditions, and shows that the periodic orbit on the edge lies in the region corresponding to the energy with 96-97 percent probability of transient chaos. This indicates that the distance of the periodic orbit on the edge from the laminar attractor is significantly higher than the average edge distance from the laminar attractor, which agrees with the equations in Fig. 2.3 and 2.10. The average distance to the edge of chaos scales like $\approx Re^{-1.8}$ (Fig. 2.10), the maximum distance to the edge of chaos scales like $\approx Re^{-1.23}$ (Fig. 2.11) and turbulent bursts in the transient turbulence region persist for an average lifetime of $\approx Re^{4.51}$ (Fig. 2.5). Thus, the average lifetime increases rapidly with Reynolds number but it does not appear that the lifetime would diverge for higher Reynolds numbers. This is in line with the observations in [3, 19–21].

Chapter 3: Robustness of periodic orbits in the presence of noise

For a smooth dynamical system $x_{n+1} = F(C, x_n)$ (depending on a parameter C), there may be infinitely many periodic windows, that is, intervals in C having a region of stable periodic behavior. However, the smaller of these windows are easily destroyed with tiny perturbations, so that only finitely many of the windows can be detected for a given level of noise. For a fixed perturbation size ϵ, we consider the system behavior in the presence of noise. We look at the "ϵ-robust windows", that is, those periodic windows such that for the superstable parameter value C in that window, the general periodic behavior persists despite noise of amplitude $\leq \epsilon$. We focus on the quadratic map, and numerically compute the number of periodic windows that are ϵ-robust. We obtain a robustness-exponent $\alpha = 0.51 \pm 0.03$, which characterizes the robustness of periodic windows in the presence of noise.

3.1 Introduction

For the map f on R given by

$$x_{n+1} = f(C, x_n) \tag{3.1}$$

we choose a parameter C for which the map has an attracting periodic orbit.

Most of these orbits can be disrupted with tiny perturbations. For $\epsilon > 0$, we

ask how common are periodic orbits that cannot be destroyed by ϵ perturbations. Let x_0 be a point of a period-k attracting orbit of Eq. 3.1. We investigate noisy trajectories starting at x_0,

$$\tilde{x}_{n+1} = f(C, \tilde{x}_n) + \delta_n \text{ for } n = 0, 1, 2, \cdots \text{ where } \tilde{x}_0 = x_0 \text{ and } |\delta_n| \leq \epsilon \tag{3.2}$$

We say that x_0 is ϵ-robust if for every choice of the sequence δ_n such that $|\delta_n| \leq \epsilon$, the distance $|\tilde{x}_n - x_n|$ remains small for all n. (We would be more precise later.) Every periodic attractor persists for small changes in C, so in such a family, we focus on the particular orbits that are most stable, and ask if it is ϵ-robust. Sometimes we instead ask if that orbit is ϵ-robust when we allow only one δ_n to be nonzero. (See Section 3.5.)

For the quadratic map

$$x_{n+1} = C - {x_n}^2 \tag{3.3}$$

we find that the number $N(\epsilon)$ of ϵ-robust super-stable periodic orbits satisfies

$$N(\epsilon) \sim \epsilon^{-\alpha} \text{ where } \alpha \approx 0.51.$$

There is a fractal nature to periodic orbits for $C - x^2$, and we investigate two problems which can be shown theoretically to have the same exponent.

We believe that the behavior of periodic orbits for many processes is very similar to those of the quadratic map (3.3). However there are special properties of (3.3) that are extremely convenient for finding periodic orbits. The studies we report here are currently only feasible for quadratic maps, so that is all we investigate. We believe these findings will provide insight into a much larger class of higher dimensional processes. From here onward, we restrict attention to (3.3).

Let C be a parameter value for which there is a stable period-k orbit $(x_i)_1^k$, i.e., $x_{i+1} = f(x_i)$ except $x_1 = f(x_k)$. The basin of attraction B for this orbit is the set of initial points x whose trajectory $(f^m(x))_{m=1}^{\infty}$ converges to this orbit. We define the ***interval basin*** for each attracting periodic point x_i, to be the largest interval (a_i, b_i) in B, containing x_i. Note that the points a_i, b_i are not in B. In particular, for all $x \in (a_i, b_i)$, $\lim_{n\to\infty} f^{nk}(x) = x_i$.

Let one of the points of the stable period-k orbit x_i, for some $i \in (1, 2, \cdots, k)$ be the starting point of the trajectory of Eq. 3.2. The trajectory 'remains in phase' with the stable period-k orbit if $f^n(C, x_i)$ and $(\tilde{x}_n)$ are in the same interval basin for all $n = 1, 2, \cdots$. The trajectory is said to go ***out of phase*** if it does not remain in phase.

Goal. A sequence of disturbances $(\delta_0, \delta_1, \cdots)$ is said to be an ***ϵ-bounded sequence*** if $|\delta_m| < \epsilon$, for $m = 0, 1, \cdots$. For each C, the map (3.3) has at most one attracting periodic orbit. Given C, x where x is an attracting periodic point, the parameter C is said to be ***ϵ-robust***, if, for every ϵ-bounded sequence of disturbances, the perturbed trajectory given by Eq. 3.2 remains in phase with the attracting orbit starting from x_0. A periodic window of period-k is an interval of the parameter, ${C_*}^{(k)} \leq C \leq {C_x}^{(k)}$, such that at the beginning of the window, as C increases through ${C_*}^{(k)}$, there is a bifurcation from a chaotic attractor to a periodic attracting orbit of period k, followed by a period-doubling cascade to chaos, followed by a sequence of band-mergings in each of which $2^m k$ separate pieces (x-intervals) of the chaotic attractor pairwise merge into a $2^{m-1}k$-piece chaotic attractor, eventually forming a

k-piece chaotic attractor, which subsequently terminates at the end of the window ($C = {C_x}^{(k)}$) through an interior crisis transition [45] to a larger chaotic attractor that is similar in size to the larger chaotic attractor just before the beginning of the window at $C = {C_*}^{(k)}$. We say that a period-k window is ϵ-***robust*** if its superstable parameter value is ϵ-robust. For a given window, we let ϵ_{max} be the largest ϵ for which the window is ϵ-robust.

Only finitely many periodic windows of f are ϵ-robust. Given ϵ, our goal is to determine the number of ϵ-robust periodic windows of the perturbed system, and how the number depends on ϵ as $\epsilon \to 0$.

In this work, we compute the location of the "primary" periodic windows of the quadratic map of periods not exceeding 25. We investigate $N(\epsilon)$, the number of windows with width $> \epsilon$, and find

$$N(\epsilon) \sim \epsilon^{-\alpha} \text{ where } \alpha = 0.51 \pm 0.03.$$

We show that our exponent α is closely related conceptually to an "uncertainty exponent" of [46]. We use our exponent to study ϵ-robust windows for the general case in Eq. 3.2 (for $f = C - x^2$), where a disturbance can be added at each iterate of the system, as well as the special case where a single disruptive perturbation is added to the system, and compute the maximum permissible disturbance bound in both the cases, beyond which, the perturbed trajectory would go out of phase. We conclude that although the maximum permissible ϵ-value is higher for the case of a single pulse as compared to the general case, the scaling is the same in the two cases. Statistically, the maximum permissible ϵ-value for the single pulse case scales

as a constant multiple of the corresponding value for the general case.

The layout of the paper is as follows. Section 4.4 introduces definitions and terminology pertaining to the problem. Section 3.3 gives the results and the robustness exponent. Section 3.4 describes the method used in determining the maximum permissible noise-bound beyond which the trajectory can be knocked out of its interval basin. Section 3.5 discusses the special case of a single disruptive perturbation destabilizing the attracting orbit. Section 3.6 compares our robustness exponent to the uncertainty exponents defined previously [46–48]. The Appendix discusses our method for computing the sequence of periodic windows. It is based on kneading theory [49].

3.2 Environment of a period-k point

The map can have infinitely many periodic windows in a range of parameter values. Fig. 3.1 shows the period-3 window of the quadratic map in black. The map has a unique attractor for each $C \in [-0.25, 2]$. Let parameter C lie in a period-k window. According to extensive numerics, for the quadratic map, the robustness of the window to perturbations is largest for the superstable period-k orbit. Hence, to study window-robustness, we consider the superstable orbit.

x-width of the window. We define the ***x-width of the period-k window*** to be the width of the smallest of the k interval basins when C equals the superstable parameter value of the window. Fig. 3.2b shows the x-width of the period-3 window.

C-width of the window. For a given period-k window, the interior-crisis point corresponds to that value of parameter C for which the interval basin has

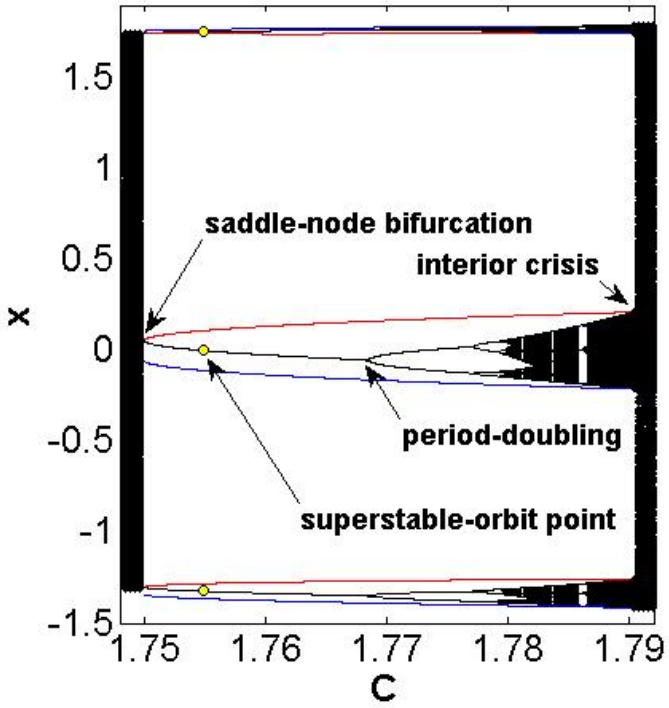

Figure 3.1: **The bifurcation diagram for the period-3 window of the quadratic map.** The bifurcation diagram shows the period-3 window of the quadratic map in Eq. 3.3. The saddle-node bifurcation, where the window is created occurs at $C = 1.75$. The interior-crisis occurs at $C \approx 1.790327$. The C-width of the window is shown. The attracting orbits of the window are shown in black. The boundaries of the interval basin are denoted by red and blue. The boundary in red is the unstable period-3 orbit created at the saddle-node bifurcation, and collides with the attractor at the interior crisis value of C. The superstable orbit points are shown as small circles. As C increases beyond the period-doubling bifurcation value, the attractor widens, and the distance of the orbit from the red and blue curves decreases.

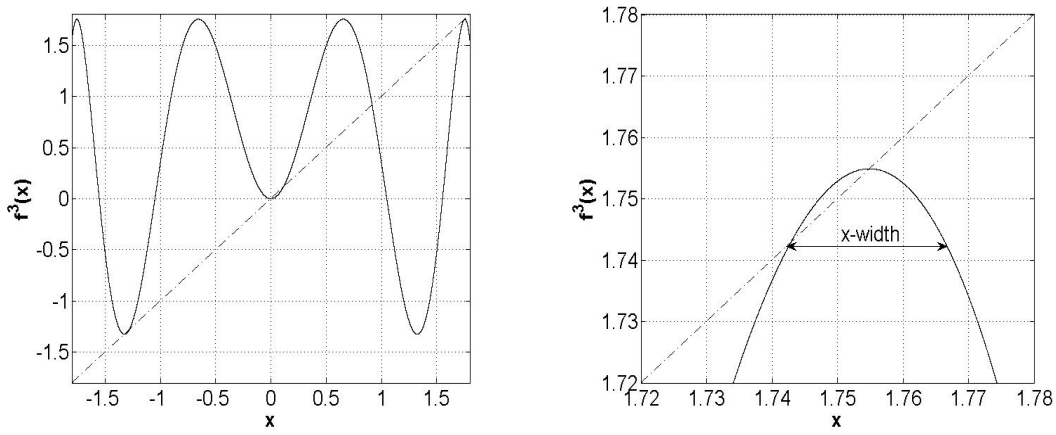

(a) (b)

Figure 3.2: **The x-width of the period-3 window.** Fig. 3.2a shows the three times iterated map $f^3(x)$ vs. x when $C \approx 1.754877$, which is the superstable parameter value of the period-3 window. The dotted line is the diagonal. Fig. 3.2b zooms in on Fig. 3.2a to show the x-width of the period-3 window, which equals the size of the smallest interval basin of the window at the superstable value of parameter C. The dotted line is the diagonal $y = x$.

an unstable period-k point on its boundary [45]. The ***C-width of the periodic window*** is defined as the parameter difference between the interior-crisis value of C for the window and the saddle-node bifurcation value of C.

Adding a disturbance. We choose a (C^*, x_0^*) where C^* corresponds to the superstable parameter value of the periodic window, and x_0^* is a point of the attracting orbit. The perturbed system is represented as (3.2). We are interested in finding if every ϵ-perturbed trajectory which starts from (C^*, x_0^*) remains in phase.

Parameter value C_{odd}. Let $C_{odd} \approx 1.543689$ denote the largest parameter value before which there are no periodic windows of odd periods other than the period-1 window. To study the distribution of C-widths of the periodic windows, we consider the parameter range $C_{odd} \leq C \leq 2$.

Number of primary windows of periods $\leq P$. Ref. [50] states that the periodic windows are dense in the interval $C_{odd} \leq C \leq 2$ and for large periods k, the number of period-k windows increases exponentially with the period. In order to characterize all the windows of periods $\leq P$, we determine the sequence in which these windows appear in the map, as the parameter C is increased. Appendix B describes the method used to determine the sequence, which is based on kneading theory [49]. There are 1402957 windows with periods ≤ 25. For the general case in (3.2) and for the special case of a single disruptive perturbation, we attempt to characterize how the total number of ϵ-robust windows scales in relation with ϵ.

3.3 Results

Fig. 3.3 shows the distribution of window C-widths for periods up to $P =$ 13, 15, 17, 19, 23, 25. As higher and higher values of P were considered, the graph behavior approximated the straight line $\log_{10}[N(\epsilon)] = (-0.51 \pm 0.03) \log_{10}[\epsilon] - 0.876$ where $N(\epsilon)$ denotes the number of primary windows whose C-width exceeds ϵ. Thus, $N(\epsilon) = K\epsilon^{-\alpha}$ where $K = 0.133, \alpha = 0.51 \pm 0.03$. We have uploaded the data for the 1402957 primary periodic windows of periods ≤ 25 lying in $C_{odd} \leq C \leq 2$ in [51].

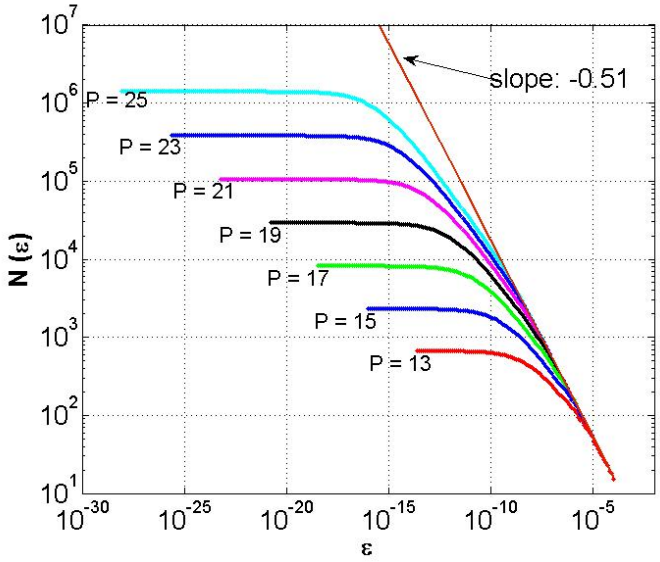

Figure 3.3: $N(\epsilon)$ **vs** ϵ**.** A curve is plotted for $P = 13, 15, 17, 19, 21, 23, 25$. The curve for each value of P includes all the periodic windows of periods not exceeding P lying in the parameter-range $C \in [C^{odd}, 2]$. In this log-log plot, as P increases, the curves appear to asymptote to the straight line shown in red, with the equation $\log_{10} N(\epsilon) = -0.51 \log_{10} \epsilon - 0.876$. Thus, $N(\epsilon) = 0.133\epsilon^{-\alpha}$ where $\alpha = 0.51 \pm 0.03$.

Robustness-Exponent. We define the robustness-exponent as

$$\alpha = \lim_{\epsilon \to 0} \frac{\log N(\epsilon)}{\log \epsilon}$$

where $N(\epsilon)$ is the number of primary windows, whose C-width exceeds ϵ. Our computations give us a robustness-exponent $\alpha = 0.51$ based on the distribution of window C-widths.

3.4 Determining the maximum permissible disturbance bound.

Computing the maximum permissible disturbance bound ϵ_{max} for a window such that the window is ϵ-robust depends on the position of the superstable orbit in the interval basin. Recall C^* denotes the superstable C of any window under

discussion. Compute the periodic trajectory (x_n) of the superstable orbit, starting from $x_0 = 0$, which is a superstable periodic point. To find ϵ_{max}, we consider the worst case scenario, wherein each δ_n in Eq. (3.2) is either ϵ or $-\epsilon$. For fixed ϵ, the perturbed trajectory, denoted $(\tilde{x}_n)$ with $\tilde{x}_0 = \pm\epsilon$, diverges from the superstable orbit, when $\delta_n = {\delta_n}^*$ is chosen as follows, for $n = 1, 2, \cdots$

$${\delta_n}^* = \begin{cases} -\epsilon, & \text{if } f(\tilde{x}_{n-1}) \leq x_n \\ \\ +\epsilon, & \text{if } f(\tilde{x}_{n-1}) > x_n \end{cases}$$

Note that $f(\tilde{x}_0 = \pm\epsilon) = C - \epsilon^2$, independent of choice of sign. Having defined ${\delta_n}^*$, let $\tilde{X}_k(x)$ be the k^{th} iterate of (3.2) starting from initial point x so that

$$\tilde{X}_{n+1} = f(\tilde{X}_n) + {\delta_n}^* \tag{3.4}$$

See Fig. 3.4 for period $k = 3$.

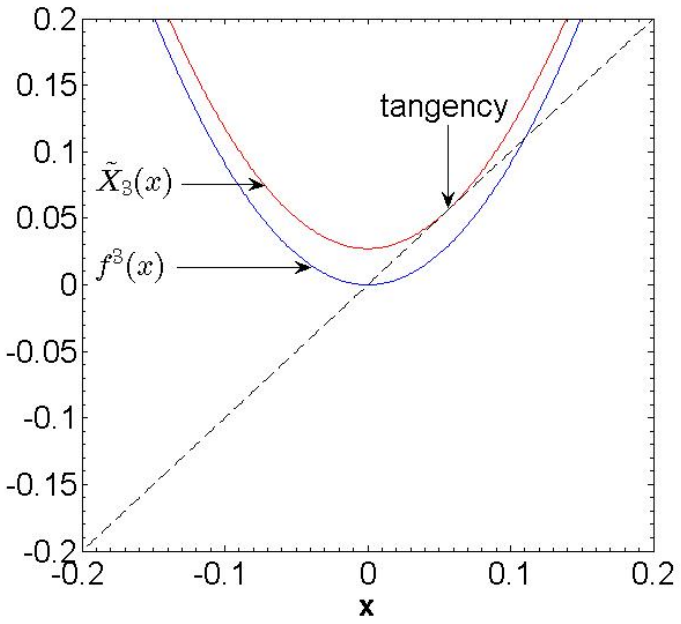

Figure 3.4: **Determining the maximum admissible perturbation ϵ_{max}.** Here we illustrate how to find ϵ_{max} via the example of a period-3 window, where the superstable C is $C^* \approx 1.754877$. The blue curve is $f^3(x)$ vs x near $x = 0$. The red curve is the graph of $\tilde{X}_3(x)$, where $\epsilon = \epsilon_{max} \approx .002111934$ is chosen so that there is a tangency. The dashed line is the diagonal.

In general, on adding tiny perturbations, up to a threshold, to each iterate of a trajectory starting from the attractor, the perturbed trajectory eventually settles down to an orbit close to the original attracting orbit. For a disturbance exceeding ϵ_{max}, the perturbed attracting orbit is no longer confined so that its k attracting points lie respectively in their original interval basins. Thus ϵ_{max} corresponds to the saddle-node bifurcation value of the perturbed attracting orbit, as in Fig. 3.4. Consequently, on adding $\pm\epsilon_{max}$, as in Eq. 3.4, the slope of the k-times-iterated map, at the x values corresponding to the perturbed attracting orbit, equals 1.

An Example. For the period-3 window, the superstable parameter value is $C^* \approx 1.754877$. Thus, the orbit of the window at the superstable value is $\{x_1 =$

$0, x_2 \approx 1.754877, x_3 \approx -1.324717\}$. To compute the maximum permissible ϵ, namely ϵ_{max}, let $\tilde{x_1}$ denote the perturbed value chosen around $x_1 = 0$. The quadratic map is symmetric about the y-axis and has a single hump at $x = 0$, so $f(\tilde{x}_1) < x_2$, irrespective of whether $\tilde{x}_1$ is greater than or less than 0. Thus $\tilde{x}_2 = f(\tilde{x}_1) - \epsilon$ and correspondingly, $\tilde{x}_3 = f(\tilde{x}_2) + \epsilon$, and $\tilde{x}_4 = f(\tilde{x}_3) + \epsilon$, so that for the attracting orbit, $\tilde{x}_4 = \tilde{x}_1 = f(f(f(\tilde{x}_1) - \epsilon) + \epsilon) + \epsilon$.

To solve for ϵ_{max}, we use the Newton's method in $\tilde{x}$ and ϵ, with $(\epsilon = 0, \tilde{x} = 0)$ as the initial approximation, and the equations

$$\tilde{x}_{k+1} = \tilde{x}_1, \frac{\partial \tilde{f}^k(\tilde{x}, \epsilon)}{\partial \tilde{x}} = 1$$

to compute ϵ_{max} at the superstable parameter value of the period-k window, and also the perturbed attracting orbit at ϵ_{max}.

3.5 The case of a single disruptive perturbation

For the quadratic map at the superstable parameter value of a period-k window, we have looked at the case where a perturbation can be added at each iterate of the system, as given by Eq. 3.2 so as to destabilize the trajectory. Here, we look at a special case of Eq. 3.2, where a *single pulse of disturbance at a single iteration* is added to the trajectory. When large enough, a single perturbation can knock the trajectory out of phase with the attracting orbit. Here we determine the *upper-bound on perturbation* ϵ such that the perturbed trajectory continues to remain in phase with the attracting orbit. For a fixed ϵ and some choice of (C, x_0) as in section 3.1, say a perturbation 'd' is added at the m^{th} iterate of the system, such that $|d| \leq \epsilon$.

The corresponding perturbed trajectory is defined as the ***ϵ-perturbed trajectory***. Let $(x_n)_{n=0}^{n=\infty}$ represent the original trajectory where $x_{n+1} = f(x_n)$. The ϵ-perturbed trajectory $(\tilde{x}_n)_{n=0}^{n=\infty}$ is given by the equation,

$$\tilde{x}_{n+1} = f(C, \tilde{x}_n) + \delta_{n,m} \text{ where } \tilde{x}_0 = x_0,$$

$$\delta_{n,m} = \begin{cases} d \text{ where } |d| \leq \epsilon, & \text{if } n = m \\ 0 & \text{if } n \neq m. \end{cases}$$

We want to determine if an ϵ-perturbed trajectory can be kicked out of the interval basin.

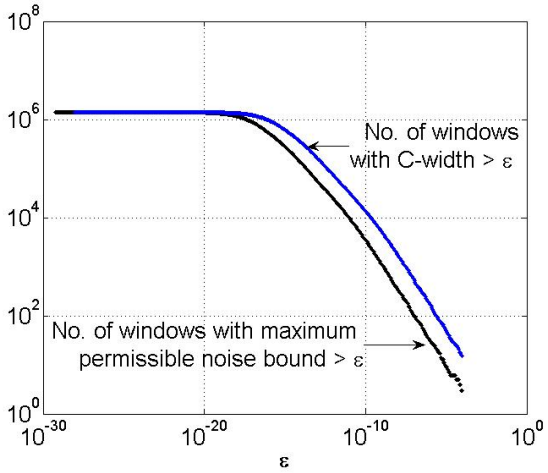

Figure 3.5: **The number of periodic windows whose C-width exceeds ϵ, and the number of periodic windows whose maximum permissible noise-bound exceeds ϵ, plotted as a function of ϵ. The blue curve is almost a horizontal shift of the black curve.** The blue curve is a plot of the number of periodic windows whose C-width exceeds ϵ, as a function of ϵ, using all periodic windows of periods not exceeding 25, lying in the parameter-range $C \in [C^{odd}, 2]$. For the same set of periodic windows, the black curve is a plot of the number of periodic windows whose maximum permissible noise-bound exceeds ϵ, as a function of ϵ.

As defined in section 3.1, k interval basins exist for a period-k window. To

understand the effects of a one-time disturbance, we need to determine which of the periodic points is closest to its interval basin's boundary and what that distance is. In particular, in order to ensure that the perturbed trajectory cannot be kicked out of any of the interval basins, it is enough to ensure that it cannot be kicked out of the smallest interval basin. We numerically observe that the maximum depth of the smallest basin occurs when C equals the superstable parameter value C^* of the periodic window. Hence, we consider trajectories starting from (C^*, x_0^*) for various periodic windows, where x_0^* lies on the attractor corresponding to the smallest interval basin.

The relation between the x-width and C-width. For the quadratic map (3.3), if there is an attracting periodic orbit, then $x = 0$ is always in one of the interval basins [52]. Say this is the central interval basin. Ref. [46] studies (3.3) using a linear approximation to the map for the $(k-1)$ non-central interval basins and defines Λ_k as $\Lambda_k = \lambda_1\lambda_2\cdots\lambda_{k-1}$ which is the product of the map-slopes at the attracting points in these $(k-1)$ interval basins, evaluated at the superstable value of parameter C. As per Ref. [46], the C-width of a window, given by ΔC_k, scales as $\Delta C_k \sim \frac{9}{4}\Lambda_k^{-2}$ and the width of the central interval basin scales as Λ_k^{-1}. The central interval basin contains $x = 0$, where the map has slope 0, and this central interval basin maps to the rightmost interval basin. Hence, the rightmost interval basin is the smallest of the k interval basins, and the x-width corresponds to this interval basin. Since the map, when applied $k-1$ times at the superstable value of C, stretches the x-width by a factor of Λ_k, it appears that the x-width scales as Λ_k^{-2}

and hence the x-width and C-width are related by a constant. This relationship was also observed by us numerically. Hence, to have a statistical understanding of the effects of noise added to one of the iterates of the map, it is enough to consider the distribution of C-widths of the periodic windows.

The relation between C-width and the maximum permissible disturbance bound. It can be observed from the histogram in Fig. 3.6 that for most of the periodic windows considered, the maximum permissible noise ϵ_{max} that can be added at each iterate at the superstable parameter value (so that the trajectory starting from an attracting orbit remains in phase) is directly proportional to the C-width of the periodic window. For a period-k window, consider the k-times-iterated map $f^k(x)$ at the superstable parameter value of the window. Each of the k regions around the period-k attracting orbit can be approximated by a quadratic map [52]. In particular, the map corresponding to the period-k attracting point x_i would be of the form $x_i - A_i(x - x_i)^2$ where A_i depends on x_i, for $i = 1, 2, \ldots, k$. Each of these k quadratic approximations has a different value of $\max|f^k(x) - x|$. Since the disturbance can be added at any iterate of the map, and we want to find the bound on the maximum disturbance that can be added so that the perturbed trajectory remains in phase, we consider the quadratic approximation from amongst the k quadratic approximations that has the minimum value of $\max|f^k(x) - x|$. For most of the periodic windows, this occurs at the rightmost period-k point (as the rightmost interval basin is typically the smallest of the k interval basins). This corresponds to the quadratic approximation around $x = C^*, y = C^*$, which is, $C^* - A^*(x - C^*)^2$

for some constant A^*. Since C^* corresponds to the superstable parameter value of the map, $\max|f^k(x) - x|$ can be approximated as being proportional to $\frac{1}{4A^*}$ and the x-width $\approx \frac{2}{A^*}$, thus the maximum permissible disturbance bound is roughly proportional to the x-width. Since x-width can be approximated as being directly proportional to the C-width, the C-width and the maximum permissible disturbance bound are approximately in direct proportion.

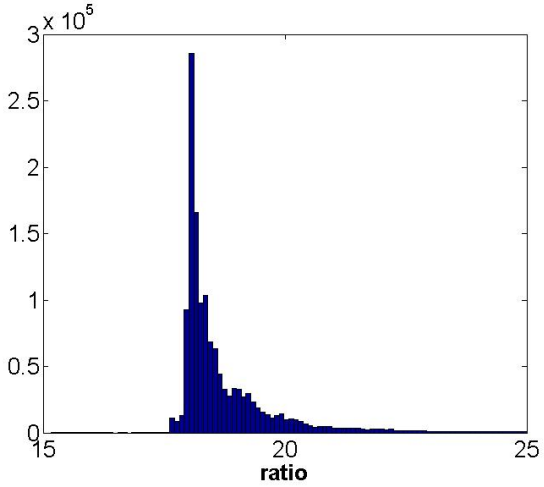

Figure 3.6: **The histogram of the ratio of the C-width to the maximum permissible single pulse.** For each periodic window of period not exceeding 25, lying in the parameter-range $C \in [C^{odd}, 2]$, we compute the ratio of the C-width to the maximum permissible single pulse. We use 100 bins for ratio values between 15 and 25 and plot the number of windows whose ratio lies in each interval. The histogram has a peak for ratios in the bin $[18, 18.1)$.

3.6 Comparing exponents.

An uncertainty exponent has been defined previously to study the distribution of chaos [46–48]. We compare our robustness-exponent to that obtained in [46–48].

Exponent according to Hunt and Ott [46]. In Ref. [46], S_c represents

the set of parameter values of the quadratic map leading to a chaotic attractor. For a given value of maximum noise ϵ, δ is chosen randomly with uniform probability density from the interval $-\epsilon \leq \delta \leq \epsilon$ and $c \in S_c$ is chosen randomly. If $S_c(\epsilon)$ denotes the set created by fattening the set S_c by the amount ϵ, [46] defines the uncertainty exponent as,

$$\alpha^* = \lim_{\epsilon \to 0} \frac{\log V[S_c(\epsilon) - S_c]}{\log(\epsilon)} \tag{3.5}$$

where V denotes Lebesgue measure. [46] studies the distribution of primary window widths of the quadratic map, and computes $\alpha^* = 0.51 \pm 0.03$. The uncertainty exponent in [46] can be derived using our computations. To derive this, assume that for each primary period-k window, the fraction of the periodic window from the saddle-node bifurcation value (where the period-k attractor emerges) to the Feigenbaum point occupies a fixed fraction of the C-width of the window. Denote this fraction by ϕ. Assume that periodic windows with C-width exceeding $2\epsilon/\phi$ contribute 2ϵ to $V[S_c(\epsilon) - S_c]$ (only the edges of the windows are filled by ϵ-fattening, see Fig. 4.6). Periodic windows with C-width less than $2\epsilon/\phi$ are entirely filled by the ϵ-fattening and hence contribute, to $V[S_c(\epsilon) - S_c]$, an amount equal to the $\phi \times$ C-width of the window (see Fig. 4.6). Assume $N(\epsilon) = 0.133\epsilon^{-\alpha}$ where $N(\epsilon)$ is the net number of primary windows, the C-width of which exceeds ϵ (see Fig. 3.3). Thus, $V[S_c(\epsilon) - S_c] \sim \int_0^{2\epsilon} x\,(-dN(x)) + 2\epsilon N(2\epsilon)$ where the negative sign preceding $dN(x)$ follows from the fact that $dN(x) < 0$. Then,

$$V[S_c(\epsilon) - S_c] = \frac{0.133 \times 0.51 \times (2\epsilon)^{1-\alpha}}{1 - 0.51} + 2\epsilon \times 0.133 \times (2\epsilon)^{-\alpha}$$

so that $\alpha^* = \lim_{\epsilon \to 0} \frac{\log V[S_c(\epsilon) - S_c]}{\log(\epsilon)} = 1 - \alpha = 0.49$. This is in close approximation with

the value $\alpha^* = 0.51 \pm 0.03$ computed in [46].

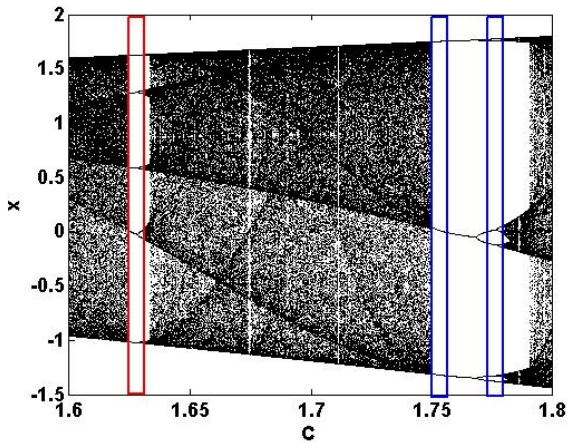

Figure 3.7: **The relation between the C-width of the window and its contribution to $V[S_c(\epsilon) - S_c]$.** The red rectangle indicates that smaller periodic windows (of C-width $< 2\epsilon/\phi$) are entirely filled up by the ϵ-fattening, where ϕ is defined in the text. The blue rectangles indicates that for large periodic windows (of C-width $> 2\epsilon/\phi$), only the edges are filled up by the ϵ-fattening. Note that the blue and red rectangles each have width ϵ.

Exponent according to Grebogi, McDonald, Ott, Yorke [47]. Ref. [47] which discusses fat fractals computes the fat fractal dimension as per Eq. 3.5 by perturbing C values in S_c by $\pm\epsilon$. This gives $\beta^* \cong 0.41$. The difference between the numerical values of this exponent and the one obtained in [46] both of which use Eq. 3.5 stems from the fact that Hunt and Ott compute their exponent taking into account only primary windows whereas [47] takes into account windows of all orders. Thus, [46] takes into account only "large chaotic attractors", that is, chaotic attractors not contained in any windows, as opposed to [47]. This will be discussed in a future paper.

Exponent according to Farmer [48]. In Ref. [48], Farmer defines the

fatness exponent in terms of widths of primary periodic windows of the map. His computations are based on his assumption that it is possible to arrange the MSS sequences in a binary tree, such that sequences lower down in the tree "generally" have smaller stable intervals. Farmer promised more details in a future paper, which has not appeared. His assumption implies that the maximum C-width of a period-n orbit is smaller than the maximum C-width of a period-$(n-1)$ orbit. Fig. 3.8 shows the C-width of the largest window, that is, the window with maximum C-width of a given period, as a function of period. The figure shows that there are frequent exceptions to the assumption in [48] at several places.

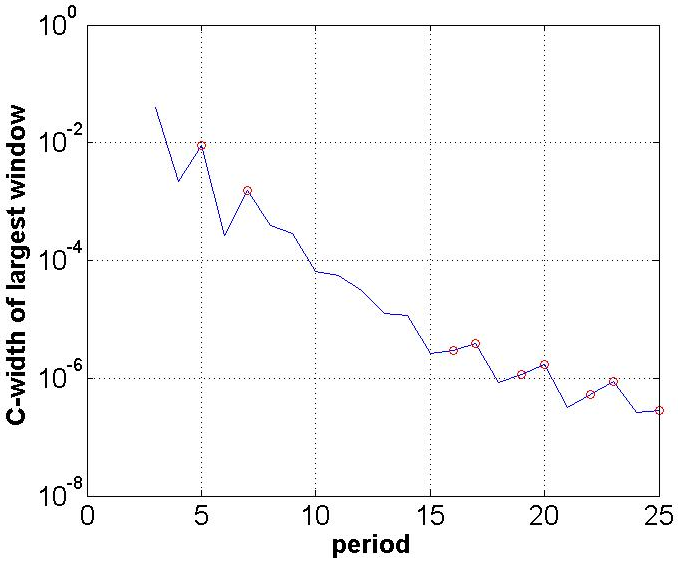

Figure 3.8: **The C-width of the largest period-k window as a function of k.** The plot shows the C-width of the largest window of a given period as a function of the period. The circles indicate those values for which the largest period-p window has C-width greater than the largest period-(p-1) window.

For the given value of ϵ, Famer considers those periodic windows for which the width of the periodic attractor region within the window exceeds ϵ. He defines

$h(\epsilon)$ as the total width of the periodic attractor regions of those periodic windows, and $\mu(\epsilon) = 1 - h(\epsilon)$. The uncertainty exponent, called the ***fatness exponent*** is defined as,

$$\beta = \lim_{\epsilon \to 0} \frac{\log[\mu(\epsilon) - \mu(0)]}{\log(\epsilon)}.$$

which he asserts gives $\beta = 0.45 \pm 0.04$.

3.7 Discussion

We have obtained a robustness exponent based on the scaling of the C-widths of the periodic windows of the quadratic map, which can be used to characterize the stability of periodic windows in the presence of bounded-perturbations. We computed maximum permissible disturbance bounds, for a general case (3.2) where a perturbation can be added to each iterate of the system, and a special case where a single perturbation is used to drive the attracting trajectory out of phase. We conclude that the maximum permissible ϵ bounds for the two cases are statistically related by a constant (see Fig. 3.6) and thus the scaling is the same in the two cases. Although we have examined ϵ-robustness for the case of the quadratic map, we expect to get the same scaling for other one-dimensional maps with one parameter having a single quadratic maximum.

Chapter 4: How Certain Can We be That a System Has a Chaotic Attractor: The Scaling of Chaos vs Periodicity.

The character of the time-asymptotic evolution of physical systems can have complex, singular behavior with variation of a system parameter, particularly when chaos is involved. A perturbation of the parameter by a small amount ϵ can convert an attractor from chaotic to non-chaotic or vice-versa. We call a parameter value where this can happen ϵ-uncertain. The probability that a random choice of the parameter is ϵ-uncertain commonly scales like a power law in ϵ. Surprisingly, two seemingly similar ways of defining this scaling, both of physical interest, yield different numerical values for the scaling exponent. We show why this happens and present a quantitative analysis of this phenomenon.

While low-dimensional chaotic attractors are common and fundamental in a vast range of physical phenomenon, it is typically the case that chaotic motions in such systems are 'structurally unstable', meaning that an *arbitrarily small* change of a system parameter can always be found that results in periodic behavior [53]. (Note that despite this structural instability, chaotic attractors are still experimentally observable because (see below) they occur with positive probability as parameters are varied.) Physical models displaying chaotic attractors that are structurally unstable

arise very often, e.g., in studies of plasma dynamics [54], Josephson junctions [55], chemical reactions [56] and many others. We also note that even the simple example of the one-dimensional quadratic map,

$$x_{n+1} = C - {x_n}^2, \tag{4.1}$$

displays this phenomenon, and, in this paper we will study this example as a convenient paradigm for such situations in general.

One reason for concern with this type of behavior is that physical systems often have uncertainties in the values of their parameters, and one might therefore ask how confident one can be about the prediction of chaotic behavior from a model calculation (even when the model and its parameter dependence are precisely known and there is no noise). Despite the fundamental importance of this question, very little study has been done to quantitatively address it [46–48]. It is the purpose of this paper to re-address this general issue, and, in particular, to resolve a long-standing puzzle. This puzzle has to do with the scaling characterization of the fractal-like chaotic/periodic interweaving structure of parameter dependence associated with structural instability. In particular, studies on the quadratic map Eq.(4.1) have addressed scaling in two slightly different ways and obtained significantly different estimates of the scaling exponent [46–48]. The reason for this surprising discrepancy has remained unresolved. In one of the two ways of addressing scaling, attention was restricted to what might seem to be the most obvious source of uncertainty, namely, when a *large* (to be defined subsequently) chaotic attractor suddenly turns into a periodic attractor, as a parameter is varied. However, we find such transitions far

too rare [46,48] to account for the observed uncertainty, applicable when all chaotic attractors of any size are considered [47], and this observation is at the heart of the resolution of the above-mentioned puzzle.

ϵ-uncertainty. Consider a dynamical system depending on a parameter C, and an attractor $A(C)$ that, as C varies continuously in some range, can be uniquely associated with C. We say that a particular value of C is *ϵ-uncertain with respect to chaos* if $A(C)$ is chaotic while either $A(C+\epsilon)$ or $A(C-\epsilon)$ or both are not chaotic. For example, for the case of the quadratic map, to which we henceforth restrict our considerations, it has been found that a random choice of C with uniform probability density yields ϵ-uncertainty with respect to chaos with a probability $\bar{F}(\epsilon)$ that scales like a power of ϵ for small ϵ [47], $\bar{F}(\epsilon) \sim \epsilon^{\beta}$. Thus, we define β as

$$\beta = \lim_{\epsilon \to 0} \frac{\log \bar{F}(\epsilon)}{\log \epsilon}. \tag{4.2}$$

As a result of the fine-scaled interweaving of C values for which $A(C)$ is chaotic and intervals of C values for which $A(C)$ is periodic, the power law exponent β turns out to be less than 1, and the set of C values with $A(C)$ chaotic has been called a "fat-fractal" [47, 48] (more precisely, it is a Cantor set with positive Lebesgue measure [57]). We have repeated the numerical determination of $\bar{F}(\epsilon)$ (Fig. 4.1) and find that for small ϵ,

$$\bar{F}(\epsilon) \sim \epsilon^{\beta} \text{ with } \beta = 0.392 \pm 0.037. \tag{4.3}$$

In performing this calculation we estimate $\bar{F}(\epsilon)$ by first randomly choosing many C values with uniform probability in the range where the quadratic map has a unique bounded attractor, $-1/4 \leq C \leq 2$. For each such C value we then compute the

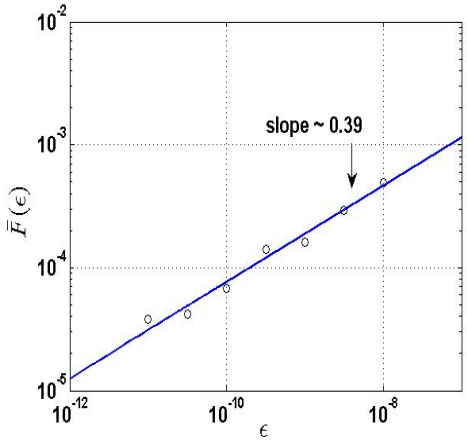

Figure 4.1: $\bar{F}(\epsilon)$ vs ϵ.

Lyapunov exponents for C, $C+\epsilon$ and $C-\epsilon$, judging the corresponding attractors to be chaotic or not depending on whether the computed Lyapunov exponent is positive. We then estimate $\bar{F}(\epsilon)$ as the fraction of those randomly chosen C-values that are computed to be ϵ-uncertain with respect to chaos. Reference [47] obtains a slightly larger β value of $\beta \approx 0.41$ using an ϵ-range with larger ϵ-values. We agree with their result in the range they tested, but, by pushing to small ϵ, obtain the result in Eq. (4.3) (See Fig. 4.1.)

We comment that Eq. (4.3) can be interpreted as implying a type of 'probabilistic stability' for chaos. That is, while chaos occuring at some parameter value C may be structurally unstable in the sense that a chaos-destroying perturbation $C \to C+\delta C$, can always be found with $|\delta C| \leq \tilde{\epsilon}$ for any given $\tilde{\epsilon}$; chaos is still stable in the sense that, for $\tilde{\epsilon}$ small, such a chaos-destroying δC may have to be very carefully chosen, and the probability that a random choice of δC in $|\delta C| \leq \tilde{\epsilon}$ destroys chaos approaches zero as $\tilde{\epsilon}$ is made smaller and smaller [58] (Eq. (4.3)). (Incidentally, we note that quasiperiodicity appears to have this same type of structural-instability /

probabilistic stability [47].)

We now recall the concept of a periodic window. A p-periodic window is an interval of the parameter, ${C_*}^{(p)} \leq C \leq {C_x}^{(p)}$, such that at the beginning of the window, as C increases through ${C_*}^{(p)}$, there is a bifurcation from a chaotic attractor to a periodic orbit attractor of period p, followed by a period-doubling cascade to chaos, followed by a sequence of band-mergings in each of which $2^m p$ separate pieces (x-intervals) of the chaotic attractor pairwise merge into a $2^{m-1}p$-piece chaotic attractor, eventually forming a 'small' p-piece chaotic attractor, which subsequently terminates ('explodes') at the end of the window ($C = {C_x}^{(p)}$) through a crisis transition [18] to a larger chaotic attractor that is similar in size to the larger chaotic attractor just before the beginning of the window at $C = {C_*}^{(p)}$. Thus, as is evident from viewing a bifurcation diagram for the quadratic map, 'small' chaotic attractors occur within windows only, and we call a chaotic attractor that is not contained in any window a 'large chaotic attractor'.

Now, instead of considering ϵ-uncertainty with respect to chaos, we consider ϵ-uncertainty with respect to the occurence of large chaotic attractors. That is, we consider C to be ϵ-uncertain if $A(C)$ is a large chaotic attractor while either $A(C+\epsilon)$ or $A(C-\epsilon)$ or both are not large chaotic attractors. Reference [46] gives a detailed consideration and analysis of the scaling of ϵ uncertainty with respect to the occurrence of large chaotic attractors for Eq. (4.1) obtaining for the probability $F_0(\epsilon)$ of ϵ-uncertainty

$$F_0(\epsilon) \sim \epsilon^{\alpha^*} \text{ with } \alpha^* = 0.51 \pm 0.03. \tag{4.4}$$

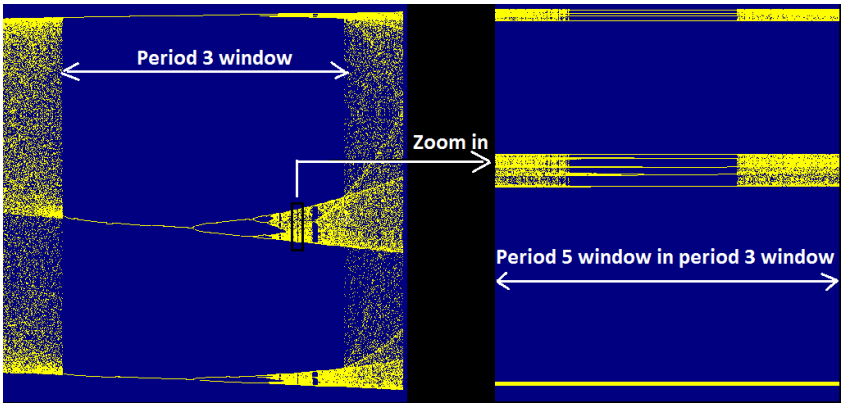

Figure 4.2: Shown is a period 5 secondary window (window of order 2) that lies in a period 3 primary window (window of order 1).

Thus, there are evidently two distinct scaling exponents, the β and α^* of Eqs. (4.3) and (4.4). We conjecture that the values of these exponents are universal for one-dimensional maps with a quadratic maximum. For example, they would apply to physical situations like those in the plasma example in Ref. [54] and the chemical example in Ref. [56], where strong phase-space attraction leads to dynamics closely approximated by a one-dimensional map.

Since $\epsilon^{0.39} >> \epsilon^{0.51}$ for small ϵ, the results (4.3) and (4.4) imply that for small ϵ most of the parameter values that are ϵ-uncertain with respect to chaos lie in windows, and, in fact, as we will demonstrate, *for a randomly chosen parameter value $\tilde{C}$ that is ϵ-uncertain with respect to chaos, the expectation value of the order of the lowest order window containing $\tilde{C}$ approaches ∞ as $\epsilon \to 0$.*

4.1 The order of a window.

This brings us to the question of where the C value that is ϵ-uncertain with respect to chaos lies. We say a periodic-window is of order 1 if it is not contained

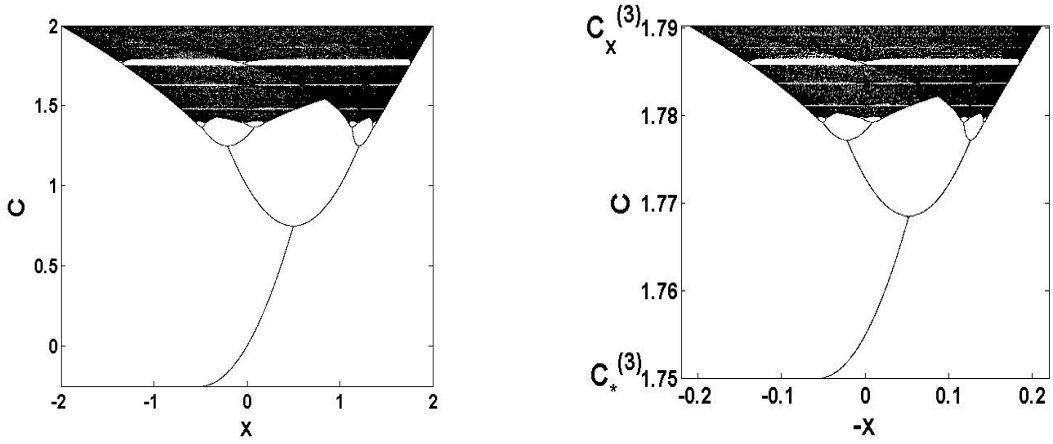

(a) (b)

Figure 4.3: (a) shows a bifurcation diagram for the quadratic map for $-0.25 \leq C \leq 2$. (b) shows a blow-up of the bifurcation diagram in the period-3 window in the region near $x = 0$.

in any other periodic window. We also call a window of order 1 a primary window. We say a window is of order $r > 1$, if it is contained within a window of order $(r-1)$, but it is not contained within a window of order $(r+1)$. Fig. 4.2 shows a case where $r = 2$, wherein the attracting periodic orbit lies in a period 5 window that lies in a period 3 window. Note that if a C value is not contained within a primary window, then it is not contained in any window (as is the case for a large chaotic attractor). Say C is ϵ-uncertain and $C + \epsilon$ results in periodic attracting behavior. Say $C + \epsilon$ lies in a window of highest order r. Then the value of r can be determined based on the sequence of points of the attracting periodic orbit at the given value of $C + \epsilon$. Let p_k denote the period of the k^{th} order window containing $C + \epsilon$, where $k \in 1, 2, \ldots, r$. The sequence of points of the attracting periodic orbit

at $C + \epsilon$ can be used to determine the periods p_k. This follows from the fact that the sequence in which attracting periodic orbits appear in a periodic window of any order as the parameter C varies, is the same for all windows. This sequence can be uniquely determined based on Kneading Theory [49]. The kneading sequence of the quadratic map monotonically decreases as the parameter C is increased [49], hence a given kneading sequence cannot occur twice as C varies.

For later reference, we define $N_r(\Delta)$ to be the number of windows of order r whose widths are greater than Δ and we write this quantity for $r = 1$ (primary windows) as

$$N_1(\Delta) = \sum_{i=1}^{\infty} U(\Delta_i - \Delta), \tag{4.5}$$

where $\Delta_1 \geq \Delta_2 \geq \Delta_3 \geq \ldots$ denote the widths of the primary windows, and U denotes the unit step function ($U(z) = 1$ for $z > 0$, $U(z) = 0$ for $z < 0$). If we consider all the windows of any order, then the number of these windows whose widths exceed Δ is

$$\bar{N}(\Delta) = \sum_{r=1}^{\infty} N_r(\Delta). \tag{4.6}$$

Preliminary to our analysis of the relationship between the exponents α^* and β, we need the following two results:

(i) *Self-similarity of windows:* Reference [52] shows that the bifurcation structure and dynamics in windows of various orders and periods are self-similar. That is, considering x near 0, by use of uniform linear stretchings (magnification) in x and C, the p-times iterated map with the parameter ranging through the interval corresponding to a period-p window, ${C_*}^{(p)} \leq C \leq {C_x}^{(p)}$, very closely

quantitatively replicates the behavior of the map in its full range, $-1/4 \leq C \leq 2$. Furthermore, this self-similarity approximation is already extremely good even for the period-3 primary window, and becomes better and better for most r-order windows as r is increased. This is illustrated in Fig. 4.3, where we see that the bifurcation diagram in the full range $-1/4 \leq C \leq 2$ in Fig. 4.3a is virtually identical to a properly magnified, inverted ($x \to -x$) version of the bifurcation diagram for the period-3 window, ${C_*}^{(3)} \leq C \leq {C_x}^{(3)}$, blown up in the region near $x = 0$ (Fig. 4.3b).

Assumption. We assume that all the periodic windows of all orders are exactly self-similar. Thus, we assume that for each window, the ratio of the length from the saddle-node bifurcation value to the Feigenbaum value of the window to the window-width is a constant. Denote this constant by ϕ. Thus,

$$\phi = \frac{C_{Feigenbaum} - C_{Saddlenode}}{C_{crisis} - C_{Saddlenode}} \tag{4.7}$$

where $C_{Feigenbaum}$, $C_{Saddlenode}$, C_{crisis} correspond to the Feigenbaum parameter value, the saddle-node bifurcation parameter value and the interior crisis parameter value of a window respectively.

(ii) *ϵ-uncertainty / window-width scaling equivalence:* It is shown in Appendix C that, for small window widths Δ, the scalings of $\bar{N}(\Delta)$ and $N_1(\Delta)$ are related to the small ϵ scalings of $\bar{F}(\epsilon)$ and $F_0(\epsilon)$:

$$\bar{F}(\epsilon) \sim \epsilon \bar{N}(\epsilon) \text{ and } F_0(\epsilon) \sim \epsilon N_1(\epsilon). \tag{4.8}$$

Thus, from Eqs. (4.3) and (4.4), Eq. (4.8) yields

$$\bar{N}(\Delta) \sim \frac{1}{\Delta^{1-\beta}} \text{ and } N_1(\Delta) \sim \frac{1}{\Delta^{1-\alpha^*}}. \tag{4.9}$$

Note that based on Eq. 4.9, α^* can be defined as

$$\alpha^* = \lim_{\Delta \to 0} \frac{\log N_1(\Delta)}{\log \Delta} + 1 = \lim_{\Delta \to 0} \frac{\log \sum_{i=1}^{\infty} U(\delta_i - \Delta)}{\log \Delta} + 1$$

where δ_i for $i = 1, 2, \ldots$ denote the C-widths of the primary windows.

4.2 Results.

The main propositions in the paper are as follows.

- ***Proposition 1***. The exponent β (as given by Eq. 4.2) is given by $\sum_{i=1}^{\infty} {\delta_i}^{\gamma} = 1$ where $\gamma = 1 - \beta$ and δ_i for $i = 1, 2, \ldots$ denote the C-widths of the primary windows. We use this equation to compute the value of β.

- ***Proposition 2***. For a randomly chosen ϵ-uncertain point a, let r denote the order of the highest order window containing a. Then, for each positive integer n,

$$\text{Prob}(r > n) \to 1 \text{ as } \epsilon \to 0$$

that is,

$$\lim_{\epsilon \to 0} \text{ Prob } (r > n) = 1$$

Thus, for small ϵ values, most uncertain points lie in an N^{th} order window (a window within a window within a window ... N times), where N is a large positive integer.

4.3 Proof of Proposition 1.

By using Eq. (4.9), we reduce our analysis of the ϵ-uncertainty exponents α^* and β to an analysis of the scaling of the distribution of window-widths. Now, using the self-similarity of windows, we can express $N_{r+1}(\Delta)$ in terms of $N_r(\Delta)$,

$$N_{r+1}(\Delta) = \int_{\Delta}^{9/4} (\frac{-dN_r(\Delta')}{d\Delta'})\ N_1(\frac{9\Delta/4}{\Delta'})\ d\Delta', \tag{4.10}$$

where $9/4 = 2 - (-1/4)$ is the width of the C-range for the quadratic map. In Eq. (4.10), we have used the window self-similarity result to write the number of $r+1$ order windows of width Δ that are contained in windows of width Δ' as $N_1(\frac{9\Delta/4}{\Delta'})$. Letting $u = \ln(9/(4\Delta))$ and $M_r(u) = N_r(\Delta)$, Eq. (4.10) becomes,

$$M_{r+1}(u) = \int_0^u M_1(u-u')\ \frac{dM_r(u')}{du'}\ du'. \tag{4.11}$$

Equation (4.11) is a convolution. It is therefore convenient to introduce the Laplace transform, $\hat{M}_r(s) = \int_0^\infty M_r(u)e^{-su}du$, in terms of which Eq. (4.6) becomes $\hat{M}_{r+1}(s) = s\hat{M}_1(s)\hat{M}_r(s)$ (where we have made use of $M_r(0) = N_r(9/4) = 0$). Iterating this result, we obtain $\hat{M}_r(s)$ in terms of $\hat{M}_1(s)$,

$$\hat{M}_r(s) = \frac{(s\hat{M}_1(s))^r}{s}. \tag{4.12}$$

Introducing the Laplace transform $\hat{\bar{M}}(s)$ of $\bar{M}(u) = \bar{N}(\Delta)$, we have from Eq. (4.6) that $\hat{\bar{M}}(s) = \sum_{r=1}^\infty \hat{M}_r(s)$, which using Eq. (4.12) gives, upon summing the resultant geometric series,

$$\hat{\bar{M}}(s) = \frac{\hat{M}_1(s)}{1 - s\hat{M}_1(s)}. \tag{4.13}$$

This expression is singular at values of s for which $s\hat{M}_1(s) = 1$. From Eq. (4.5), $M_1(u) = \sum_{i=1}^{\infty} U(u - u_i)$, where $u_i = \ln(9/(4\Delta_i))$. Thus, $\hat{M}_1(s) = s^{-1} \sum_{i=1}^{\infty} e^{-su_i} = \sum_{i=1}^{\infty} (4\Delta_i/9)^s$ and we have that singularities of $\hat{\bar{M}}(s)$ occur at s values satisfying $1 = \sum_{i=1}^{\infty} {\delta_i}^s$, where $\delta_i = (4\Delta_i/9)$ are the normalized widths of the primary windows.

Now consider the inverse Laplace transform [59] of $\hat{\bar{M}}(s)$ for large u (i.e., small Δ); we see that $\bar{M}(u) \sim e^{\gamma u}$ where γ is the solution for s of $1 = \sum_i {\delta_i}^s$ with the largest real part. It can be shown that this solution is real. Thus we obtain for $\bar{N}(\Delta)$ at small Δ, $\bar{N}(\Delta) \sim \Delta^{-\gamma}$, which when compared with the first part of our result Eq. (4.9) shows that $\gamma = 1 - \beta$. We conclude that we can obtain the exponent β as the real positive root of

$$\sum_{i=1}^{\infty} {\delta_i}^{\gamma} = 1, \ \gamma = 1 - \beta. \tag{4.14}$$

Note that based on our model of exact self-similarity of windows, if we compute the fraction of ϵ-uncertain values of C, we get the same exponent α^* as in Eq. 4.4 if we restrict the ϵ-uncertain C values to lie in a window of highest order k, for any positive integer k. It is only as k approaches ∞ that there is a sudden change in the exponent to β in Eq. 4.3.

4.3.1 Computing β.

We now use Eq. (4.14) to investigate the relationship of the exponents α^* and β to the widths of the primary windows. Writing Eq. (4.14) as $\sum_{i=1}^{I-1} {\delta_i}^{\gamma} + \sum_{i=I}^{\infty} {\delta_i}^{\gamma} = 1$, for sufficiently large I, we can approximate the second summation by

$$\sum_{i=I}^{\infty} {\delta_i}^{\gamma} \approx \int_0^{\delta_I} (-dN_1(\delta)/d\delta)\delta^{\gamma} d\delta. \tag{4.15}$$

Since $N_1(\delta) \sim \delta^{-(1-\alpha^*)}$, the integrand is proportional to $\delta^{\gamma+\alpha^*-2}$,and the integral diverges unless $\gamma+\alpha^* > 1$. Thus, the summation in (4.14) is infinity unless $\gamma > (1-\alpha^*)$, and, since each term in the sum decreases monotonically with increasing γ, we conclude that as γ increases past $(1-\alpha^*)$, the sum in (4.14) decreases monotonically.

For $\gamma = 1$, the sum is the normalized total length of all windows, which, by definition, is less than 1. We conclude that Eq. (4.14) has a single root for γ and that this root satisfies $\gamma < (1-\alpha^*)$. Thus, for $\gamma = 1-\beta$, we must have that $\alpha^* > \beta$, in agreement with the numerical results $\alpha^* \approx 0.51, \beta \approx 0.39$. Taking $N_1(\delta_I) = I(\delta_I/\delta)^{1-\alpha^*}$ and performing the integration in (4.15), we obtain

$$\sum_{i=1}^{I-1} {\delta_i}^{1-\beta} + \frac{1-\alpha^*}{\alpha^*-\beta} I {\delta_I}^{1-\beta} = 1. \tag{4.16}$$

For example, assuming availability of an estimate of α^*, one can use (4.16) to estimate β given numerical determinations of $(\delta_1, \delta_2, \ldots, \delta_I)$. (Note that the second term in (4.16) becomes smaller and smaller as I is increased and can be omitted for very large I.)

Figure 4.4 shows a plot of the estimated value of β obtained from (4.16) as a function of I for $\alpha^* = 0.51$. The result from Fig. 4.4 is $\beta = 0.39$ in good agreement with the estimate from Fig. 4.1.

4.4 Environment of a period-k point

We define the following to prove Proposition 2.

C-width of the window. For a given period-k window, the interior-crisis point corresponds to that value of parameter C for which the interval basin has

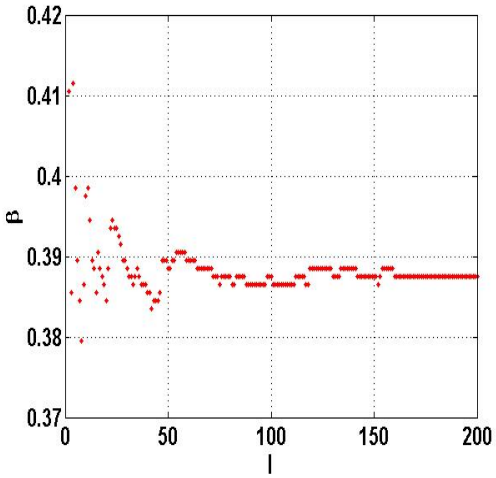

Figure 4.4: Estimated value of β vs I. As I is increased, the estimated value of β converges to ≈ 0.39.

an unstable period-k point on its boundary [45, 60]. We define the *C-width of the periodic window* as the parameter difference between the interior-crisis value of C for the window and the saddle-node bifurcation value of C.

Parameter value C_{odd}. Let $C_{odd} \approx 1.543689$ denote the parameter value before which there are no periodic windows of odd periods other than the period-1 window. To study the distribution of C-widths of the periodic windows, we consider the parameter range $C_{odd} \leq C \leq 2$.

Maximum period P. The periodic windows are dense in the interval $C_{odd} \leq C \leq 2$ [50] and for large period k, the number of windows of period k is given by $N_k \cong \frac{2^k-2}{2k}$. The value is exact when k is prime and the precise value is not hard to compute otherwise [61]. Thus, the number of period-k windows increases exponentially with the period. Hence, we consider a maximum period P, and try to characterize all the periodic windows of periods not exceeding P. In order to characterize all the windows of periods till P, we determine the sequence in which

these windows appear in the map, as the parameter C is increased. This method is based on kneading theory [49].

The C-width exponent. We define the C-width exponent as $\alpha = \lim_{\epsilon \to 0} \frac{\log N_1(\epsilon)}{\log \epsilon}$ where $N_1(\epsilon)$ is the net number of primary windows, the C-width of which exceeds ϵ. The C-width exponent characterizes the scaling of C-widths of primary windows. Our data looks at the primary windows of periods up to 25 for the quadratic map. There are 1402957 such windows. Fig.4.5 shows the distribution of window widths for $P = 13, 15, 17, 19, 23, 25$. As higher and higher values of P were considered, the graph behavior approximated the straight line $\log_{10}[N_1(\epsilon)] = (-0.51 \pm 0.03) \log_{10}[\epsilon] - 0.876$. In our computations based on these windows, it appears that if all the periods were to be considered, $N_1(\epsilon)$ satisfies the following for all small values of ϵ,

$$N_1(\epsilon) \approx K \epsilon^{-\alpha} \tag{4.17}$$

where, $K \approx 0.133$ and $\alpha = 0.51 \pm 0.03$. See Fig. 4.5 over the range of ϵ given by $\epsilon \in (10^{-8}, 10^{-5})$. Let us order the primary windows in the descending order with respect to their C-width, where δ_n denotes the C-width of the n^{th} largest primary window. Then, $N_1(\epsilon)^{\frac{-1}{\alpha}} \approx K^{\frac{-1}{\alpha}} \epsilon$ and hence, Eq. 4.17 implies,

$$\delta_n \approx \frac{K_0}{n^{\frac{1}{\alpha}}} \text{ where } K_0 = K^{\frac{1}{\alpha}} \text{ and } n = 1, 2, \ldots \tag{4.18}$$

Deriving the exponent α^* in [46] from α. The uncertainty exponent in [46] can be derived using our computations. To derive this, assume that a fixed fraction of each periodic window lies in the region before the Feigenbaum point. To derive this, assume that for each primary window, the fraction of the periodic

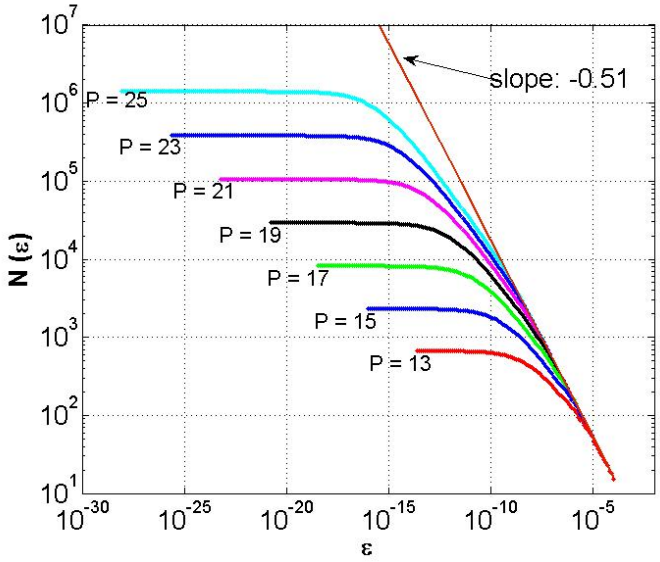

Figure 4.5: $N(\epsilon)$ **vs** ϵ**.** A curve is plotted for $P = 13, 15, 17, 19, 21, 23, 25$. The curve for each value of P includes all the periodic windows of periods not exceeding P lying in the parameter-range $C \in [C^{odd}, 2]$. In this log-log plot, as P increases, the curves appear to asymptote to the straight line shown in red, with the equation $\log_{10} N(\epsilon) = (-0.51 \pm 0.03) \log_{10} \epsilon - 0.876$. Thus, $N(\epsilon) = 0.133\epsilon^{-\alpha}$ where $\alpha = 0.51 \pm 0.03$.

window from the saddle-node bifurcation value (the starting point of the window) to the Feigenbaum point occupies a fixed fraction of the C-width of the window. Denote this fraction by ϕ. Assume that periodic windows with C-width exceeding $2\epsilon/\phi$ contribute 2ϵ to $V[S_c(\epsilon) - S_c]$ (only the edges of the windows are filled by ϵ-fattening, see Fig. 4.6). Periodic windows with C-width less than $2\epsilon/\phi$ are entirely filled by the ϵ-fattening and hence contribute, to $V[S_c(\epsilon) - S_c]$, an amount equal to the $\phi \times$ C-width of the window (see Fig. 4.6). Thus, $V[S_c(\epsilon) - S_c] \sim \int_{2\epsilon}^{0} x\, dN(x) + 2\epsilon N(2\epsilon)$ where $N(\epsilon)$ is the net number of windows, the C-width of which exceeds ϵ. Assuming $N(\epsilon) = 0.133\epsilon^{-\alpha}$ (see Fig. 4.5), $V[S_c(\epsilon) - S_c] = 0.133 \times 0.51 \times (2\epsilon)^{1-\alpha}/(1 - 0.51) + 2\epsilon \times 0.133 \times (2\epsilon)^{-\alpha}$ so that $\alpha^* = \lim_{\epsilon \to 0} \frac{\log V[S_c(\epsilon) - S_c]}{\log(\epsilon)} = 1 - \alpha = 0.49$. This is

in close approximation with the value $\alpha^* = 0.51 \pm 0.03$ computed in [46].

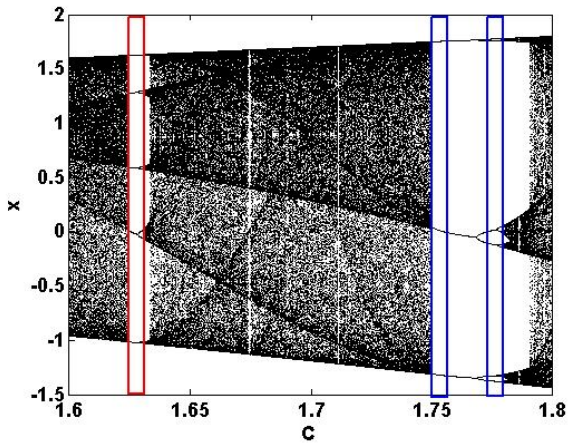

Figure 4.6: **The relation between the C-width of the window and its contribution to $V[S_c(\epsilon) - S_c]$.** The red rectangle indicates that smaller periodic windows (of C-width $< 2\epsilon/\phi$) are entirely filled up by the ϵ-fattening. The blue rectangles indicates that for large periodic windows (of C-width $> 2\epsilon/\phi$), only the edges are filled up by the ϵ-fattening.

4.5 Proof of Proposition 2.

Size-distribution of (k+1)-order windows in terms of k-order windows.

Based on self-similarity, $N_{k+1}(\epsilon)$ such that the (k+1)-order windows lie in $\Delta_{i_1 i_2 \ldots i_k}$ is given by $K(\frac{L\epsilon}{\delta})^{-\alpha}$ where $\frac{\epsilon L}{\delta} \geq M$.

In general, for the k^{th} order window to have a $(k+1)$-order window of C-width at least ϵ, the minimum C-width of the k^{th} order window can be approximated by $\frac{L\epsilon}{M}$. The C-widths of the primary windows range from 0 to M. Similarly, the C-widths of secondary windows range from 0 to $\frac{M^2}{L}$. In general, the C-widths of k^{th} order windows range from 0 to $\frac{M^k}{L^{k-1}}$. Let $dN_k(\delta)$ denote the number of k^{th} order windows

with C-widths lying in $[\delta, \delta + d\delta]$. Thus, $N_{k+1}(\epsilon)$ is given by,

$$N_{k+1}(\epsilon) \approx \int_{L\epsilon/M}^{M^k L^{(1-k)}} K(\frac{L\epsilon}{\delta})^{-\alpha}\, dN_k(\delta) \tag{4.19}$$

Note that $N_{k+1}(\epsilon)$ has to be an integer and the $\approx$ sign in the above expression denotes the nearest integer.

Lemma 1: For $k \geq 2$,

$$N_k(\epsilon) \approx A(k)\epsilon^{-\alpha} P_{k-1}(u_{k-1}(\epsilon)) \tag{4.20}$$

where $A(k) = K^k \alpha L^{-(k-1)\alpha}$, $u_{k-1}(\epsilon) = \log(\frac{M^k}{\epsilon L^{k-1}})$ and $P_{k-1}(u_{k-1}(\epsilon))$ is a $(k-1)$-order polynomial in $u_{k-1}(\epsilon)$ such that the constant term of the polynomial equals 0.

Proof of Lemma 1:

We use an inductive argument to show that Eq.4.20 holds.

For $k = 1$,

$$N_1(\delta) \approx K\delta^{-\alpha}, \text{ so, } dN_1(\delta) \approx -K\alpha\delta^{-\alpha-1}d\delta$$

Note that the negative sign follows from the fact that for each k, $N_k(\delta)$ is a decreasing function of δ. Hence, for the purpose of computation, we use $|dN_1(\delta)| \approx K\alpha\delta^{-\alpha-1}d\delta$. Now, for $k = 2$, based on Eq. 4.19,

$$N_2(\epsilon) \approx \int_{L\epsilon/M}^{M} K(\frac{L\epsilon}{\delta})^{-\alpha} K\alpha\delta^{-\alpha-1}\, d\delta \approx K^2\alpha L^{-\alpha}\epsilon^{-\alpha} \log(\frac{M^2}{\epsilon L}) \tag{4.21}$$

This is of the form $N_2(\epsilon) \approx A(2)\epsilon^{-\alpha} P_1(u_1(\epsilon))$. Thus, Eq. 4.20 holds when $k = 2$.

In general, let us assume that for some $k \geq 2$, Eq. 4.20 holds, that is,

$$N_k(\epsilon) \approx A(k)\epsilon^{-\alpha} P_{k-1}(u_{k-1}(\epsilon))$$

We will then prove that Eq. 4.20 holds when k is replaced by k+1.

Assuming Eq. 4.20 holds, say, $\{p_{m,k-1}\}_{m=1}^{m=k-1}$ are the (k-1) coefficients of the polynomial $P_{k-1}(u_{k-1}(\epsilon))$. Now,

$$dN_k(\epsilon) \approx A(k)\left[-\alpha\epsilon^{-\alpha-1}P_{k-1}(u_{k-1}(\epsilon))d\epsilon + \epsilon^{-\alpha}P'_{k-1}(u_{k-1}(\epsilon))(\frac{-1}{\epsilon})d\epsilon\right]$$

Thus,

$$|dN_k(\epsilon)| \approx A(k)\left[\alpha\epsilon^{-\alpha-1}P_{k-1}(u_{k-1}(\epsilon)) + \epsilon^{-\alpha-1}P'_{k-1}(u_{k-1}(\epsilon))\right]d\epsilon \tag{4.22}$$

Thus,

$$\begin{aligned} N_{k+1}(\epsilon) &\approx \int_{L\epsilon/M}^{M^kL^{(1-k)}} K(\frac{L\epsilon}{\delta})^{-\alpha}\, dN_k(\delta) \\ &\approx \int_{L\epsilon/M}^{M^kL^{(1-k)}} K(\frac{L\epsilon}{\delta})^{-\alpha}A(k)\left[\alpha P_{k-1}(u_{k-1}(\delta)) + P'_{k-1}(u_{k-1}(\delta))\right]\delta^{-\alpha-1}d\delta \\ &\approx K(L\epsilon)^{-\alpha}A(k)\int_{L\epsilon/M}^{M^kL^{(1-k)}} \left[\alpha P_{k-1}(u_{k-1}(\delta)) + P'_{k-1}(u_{k-1}(\delta))\right]\delta^{-1}d\delta \end{aligned}$$

Now, $u_{k-1}(\delta) = \log(\frac{M^k}{\delta L^{k-1}})$. Then, $du_{k-1}(\delta) = -\frac{d\delta}{\delta}$. Therefore,

$$N_{k+1}(\epsilon) \approx K(L\epsilon)^{-\alpha}A(k)\int_0^{M^{k+1}L^{-k}/\epsilon} \left[\alpha P_{k-1}(u_{k-1}(\delta)) + P'_{k-1}(u_{k-1}(\delta))\right]du_{k-1}(\delta)$$

Let $Q_k(u_{k-1}(\delta))$ denote $\int P_{k-1}(u_{k-1}(\delta))du_{k-1}(\delta)$. Then the coefficients $\{q_{m,k}\}_{m=1}^{m=k}$ of $Q_k(u)$ are given by

$$q_{m,k} = \frac{p_{m-1,k-1}}{m} \tag{4.23}$$

Then,

$$\begin{aligned} N_{k+1}(\epsilon) &\approx K(L\epsilon)^{-\alpha}A(k)\left[\alpha Q_k(u_k(\epsilon)) + P_{k-1}(u_k(\epsilon))\right] \\ &\approx K^{k+1}\alpha L^{-k\alpha}\epsilon^{-\alpha}\left[\alpha Q_k(u_k(\epsilon)) + P_{k-1}(u_k(\epsilon))\right] \\ &\approx A(k+1)\epsilon^{-\alpha}\left[\alpha Q_k(u_k(\epsilon)) + P_{k-1}(u_k(\epsilon))\right] \end{aligned}$$

This is of the form Eq. 4.20, with k replaced by (k+1), that is,

$$N_{k+1}(\epsilon) \approx A(k+1)\epsilon^{-\alpha}P_k(u_k(\epsilon))$$

where $P_k(u_k(\epsilon))$ is a k^{th} order polynomial in $u_k(\epsilon)$. The coefficients of $P_k(u_k(\epsilon))$ are given by $p_{m,k} = \alpha q_{m,k} + p_{m,k-1}$. Thus, from Eq. 4.23 and 4.21,

$$p_{m,k} = \alpha\frac{p_{m-1,k-1}}{m} + p_{m,k-1} \text{ where } m = 1, 2, \ldots, (k-1) \tag{4.24}$$

$$= \alpha\frac{p_{k-1,k-1}}{k} \text{ where } m = k \tag{4.25}$$

$$p_{1,1} = 1 \tag{4.26}$$

This proves Lemma 1.

Proposition 1/2. Given any $k \in \mathbb{N}$ and any $\delta > 0$, there exists an $\epsilon' > 0$ such that for all $\epsilon < \epsilon'$, the ratio $\frac{N_{k+1}(\epsilon)}{N_k(\epsilon)} > \frac{1}{\delta}$. In particular, the ratio $\frac{N_{k+1}(\epsilon)}{N_k(\epsilon)}$ scales as $(\frac{1}{k})\log(\frac{1}{\epsilon})$ for small values of ϵ.

Proof of Proposition 1/2.

For a given value of $k \in \mathbb{N}$, let r_k denote the ratio $\frac{N_{k+1}(\epsilon)}{N_k(\epsilon)}$. Then,

$$\begin{aligned} r_k &= \frac{N_{k+1}(\epsilon)}{N_k(\epsilon)} \\ &= \frac{A(k+1)\epsilon^{-\alpha}P_k(u_k(\epsilon))}{A(k)\epsilon^{-\alpha}P_{k-1}(u_{k-1}(\epsilon))} \\ &= \frac{KL^{-\alpha}P_k(u_k(\epsilon))}{P_{k-1}(u_{k-1}(\epsilon))} \end{aligned} \tag{4.27}$$

Now $P_k(u_k(\epsilon))$ is a polynomial of order k in $u_k(\epsilon)$. Note that $u_k(\epsilon) = \log(\frac{M^{k+1}}{\epsilon L^k})$. Thus, for a given value of k, $P_k(u_k(\epsilon))$ is a k^{th} order polynomial in $\log(\frac{1}{\epsilon})$. Thus, rewrite $P_k(u_k(\epsilon))$ as $P_k(\log(\frac{1}{\epsilon}))$. Similarly, rewrite the denominator as $P_{k-1}(\log(\frac{1}{\epsilon}))$.

The leading coefficient of $P_k(\log(\frac{1}{\epsilon}))$ is $p_{k,k}$ while that of $P_{k-1}(\log(\frac{1}{\epsilon}))$ is $p_{k-1,k-1}$. Thus, from Eq. 4.29,

$$\begin{aligned} r_k &= \frac{KL^{-\alpha}P_k(\log(\frac{1}{\epsilon}))}{P_{k-1}(\log(\frac{1}{\epsilon}))} \\ &= \frac{KL^{-\alpha}[(\frac{p_{k,k}}{p_{k-1,k-1}})W_1(\log(\frac{1}{\epsilon}))P_{k-1}(\log(\frac{1}{\epsilon})) + U_{k-2}(\log(\frac{1}{\epsilon}))]}{P_{k-1}(\log(\frac{1}{\epsilon}))} \end{aligned}$$

where $W_1(\log(\frac{1}{\epsilon}))$ is a polynomial of order 1 in $(\log(\frac{1}{\epsilon}))$ with leading coefficient equal to 1, and $U_{k-2}(\log(\frac{1}{\epsilon}))$ is a polynomial of order (k-2) in $\log(\frac{1}{\epsilon})$. Thus,

$$\begin{aligned} r_k &= KL^{-\alpha}\left[(\frac{p_{k,k}}{p_{k-1,k-1}})W_1(\log(\frac{1}{\epsilon})) + \frac{U_{k-2}(\log(\frac{1}{\epsilon}))}{P_{k-1}(\log(\frac{1}{\epsilon}))}\right] \\ &= KL^{-\alpha}\left[(\frac{\alpha}{k})W_1(\log(\frac{1}{\epsilon})) + \frac{U_{k-2}(\log(\frac{1}{\epsilon}))}{P_{k-1}(\log(\frac{1}{\epsilon}))}\right] \end{aligned} \tag{4.28}$$

For some $m > 0$, choose an $\epsilon_1 > 0$ such that $KL^{-\alpha}\frac{U_{k-2}(\log(\frac{1}{\epsilon_1}))}{P_{k-1}(\log(\frac{1}{\epsilon_1}))} > -m$. The required ϵ_1 exists since the degree of the denominator exceeds that of the numerator. Given a $\delta > 0$, choose an $\epsilon_2 > 0$ such that $KL^{-\alpha}(\frac{\alpha}{k})W_1(\log(\frac{1}{\epsilon_2})) > \frac{1}{\delta} + m$.

Let $\epsilon' = \min(\epsilon_1, \epsilon_2)$. Then, for all $\epsilon < \epsilon'$,

$$r_k = \frac{N_{k+1}(\epsilon)}{N_k(\epsilon)} > \frac{1}{\delta} \tag{4.29}$$

From Eq. 4.28, for small values of ϵ,

$$r_k \approx KL^{-\alpha}\left[(\frac{\alpha}{k})\log(\frac{1}{\epsilon})\right]$$

Thus, the ratio $\frac{N_{k+1}(\epsilon)}{N_k(\epsilon)}$ scales as $(\frac{1}{k})\log(\frac{1}{\epsilon})$. This proves the proposition.

Let $\beta \in (0,1)$. Define $N_k(\beta\epsilon, \epsilon)$ to be the number of k^{th} order windows with diameters lying between $\beta\epsilon$ and ϵ.

Proposition 2/3. Given a $k \in \mathbb{N}$ and any $\delta > 0$, there exists an $\epsilon' > 0$ such that $\lim_{\epsilon\to 0} \frac{N_{k+1}(\beta\epsilon,\epsilon)}{N_k(\beta\epsilon,\epsilon)} \to \infty$ for each $\epsilon < \epsilon'$, for each $\beta \in (0,1)$.

Proof of Proposition 2/3: To prove the proposition, it is sufficient to prove that given a $k \in \mathbb{N}$ and any $\delta > 0$, there exists an $\epsilon' > 0$ such that the ratio $\frac{N_{k+1}(\beta\epsilon,\epsilon)}{N_k(\beta\epsilon,\epsilon)} > \frac{1}{\delta}$ for each $\epsilon < \epsilon'$, for each $\beta \in (0,1)$.

Denote $r_{k,\epsilon,\beta} = \frac{N_{k+1}(\beta\epsilon,\epsilon)}{N_k(\beta\epsilon,\epsilon)}$.

Based on Eq. 4.20,

$$\begin{aligned} r_{k,\epsilon,\beta} &= \frac{A(k+1)[(\beta\epsilon)^{-\alpha}P_k(u_k(\beta\epsilon)) - \epsilon^{-\alpha}P_k(u_k(\epsilon))]}{A(k)[(\beta\epsilon)^{-\alpha}P_{k-1}(u_{k-1}(\beta\epsilon)) - \epsilon^{-\alpha}P_{k-1}(u_{k-1}(\epsilon))]} \\ &= KL^{-\alpha}\frac{\beta^{-\alpha}P_k(u_k(\beta\epsilon)) - P_k(u_k(\epsilon))}{\beta^{-\alpha}P_{k-1}(u_{k-1}(\beta\epsilon)) - P_{k-1}(u_{k-1}(\epsilon))} \\ &= KL^{-\alpha}\frac{\beta^{-\alpha}P_k(\log(\frac{M^{k+1}}{\beta\epsilon L^k})) - P_k(\log(\frac{M^{k+1}}{\epsilon L^k}))}{\beta^{-\alpha}P_{k-1}(\log(\frac{M^k}{\beta\epsilon L^{k-1}})) - P_{k-1}(\log(\frac{M^k}{\epsilon L^{k-1}}))} \end{aligned}$$

Denote $c = \frac{M^{k+1}}{L^k}, d = \frac{M^k}{L^{k-1}}$. Then,

$$\begin{aligned} r_{k,\epsilon,\beta} &= KL^{-\alpha}\frac{\beta^{-\alpha}P_k(\log(\frac{c}{\beta\epsilon})) - P_k(\log(\frac{c}{\epsilon}))}{\beta^{-\alpha}P_{k-1}(\log(\frac{d}{\beta\epsilon})) - P_{k-1}(\log(\frac{d}{\epsilon}))} \\ &= KL^{-\alpha}\frac{\sum_{m=1}^{m=k} p_{k,m}[\beta^{-\alpha}(\log(\frac{c}{\beta\epsilon}))^m - (\log(\frac{c}{\epsilon}))^m]}{\sum_{m=1}^{k-1} p_{k-1,m}[\beta^{-\alpha}(\log(\frac{d}{\beta\epsilon}))^m - (\log(\frac{d}{\epsilon}))^m]} \end{aligned} \tag{4.30}$$

where the coefficients are defined as per Eq. 4.24, 4.25, 4.26.

Consider the numerator of the fraction. Let t denote the term corresponding to $m = 1$. Thus,

$$\begin{aligned} t &= p_{k,1}[\beta^{-\alpha}(\log(\frac{c}{\beta\epsilon})) - (\log(\frac{c}{\epsilon}))] \\ &= p_{k,1}[(\log\frac{c}{\epsilon})(\beta^{-\alpha} - 1) + \beta^{-\alpha}(\log\frac{1}{\beta})] \end{aligned}$$

Now, choose an ϵ such that $\frac{c}{\epsilon} > 1$ so that $\log \frac{c}{\epsilon} > 0$. As per Eq. 4.25 and 4.26, $p_{k,1} > 0$. For $\alpha, \beta \in (0,1)$, $\beta^{-\alpha} > 1$, $\frac{1}{\beta} > 1$. Thus, $t > 0$. Also $KL^{-\alpha} > 0$. Hence,

$$\begin{aligned} r_{k,\epsilon,\beta} &> KL^{-\alpha} \frac{\sum_{m=2}^{m=k} p_{k,m}[\beta^{-\alpha}(\log(\frac{c}{\beta\epsilon}))^m - (\log(\frac{c}{\epsilon}))^m]}{\sum_{m=1}^{k-1} p_{k-1,m}[\beta^{-\alpha}(\log(\frac{d}{\beta\epsilon}))^m - (\log(\frac{d}{\epsilon}))^m]} \\ &= KL^{-\alpha} \frac{\sum_{m=1}^{k-1} p_{k,m+1}[\beta^{-\alpha}(\log(\frac{c}{\beta\epsilon}))^{m+1} - (\log(\frac{c}{\epsilon}))^{m+1}]}{\sum_{m=1}^{k-1} p_{k-1,m}[\beta^{-\alpha}(\log(\frac{d}{\beta\epsilon}))^m - (\log(\frac{d}{\epsilon}))^m]} \end{aligned}$$

Let $d = c\phi$ where $\phi = L/M$. Thus $\phi > 1$. Then,

$$\begin{aligned} r_{k,\epsilon,\beta} &> KL^{-\alpha} \frac{\sum_{m=1}^{k-1} p_{k,m+1}[\beta^{-\alpha}(\log\frac{c}{\epsilon} + \log\frac{1}{\beta})^{m+1} - (\log(\frac{c}{\epsilon}))^{m+1}]}{\sum_{m=1}^{k-1} p_{k-1,m}[\beta^{-\alpha}(\log\frac{c\phi}{\epsilon} + \log\frac{1}{\beta})^m - (\log(\frac{c\phi}{\epsilon}))^m]} \\ &= KL^{-\alpha} \frac{\sum_{m=1}^{k-1} p_{k,m+1}(\log\frac{c}{\epsilon})^{m+1}[\beta^{-\alpha}(1 + \frac{\log\frac{1}{\beta}}{\log\frac{c}{\epsilon}})^{m+1} - 1]}{\sum_{m=1}^{k-1} p_{k-1,m}(\log\frac{c\phi}{\epsilon})^m[\beta^{-\alpha}(1 + \frac{\log\frac{1}{\beta}}{\log\frac{c\phi}{\epsilon}})^m - 1]} \end{aligned}$$

It follows from Eq. 4.24, 4.25, 4.26 and the choice of ϵ that for each $m = 1, 2, \ldots, k-1$,

$$\frac{p_{k,m+1}(\log\frac{c}{\epsilon})^{m+1}[\beta^{-\alpha}(1 + \frac{\log\frac{1}{\beta}}{\log\frac{c}{\epsilon}})^{m+1} - 1]}{p_{k-1,m}(\log\frac{c\phi}{\epsilon})^m[\beta^{-\alpha}(1 + \frac{\log\frac{1}{\beta}}{\log\frac{c\phi}{\epsilon}})^m - 1]} > 0$$

Note that if I is a positive integer, and $a_1, a_2, \ldots, a_I > 0, b_1, b_2, \ldots, b_I > 0$, then

$$\frac{\sum_{i=1}^{I} a_i}{\sum_{i=1}^{I} b_i} > \min\{\frac{a_j}{b_j}\}_{j=1}^{I} \tag{4.31}$$

Thus,

$$r_{k,\epsilon,\beta} > KL^{-\alpha} \min \left\{ \frac{p_{k,m+1}(\log\frac{c}{\epsilon})^{m+1}[\beta^{-\alpha}(1 + \frac{\log\frac{1}{\beta}}{\log\frac{c}{\epsilon}})^{m+1} - 1]}{p_{k-1,m}(\log\frac{c\phi}{\epsilon})^m[\beta^{-\alpha}(1 + \frac{\log\frac{1}{\beta}}{\log\frac{c\phi}{\epsilon}})^m - 1]} \right\}_{m=1}^{k-1}$$

Let $M_1 = KL^{-\alpha} \min \left\{ \frac{p_{k,m+1}(\log\frac{c}{\epsilon})^{m+1}}{p_{k-1,m}(\log\frac{c\phi}{\epsilon})^m} \right\}_{m=1}^{k-1}$, $M_2 = \min \left\{ \frac{\beta^{-\alpha}(1+\frac{\log\frac{1}{\beta}}{\log\frac{c}{\epsilon}})^{m+1}-1}{\beta^{-\alpha}(1+\frac{\log\frac{1}{\beta}}{\log\frac{c\phi}{\epsilon}})^m-1} \right\}_{m=1}^{k-1}$ so that

$$r_{k,\epsilon,\beta} > M_1 M_2 \tag{4.32}$$

Now,

$$
\begin{aligned}
M_2 &= \min\left\{\frac{\beta^{-\alpha}(1+\frac{\log\frac{1}{\beta}}{\log\frac{c}{\epsilon}})^{m+1}-1}{\beta^{-\alpha}(1+\frac{\log\frac{1}{\beta}}{\log\frac{c\phi}{\epsilon}})^{m}-1}\right\}_{m=1}^{k-1} \\
&= \min\left\{\frac{\left(\sum_{g=0}^{m+1} C_g^{m+1}\beta^{-\alpha}(\frac{\log\frac{1}{\beta}}{\log\frac{c}{\epsilon}})^g\right)-1}{\left(\sum_{g=0}^{m} C_g^{m}\beta^{-\alpha}(\frac{\log\frac{1}{\beta}}{\log\frac{c\phi}{\epsilon}})^g\right)-1}\right\}_{m=1}^{k-1} \\
&= \min\left\{\frac{\left(\sum_{g=1}^{m+1} C_g^{m+1}\beta^{-\alpha}(\frac{\log\frac{1}{\beta}}{\log\frac{c}{\epsilon}})^g\right)+[\beta^{-\alpha}-1]}{\left(\sum_{g=1}^{m} C_g^{m}\beta^{-\alpha}(\frac{\log\frac{1}{\beta}}{\log\frac{c\phi}{\epsilon}})^g\right)+[\beta^{-\alpha}-1]}\right\}_{m=1}^{k-1}
\end{aligned}
$$

Considering the term corresponding to $g = m+1$ in the numerator of the above fraction, $C_{m+1}^{m+1}\beta^{-\alpha}(\frac{\log\frac{1}{\beta}}{\log\frac{c}{\epsilon}})^{m+1} > 0$ and hence,

$$
M_2 > \min\left\{\frac{\left(\sum_{g=1}^{m} C_g^{m+1}\beta^{-\alpha}(\frac{\log\frac{1}{\beta}}{\log\frac{c}{\epsilon}})^g\right)+[\beta^{-\alpha}-1]}{\left(\sum_{g=1}^{m} C_g^{m}\beta^{-\alpha}(\frac{\log\frac{1}{\beta}}{\log\frac{c\phi}{\epsilon}})^g\right)+[\beta^{-\alpha}-1]}\right\}_{m=1}^{k-1}
$$

Based on Eq. 4.31 and since $\phi > 1$,

$$
\begin{aligned}
M_2 &> \min\left\{\min\left\{\frac{C_g^{m+1}\beta^{-\alpha}(\frac{\log\frac{1}{\beta}}{\log\frac{c}{\epsilon}})^g}{C_g^{m}\beta^{-\alpha}(\frac{\log\frac{1}{\beta}}{\log\frac{c\phi}{\epsilon}})^g}\right\}_{g=1}^{m}, \frac{\beta^{-\alpha}-1}{\beta^{-\alpha}-1}\right\}_{m=1}^{k-1} \\
&= \min\left\{\min\left\{\frac{(m+1)}{(m+1-g)}(\frac{\log\frac{c\phi}{\epsilon}}{\log\frac{c}{\epsilon}})^g\right\}_{g=1}^{m}, 1\right\}_{m=1}^{k-1}
\end{aligned}
$$

It follows that

$$
M_2 > 1 \tag{4.33}
$$

Now,

$$\begin{aligned} M_1 &= KL^{-\alpha} \min \left\{ \frac{p_{k,m+1}(\log \frac{c}{\epsilon})^{m+1}}{p_{k-1,m}(\log \frac{c\phi}{\epsilon})^m} \right\}_{m=1}^{k-1} \\ &> KL^{-\alpha} \min \left\{ \frac{p_{k,m+1}}{p_{k-1,m}} \right\}_{m=1}^{k-1} \min \left\{ \frac{(\log \frac{c}{\epsilon})^{m+1}}{(\log \frac{c\phi}{\epsilon})^m} \right\}_{m=1}^{k-1} \\ &> KL^{-\alpha} \min \left\{ \frac{p_{k,m+1}}{p_{k-1,m}} \right\}_{m=1}^{k-1} (\log \frac{c}{\epsilon}) \min \left\{ (\frac{\log \frac{c}{\epsilon}}{\log \phi + \log \frac{c}{\epsilon}})^m \right\}_{m=1}^{k-1} \\ &= KL^{-\alpha} \min \left\{ \frac{p_{k,m+1}}{p_{k-1,m}} \right\}_{m=1}^{k-1} (\log \frac{c}{\epsilon}) (\frac{\log \frac{c}{\epsilon}}{\log \phi + \log \frac{c}{\epsilon}})^{k-1} \end{aligned}$$

For some $w \in (0,1)$, choose an $\epsilon*$ such that $(\frac{\log \frac{c}{\epsilon*}}{\log \phi + \log \frac{c}{\epsilon*}})^{k-1} > w$. Further, choose an $\epsilon' < \epsilon*$ such that $(\log \frac{c}{\epsilon'}) > (KL^{-\alpha} \min \left\{ \frac{p_{k,m+1}}{p_{k-1,m}} \right\}_{m=1}^{k-1} w)^{-1} \frac{1}{\delta}$ so that

$$M_1 > \frac{1}{\delta} \tag{4.34}$$

Then, by Eq. 4.32, 4.33 and 4.34, for each $\epsilon < \epsilon'$, for each $\beta \in (0,1)$,

$$r_{k,\epsilon,\beta} = \frac{N_{k+1}(\beta\epsilon, \epsilon)}{N_k(\beta\epsilon, \epsilon)} > \frac{1}{\delta} \tag{4.35}$$

This proves the proposition.

Proposition 2. For a randomly chosen ϵ-uncertain point a, let r denote the order of the highest order window containing a. Then, for each positive integer n,

$$\text{Prob}(r > n) \to 1 \text{ as } \epsilon \to 0$$

This proposition can also be restated as follows.

Proposition 2' (restatement of Proposition 2). Assume we randomly choose an ϵ-uncertain point a. Assume the highest order window containing the ϵ-uncertain point has order r. Then, for each positive integer n, $\lim_{\epsilon \to 0} \text{Prob}(r > n) = 1$.

Proof of Proposition 2. Note that

$$\sum_{n=1}^{\infty} \text{Prob}(r = n) = 1 \tag{4.36}$$

Assume that the proposition does not hold. Then, there exists some value of n such that $\text{Prob}(r = n) > 0$ as $\epsilon \to 0$. Say, this occurs at $n = n_0$. To reach a contradiction, it is enough to show that for each $\delta > 0$, there exists an $\epsilon' > 0$ such that

$$\frac{\text{Prob}(r = n_0 + 1)}{\text{Prob}(r = n_0)} > \frac{1}{\delta} \text{ for } \epsilon < \epsilon'$$

that is, the ratio $\frac{\text{Prob}_{(r=n_0+1)}}{\text{Prob}_{(r=n_0)}}$ becomes arbitrarily large as ϵ approaches 0.

Given a value of ϵ and an order k of the window, we want to approximate the probability of a randomly chosen point being ϵ-uncertain. The k^{th} order windows can be divided into those with C-width exceeding $2\epsilon/\phi$ and those with C-width less than $2\epsilon/\phi$, where ϕ is defined in Eq. 4.7. The windows with C-width exceeding $2\epsilon/\phi$ contribute 2ϵ to $V[S_c(\epsilon) - S_c]$, while those with C-width less than $2\epsilon/\phi$ contribute, to $V[S_c(\epsilon) - S_c]$, an amount equal to the $\phi \times$ C-width of the window (see Fig. 4.6). Now $\text{Prob}(r = k)$ is proportional to the contribution to $V[S_c(\epsilon) - S_c]$ corresponding to the k^{th} order windows. Let $C_{1,k,\epsilon}$ denote the contribution to $V[S_c(\epsilon) - S_c]$ from the k^{th} order windows with C-width exceeding $2\epsilon/\phi$. Then, $C_{1,k,\epsilon} = 2\epsilon N_k(\epsilon)$. Let $P_\epsilon = [0, \epsilon_1, \epsilon_2, \ldots, \epsilon]$ be a partition of the interval $[0, \epsilon]$. Let $\beta_{k+1} = \frac{\epsilon_k}{\epsilon_{k+1}}$ for $k = 1, 2, \ldots$. Thus, $\beta_{k+1} \in (0, 1)$. Let $C_{2,k,\epsilon}$ denote the contribution to $V[S_c(\epsilon) - S_c]$ from the k^{th} order windows with C-width less than $2\epsilon/\phi$. Then, $C_{2,k,\epsilon} = \sum_{i=2}^{\infty} \phi\epsilon_i N_k(\beta_i\epsilon_i, \epsilon_i)$. Thus,

$$\frac{\text{Prob}(n=k+1)}{\text{Prob}(n=k)} = \frac{\epsilon N_{k+1}(\epsilon) + \sum_{i=2}^{\infty} \epsilon_i N_{k+1}(\beta_i \epsilon_i, \epsilon_i)}{\epsilon N_k(\epsilon) + \sum_{i=2}^{\infty} \epsilon_i N_k(\beta_i \epsilon_i, \epsilon_i)}$$

Based on Eq. 4.31,

$$\frac{\text{Prob}(n=k+1)}{\text{Prob}(n=k)} > \min\left\{ \frac{N_{k+1}(\epsilon)}{N_k(\epsilon)}, \min\left\{ \frac{N_{k+1}(\beta_i \epsilon_i, \epsilon_i)}{N_k(\beta_i \epsilon_i, \epsilon_i)} \right\}_{i=2}^{\infty} \right\}$$

Based on Eq. 4.29, given any $\delta > 0$, it is possible to choose an ϵ_1 such that, for all $\epsilon < \epsilon_1$, the ratio $\frac{N_{k+1}(\epsilon)}{N_k(\epsilon)} > \frac{1}{\delta}$.

Based on Eq. 4.35, it is possible to choose an ϵ_2 such that the ratio $\frac{N_{k+1}(\beta\epsilon,\epsilon)}{N_k(\beta\epsilon,\epsilon)} > \frac{1}{\delta}$ for each $\epsilon < \epsilon_2$, for each $\beta \in (0,1)$.

Choose $\epsilon' = \min(\epsilon_1, \epsilon_2)$. Then, for each $\epsilon < \epsilon'$, for each $\beta \in (0,1)$,

$$\frac{\text{Prob}(n=k+1)}{\text{Prob}(n=k)} > \frac{1}{\delta}$$

where δ can be chosen arbitrarily. Based on Eq. 4.36, our assumption that for some $n_0 \in \mathbb{N}$, $\text{Prob}(r = n_0) > 0$ as $\epsilon \to 0$ is incorrect. Thus, for each positive integer n, $\text{Prob}(r > n) \to 1$ as $\epsilon \to 0$. This proves the proposition.

In conclusion, most points which are ϵ-uncertain with respect to chaos are nested in higher order periodic windows, and this order approaches infinity as ϵ approaches zero. We have derived an analytic estimate Eq. (4.14) for β which yields good agreement with the numerical result in Eq. (4.3) and shows why $\alpha^* > \beta$. More generally, letting Q_0 and $\bar{Q}$ respectively denote the set of C values yielding large chaotic attractors and the set of C values yielding chaotic attractors of any size, one can view our work as using the self-similarity of windows to establish a quantitative link between the structure of these two sets. In particular, Eq. (4.14)

relates the primary window widths $\{\delta_1, \delta_2, \delta_3, \ldots\}$ (a characterization of Q_0) to the exponent β (a characterization of $\bar{Q}$.) Although our considerations have focused on the quadratic map, we believe that the numerical results for the exponents α^* and β are universal for one-dimensional maps with a single quadratic maximum, and thus apply for situations as in [54], [56] where there is a strong phase-space contraction.

Chapter 5: A map with increasing topological entropy

5.1 Introduction.

As a parameter μ is increased, many dynamical systems reach a level of maximum topological entropy followed by a decrease to zero entropy. Consider the forced damped pendulum, and the forced Duffing equation, where T is the period and μ is the strength of the forcing. The time T map for both the differential equations has that property; there is no chaos for large $|\mu|$. For the quadratic map and the Henon map, the entropy reaches a maximum, namely ln 2, and is thereafter, a constant. In this chapter we give an example such that the number of cascades continues to increase for arbitrarily large values of the parameter. Specifically, we investigate the map $S_\mu : [0,1] \to [0,1)$ defined by

$$S_\mu(x) := \mu \sin(2\pi x) \bmod 1. \tag{5.1}$$

(The map is depicted in Figures 5.1 and 5.2 for $\mu = 1$ and $\mu = 3$ respectively.) For this map, the entropy increases without bound as $\mu \to \infty$. In fact, the number of cascades in the system and consequently the chaos in the system increases as μ increases, and the system has an ever-increasing number of solitary cascades for $\mu \in [0, m]$ as m is increased to higher and higher integer values. Specifically, we

calculate the number of period-k cascades of the map, for $k > 1$, for positive integer values of $\mu \in [0, m]$, where $m \in \mathbb{N}$. We show that for positive integer values of μ, S_μ is conjugate to a map T_μ for which $\inf |T'_\mu| > 1$. Thus $S_\mu(x)$ is unstable for $\mu > 0$ an integer. This allows us to conclude that for each positive integer μ, the map S_μ is chaotic, and every periodic orbit is unstable.

The number of cascades of the S_μ map for $\mu \in [0, m]$ where $m \in \mathbb{N}$ equals the number of unstable regular orbits of the S_μ map at $\mu = m$ [61]. We define a map T_μ, which is conjugate to the map S_μ. Proposition 1 proves that for every positive integer value of μ, every periodic orbit of the map T_μ is unstable. Lemmas 1, 2 and 3 count the number of regular orbits of the map S_μ for a given positive integer μ. Lemma 1 gives the number of periodic orbits of a given period p, for positive integral values of μ. Lemma 2 considers the points of period either equal to p, or to any other positive divisor of p, and gives the number of such points corresponding to regular and flip orbits of the map. Lemma 3 gives a method of calculating the number of regular and flip orbits of period p.

5.2 The map S_μ.

The map S_μ is given in Eq. 5.1. For each positive integer μ, i.e., $\mu \in \mathbb{N}$, the map is rotationally symmetric with respect to point $(\frac{1}{2}, \frac{1}{2})$. The interval $[0, 1)$ is divided into 4μ parts, each of which maps onto $[0, 1)$. Let us name these parts as $S_1, S_2, \ldots, S_{4\mu}$. To construct a period p orbit, one can choose the p points from any of the 4μ regions, since each of these regions maps onto $[0, 1)$. However, note that

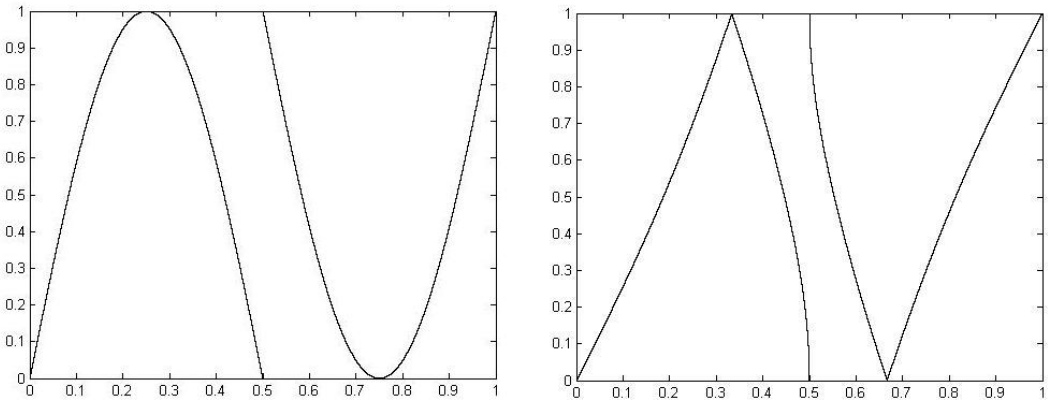

Figure 5.1: $S_\mu(x)$ and $T_\mu(y)$ for $\mu = 1$

the resulting orbit could also have period k, for some positive integer k that divides p. Let us denote the set of such k, which divide p but do not equal p as D_p. Hence, the number of points of period p (or of period k where $k \in D_p$) is given by $(4\mu)^p - 1$. Thus,

$$(4\mu)^p - 1 = P_p + \sum_{k \in D_p} kP_k$$

where P_k is the number of points of period k. The -1 is to account for the fact that $(0, 0)$ and $(1, 1)$, which are both fixed points of the map, correspond to the same point.

The map $C : [-1, 1] \to [0, 1]$ given by

$$C(y) = \frac{1 - \cos(\pi y)}{2}$$

has been used to establish a conjugacy between the logistic map and the tent map [45].

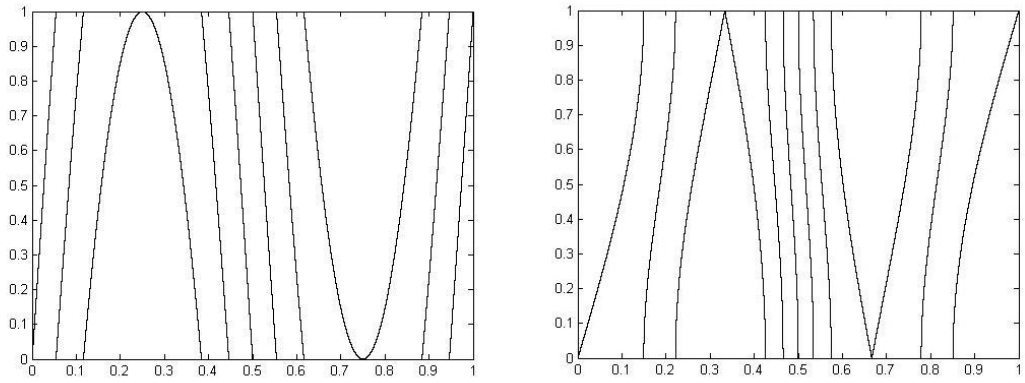

Figure 5.2: $S_\mu(x)$ and $T_\mu(y)$ for $\mu = 3$

5.3 The conjugate map.

We define the map $T_\mu := C^{-1}(S_\mu(C))$ where

$$C^{-1}(x) = \frac{\cos^{-1}(1-2x)}{\pi}.$$

Proposition 1. For $\mu \in \mathbb{N}$, the conjugate map T_μ satisfies $\inf |T'_\mu| > 1$.[1]

Proof of Proposition 1.

$$\begin{aligned} T_\mu(y) &= C^{-1}(S_\mu(C(y))) \\ &= \frac{\cos^{-1}(1-2[\mu \sin(\pi \cos(\pi y)) \bmod 1])}{\pi} \end{aligned} \tag{5.2}$$

Hence,

$$\begin{aligned} \frac{dT_\mu(y)}{dy} &= \frac{2(\mu \sin(\pi \cos(\pi y)) \bmod 1)'}{\pi\sqrt{(1-(1-2[\mu \sin(\pi \cos(\pi y)) \bmod 1])^2}} \text{ where } ' \text{ denotes derivative} \\ &= \frac{(\mu \sin(\pi \cos(\pi y)) \bmod 1)'}{\pi\sqrt{(\mu \sin(\pi \cos(\pi y)) \bmod 1) - (\mu \sin(\pi \cos(\pi y)) \bmod 1)^2}} \\ &= \frac{(\mu \sin(\pi \cos(\pi y)))'}{\pi\sqrt{(\mu \sin(\pi \cos(\pi y)) \bmod 1) - (\mu \sin(\pi \cos(\pi y)) \bmod 1)^2}} \end{aligned} \tag{5.3}$$

[1]Note that $|\frac{dT_\mu(0)}{dy}| = \sqrt{2\pi\mu}$ which appears to be $\inf_{y\in(0,\frac{1}{2})} |\frac{dT_\mu(y)}{dy}|$

Therefore,

$$\left|\frac{dT_\mu(y)}{dy}\right|^2 = \frac{[(\mu \sin[\pi \cos(\pi y)])']^2}{\pi^2[(\mu \sin(\pi \cos(\pi y)) \bmod 1) - (\mu \sin(\pi \cos(\pi y)) \bmod 1)^2]}$$

since the 'mod1' does not affect the derivative of the function at a point, so long as the derivative is defined at that point.

The derivative $dT_\mu(y)/dy$ is defined everywhere on $[0,1]$ except for a finite number of points. In this section, our notation will ignore the fact that we are taking infima of functions which are not defined at a finite number of points.

Define $L_\mu = \inf_{y\in(0,\frac{1}{2})} |dT_\mu(y)/dy|$. Considering $y \in [0,1]$, ${T_\mu}'(y) = {T_\mu}'(1-y)$. Hence, ${T_\mu}'(y)$ is symmetric with respect to line $y = \frac{1}{2}$. Hence, it is enough to prove that $L_\mu > 1$ which is equivalent to showing ${L_\mu}^2 > 1$. For convenience, write, $\theta(y) = \theta = \pi \cos(\pi y)$ for $y \in (0, \frac{1}{2})$ which gives $\theta \in (0, \pi)$. Rewrite $[\mu \sin(\pi \cos(\pi y)) \bmod 1] = [\mu \sin\theta \bmod 1]$ as $(\mu \sin\theta - k)$ where k is an integer such that $0 \leq (\mu \sin\theta - k) < 1$, i.e., k is the integer part of $\mu \sin\theta$. Depending on $\theta \in (0, \pi)$, k ranges from 0 to $\mu - 1$.

Thus, we prove,

$${L_\mu}^2 = \inf_{\theta\in(0,\pi)} \frac{\mu^2(\pi^2 - \theta^2)\cos^2\theta}{(\mu \sin\theta - k) - (\mu \sin\theta - k)^2} > 1. \tag{5.4}$$

Case 1: $\mu = 1$

For $\mu = 1$, $k = 0$.

$$
\begin{aligned}
{L_1}^2 &= \inf_{\theta\in(0,\pi)} \frac{(\pi^2-\theta^2)\cos^2\theta}{\sin\theta-\sin^2\theta} \\
&= \inf_{\theta\in(0,\pi)} \frac{(1+\sin\theta)(1-\sin\theta)(\pi^2-\theta^2)}{\sin\theta(1-\sin\theta)} \\
&= \inf_{\theta\in(0,\pi)} \left(1+\frac{1}{\sin\theta}\right)(\pi^2-\theta^2). \qquad (5.5)
\end{aligned}
$$

However,

$$
\inf_{\theta\in(0,\pi)} \left(1+\frac{1}{\sin\theta}\right)(\pi^2-\theta^2) > \inf_{\theta\in(0,\pi)} \left(\frac{1}{\sin\theta}\right)(\pi-\theta).
$$

Hence, it is enough to show that

$$
\left(\frac{1}{\sin\theta}\right)(\pi-\theta) \geq 1 \text{ for } \theta\in(0,\pi),
$$

which is equivalent to showing

$$
g(\theta) = \pi-\theta-\sin\theta \geq 0 \text{ for } \theta\in(0,\pi). \qquad (5.6)
$$

Now, $g'(\theta) = -1-\cos\theta < 0$ for $\theta\in(0,\pi)$. Hence, $g(\theta)$ is a decreasing function for $\theta\in(0,\pi)$, so g attains a minimum as $\theta\to\pi^-$ and $\lim_{\theta\to\pi^-} g(\theta) = 0$. Therefore, (5.6) holds, and hence

$$
{L_1}^2 = \inf_{\theta\in(0,\pi)} \frac{(\pi^2-\theta^2)\cos^2\theta}{\sin\theta-\sin^2\theta} > 1. \qquad (5.7)
$$

This finishes the case $\mu = 1$.

Figure 5.1 shows the graph of $S_\mu(x)$ and the corresponding graph of $T_\mu(y)$ for $\mu = 1$.

Case 2: $\mu > 1$

Assume $\mu\in\mathbb{N}$, $\mu > 1$. In this case, we show

$$
{L_\mu}^2 = \inf_{\theta\in(0,\pi)} \frac{\mu^2(\pi^2-\theta^2)\cos^2\theta}{(\mu\sin\theta-k)-(\mu\sin\theta-k)^2} > 1.
$$

From (5.7), it is enough to show that for $\theta \in (0, \pi)$,

$$\begin{aligned} \frac{\mu^2(\pi^2-\theta^2)\cos^2\theta}{(\mu\sin\theta-k)-(\mu\sin\theta-k)^2} &\geq \frac{(\pi^2-\theta^2)\cos^2\theta}{\sin\theta-\sin^2\theta} \qquad (5.8)\\ \iff \frac{\mu^2}{(\mu\sin\theta-k)-(\mu\sin\theta-k)^2} &\geq \frac{1}{\sin\theta-\sin^2\theta} \\ \iff \mu^2(\sin\theta-\sin^2\theta) &\geq (\mu\sin\theta-k)-(\mu\sin\theta-k)^2 \\ \iff \mu^2\sin\theta &\geq \mu\sin\theta-k-k^2+2\mu k\sin\theta \\ \iff (\mu^2-\mu-2\mu k)\sin\theta &\geq -k-k^2. \qquad (5.9) \end{aligned}$$

Note that k is an integer and a function of θ, that is, $k = k(\theta)$ such that $0 \leq \mu\sin\theta - k < 1$. Since $\sin\theta$ is a continuous function, $k(\theta)$ is piecewise continuous with jump discontinuities. Also,

$$(\mu^2-\mu-2\mu k)\sin\theta \geq (\mu^2-\mu-2\mu k).$$

Hence, from (5.9), it is enough to show $(\mu^2-\mu-2\mu k) \geq -k-k^2$. This is equivalent to showing

$$(\mu-k)^2 \geq (\mu-k).$$

This is always true since $(\mu-k)$ is an integer. This proves (5.8). Hence,

$$\inf_{y\in(0,\frac{1}{2})} |T'_\mu(y)| > 1$$

for $\mu > 1$, when μ is an integer.

Figure 5.2 shows the graphs of $S_\mu(x)$ and the corresponding graphs of $T_\mu(y)$ for $\mu = 3$.

Proposition 1 shows that every periodic orbit of the map $T_\mu(y)$ is unstable, and since $T_\mu(y)$ and $S_\mu(x)$ are conjugates, every periodic orbit of the map $S_\mu(x) = \mu \sin(2\pi x) \bmod 1$ is unstable, for positive integer values of μ.

5.4 Counting cascades for S_μ.

The number of cascades of the S_μ map for $\mu \in [0, m]$ where $m \in \mathbb{N}$ equals the number of unstable regular orbits of the S_μ map at $\mu = m$ [61]. In this section, we compute the number of regular orbits and use the fact that every periodic orbit of $S_\mu(x)$ is unstable, to count the number of cascades of the map for $\mu \in [0, m]$.

Lemma 1: The number of orbits of period p of the map $f(x_n) = \mu \sin(2\pi x_n) \bmod 1$ is given by $\frac{\Psi(p)}{p}$, where, $\Psi(m) = \Omega(m) - \sum_{j \in D_m} \Psi(j)$ and $\Omega(m) = (4\mu)^m - 1$, where m is a positive integer.

Proof of Lemma 1. We want to find the number of orbits of period p. Let $(4\mu)^p - 1$ be denoted as $\Omega(p)$. Define a recursive function $\Psi(p)$ as follows,

$$\Psi(p) = \Omega(p) - \sum_{k \in D_p} \Psi(k).$$

This recursive formula subtracts from the number of points of period p or k, where $k \in D_p$, the sum of the number of points of period exactly equal to k. Also, note that $\Psi(1) = 4 - 1 = 3$. Thus, we can conclude that $\Psi(p)$ denotes the number of points of period exactly equal to p. Thus, the number of period-p orbits would be $\frac{\Psi(p)}{p}$.

Now, note that amongst the 4μ parts $S_1, S_2, \ldots, S_{4\mu}$ into which the domain

$[0, 1]$ is divided, 2μ regions have a non-negative slope, namely the regions,

$$S_1, S_3, \ldots, S_{2\mu-1}, S_{2\mu+2}, S_{2\mu+4}, \ldots, S_{4\mu}.$$

Let us call these regions S_{pos}. The remaining 2μ regions, namely,

$$S_2, S_4, \ldots, S_{2\mu}, S_{2\mu+1}, S_{2\mu+3}, \ldots, S_{4\mu-1}$$

have a non-positive slope. Let us call these regions S_{neg}. The orbit having p points (or period equal to p or k, where $k \in D_p$) would be a flip orbit if an odd number of these p points are chosen from amongst the regions S_{neg}. It would be a regular orbit if an even number of the p points are chosen from S_{neg}.

Lemma 2: Amongst the $(4\mu)^p - 1$ points (of period p or k, where $k \in D_p$), $\frac{(4\mu)^p}{2}$ correspond to flip orbits and $\frac{(4\mu)^p}{2} - 1$ to regular orbits.

Proof of Lemma 2. To prove this, let us assume that the number of points corresponding to flip and regular orbits for $p = k$, where k is a positive integer are F_k and R_k respectively. Now let us increment k by 1. For $p = k$, each of the k places of the orbit, say $P_1, P_2, \cdots, P_k$ can be chosen in 4μ ways as discussed. Consider any point, say M, such that $M \in F_{k+1}$. If the corresponding $p = k$ point, namely the point before the $(k+1)^{th}$ place was filled is to belong to F_k, then the $(k+1)^{th}$ place would have to be chosen from S_{pos}. The number of ways corresponding to this would be $F_k S_{pos} = F_k 2\mu$. Now, consider the case where $M \in F_{k+1}$, but the corresponding $p = k$ point belongs to R_k. The points corresponding to $S_1, S_1, \cdots$ k times and $S_{4\mu}, S_{4\mu}, \cdots$ k times which are actually the same point, belong to R_k. This has to be accounted for while calculating the number of points which belong to F_{k+1}, when the corresponding $p = k$ belongs to R_k. Hence the number of such points would be

$(R_k + 1)2\mu$ where the 2μ factor comes from the fact that the $(k+1)^{th}$ place can belong to any of the S_{neg} and the $+1$ is to account for the fact that $S_1, S_1, \cdots$ k times and $S_{4\mu}, S_{4\mu}, \cdots$ k times are the same point. So, combining both the cases,

$$F_{k+1} = (R_k + 1)2\mu + F_k 2\mu = 2\mu(1 + T_k)$$

where $T_k = R_k + F_k$ is the total number of points corresponding to $p = k$ which is $(4\mu)^k - 1$. Therefore,

$$F_{k+1} = \frac{4\mu(4\mu)^k}{2} = \frac{(4\mu)^{k+1}}{2}. \tag{5.10}$$

Now, let us calculate the number of points in R_{k+1}. If a point is to belong to R_{k+1}, and the corresponding $p = k$ point is to belong to F_k, then the $(k+1)^{th}$ place would have to be chosen from S_{neg}. The number of ways corresponding to this would be $F_k S_{neg} = F_k 2\mu$. Now, consider the case where $M \in R_{k+1}$, but the corresponding $p = k$ point belongs to R_k. The points corresponding to $S_1, S_1, \cdots$ k times and $S_{4\mu}, S_{4\mu}, \cdots$ k times which are actually the same point, belong to R_k. This has to be accounted for while calculating the number of points which belong to R_{k+1}, when the corresponding $p = k$ belongs to R_k. Hence the number of such points would be $(R_k + 1)2\mu$ where the 2μ factor comes from the fact that the $(k+1)^{th}$ place can belong to any of the S_{pos} and the $+1$ is to account for the fact that $S_1, S_1, \cdots$ k times and $S_{4\mu}, S_{4\mu}, \cdots$ k times are the same point. However, this would consider the points corresponding to $S_1, S_1, \cdots (k+1)$ times and $S_{4\mu}, S_{4\mu}, \cdots (k+1)$ times separately, which are actually the same point. This needs to be accounted for. Hence, the number of such points would be $(R_k + 1)2\mu - 1$. So, combining both the cases,

$$R_{k+1} = (R_k + 1)2\mu + F_k 2\mu = 2\mu(1 + T_k) - 1$$

where $T_k = R_k + F_k$ is the total number of points corresponding to $p = k$ which is $(4\mu)^k - 1$. Therefore,

$$R_{k+1} = \frac{4\mu(4\mu)^k}{2} - 1 = \frac{(4\mu)^{k+1}}{2} - 1. \tag{5.11}$$

Thus, from (5.10) and (5.11), the number of points corresponding to flip and regular orbits for $p = k$ would be,

$$F_k = \frac{(4\mu)^k}{2}, R_k = \frac{(4\mu)^k}{2} - 1.$$

Now let us consider the parity of $\frac{p}{k}$, where $k \in D_p$. Say $k \in E$ if $\frac{p}{k}$ is even and $k \in O$ if $\frac{p}{k}$ is odd.

Lemma 3: For an odd value of p, the number of regular and flip orbits are equal, namely, $P_{pr} = P_{pf} = \frac{\Psi(p)}{2p}$. For an even value of p, the number of regular orbits of period p are given by

$$P_{pr} = \frac{\frac{(4\mu)^p}{2} - 1 - \sum_{k\in E} kP_k - \sum_{j\in O} jP_{jr}}{p} \tag{5.12}$$

and the number of flip orbits are given by

$$P_{pf} = \frac{\frac{(4\mu)^p}{2} - \sum_{j\in O} jP_{jf}}{p} \tag{5.13}$$

Proof of Lemma 3. Consider the following two cases,

1. Case 1. $k \in E$ A period-k orbit can either be a regular or a flip orbit. In either case however, the orbit corresponding to $(S_1, S_2, \cdots, S_p)$ would have $\Pi_{i=1}^{p} f'(S_i) > 1$ since $k \in E$ and hence acts as a regular orbit.

2. Case 2. As opposed to the above case, if $k \in O$, then the orbit corresponding to $(S_1, S_2, \cdots, S_p)$ would be a regular (or flip) orbit, with $\Pi_{i=1}^{p} f'(S_i) > 1$ (or

$\Pi_{i=1}^{p} f'(S_i) < -1$) only if the corresponding period-k orbit is a regular (or flip) orbit.

Hence, the $(4\mu)^p - 1$ points can be divided into 2 groups: Group 1 consisting of the $\frac{(4\mu)^p}{2}$ points corresponding to the flip orbits and Group 2 consisting of the $\frac{(4\mu)^p}{2} - 1$ points corresponding to the regular orbits. Group 1 contains the points corresponding to the orbits mentioned in the Case 1 above. For Case 2, let P_{kr} and P_{kf} denote the number of regular and flip orbits of period k if $k \in O$. The orbits would belong to Group 1 and Group 2 respectively. Hence, for Group 1,

$$\frac{(4\mu)^p}{2} - 1 = \sum_{k \in E} kP_k + \sum_{j \in O} jP_{jr} + pP_{pr} \Rightarrow P_{pr} = \frac{\frac{(4\mu)^p}{2} - 1 - \sum_{k \in E} kP_k - \sum_{j \in O} jP_{jr}}{p} \tag{5.14}$$

For Group 2,

$$\frac{(4\mu)^p}{2} = \sum_{j \in O} jP_{jf} + pP_{pf} \Rightarrow P_{pf} = \frac{\frac{(4\mu)^p}{2} - \sum_{j \in O} jP_{jf}}{p} \tag{5.15}$$

where P_{pr} and P_{pf} are the number of regular and flip orbits of period p respectively.

The number of orbits of period 1 are evenly distributed amongst flip and regular; however, the fact that $(0, 0)$ and $(1, 1)$ are the same point must be taken into account. Thereby, the orbits of the primes are also evenly distributed, that is, if p is prime, it would have an equal number of regular and flip orbits, given by $P_{pr} = P_{pf} = \frac{((4\mu)^p - 1) - (4\mu - 1)}{2p} = \frac{(4\mu)^p - 4\mu}{2p}$. This can be shown using formulae (5.14) and (5.15) above and the fact that the only divisors of a prime are one and itself.

In general, if p is odd, then for any k that divides p, k is odd. Hence the orbits $(S_1, S_2, \cdots, S_p)$ corresponding to period k would be regular or flip in accordance to whether the original period-k orbits are regular or flip. Further, each divisor of

k is odd, and the regular/flip orbits of k would depend on the regular/flip orbits of its divisors, all of which are such that, d divides k, $k/d \in O$. On successively seeking smaller and smaller divisors, we eventually reach the odd prime divisors of the number, for which the number of regular and flip orbits are equal. Repeating this process in the reverse direction, and from formulae (5.14) and (5.15), it follows that for any odd p, the number of regular and flip orbits are equal, namely $P_{pr} = P_{pf} = \frac{\Psi(p)}{2p}$. The formulae (5.14) and (5.15) can be used to find the number of regular and flip orbits for even p.

The number of cascades of the S_μ map for $\mu \in [0, m]$ where $m \in \mathbb{N}$ equals the number of unstable regular orbits of the S_μ map at $\mu = m$ [61]. Thus, Lemma 3 along with the fact that every periodic orbit of S_μ is unstable, can be used to compute the number of cascades in the system. Thus, the number of cascades in the system and consequently, the chaos in the system increases as μ increases, and the system never reaches a stable state. This number of cascades of the map is given for two sample intervals in Table 5.1.

$Period-k$	S_μ on $[0,2]$	S_μ on $[0,3]$
1	4	6
2	12	30
3	84	286
4	496	2556
5	3276	24,882
6	21756	248,534
7	149,796	2,559,414
8	1,048,064	26,871,264
9	7,456,512	286,654,368
$k \gg 10$	$\sim 8^k/2k$	$\sim 12^k/2k$

Table 5.1: The number of period-k cascades of the map $S_\mu(x)$ on $\mu \in [0,2]$ and $\mu \in [0,3]$.

Appendix A

Supplement for Chapter 3: Methods for primary-window computation

To compute the C-widths of the windows and the maximum permissible ϵ, we used the NTL library [62], which is an arbitrary precision library in C++. The computation is done using a server cluster, with 200 processors running for 15 days. P values of 13, 15, 17, 19, 23, 25 are considered. Tolerance values not exceeding 10^{-34} were considered when computing window C-widths.

Characterizing the window by finding C values

Given a maximum period P and a starting parameter value C, we successively determine the periods of the next periodic windows such that the period $\leq P$. We also determine the kneading sequence corresponding to the superstable parameter value of each following window. We numerically characterize each primary window by computing its superstable parameter value and determining its C-width.

Determining the superstable parameter value of the window. We start from $C = C_{odd}$ and determine the period and sequence of the next window.

Thereby, we use the Newton's method in x and C, with $(C = C_{odd}, x = 0)$ as the initial approximation, and the equations

$$f^k(x, C) = x, \frac{\partial f^k(x, C)}{\partial x} = 0$$

to compute the superstable parameter value, C^* of the window. The second equation is the criterion for being superstable. For all other windows, we use the interior crisis parameter value of the previous window as the initial C approximation, and $x = 0$ as the initial x approximation. The $x = 0$ approximation is based on the fact that $x = 0$ always lies in one of the k interval basins of a period-k window [52].

Determining the saddle-node bifurcation value of the window. Once we determine the superstable parameter value C^* of the window, we use Newton's method in x and C, with $(C = C^*, x = 0)$ as the initial approximation, and the equations

$$f^k(x, C) = x, \frac{\partial f^k(x, C)}{\partial x} = 1$$

to compute the saddle-node bifurcation value $C_{SadNode}$ of the window.

Determining the interior crisis value of the window. The interior crisis value of the window is determined in three steps. In the first step, we determine the period-doubling bifurcation value of the window. We use the Newton's method in x and C, with $(C = C^*, x = 0)$ as the initial approximation, and the equations

$$f^k(x, C) = x, \frac{\partial f^k(x, C)}{\partial x} = -1$$

to compute the period-doubling bifurcation value $C_{PerDoub}$ of the window.

In the second step, we make our first approximation for the interior crisis parameter value, C_{Crisis} as follows [52],

$$C_{Crisis} = C_{SadNode} + (9/4)(C_{PerDoub} - C_{SadNode}) \tag{1}$$

Thereafter, in the third step, we use the fact that for a period-k window, at the interior crisis value of parameter C, the interval basin has an unstable period-k point on its boundary. The Newton's method is used in C with the equations

$$f^{2k}(0) = f^{3k}(0)$$

to compute the exact interior crisis value C_{Crisis}.

The C-width of the window is computed as $C_{width} = C_{Crisis} - C_{SadNode}$

Thereafter, for the next periodic window, the superstable value is computed using

$$C = C_{Crisis}, x = 0$$

as the initial approximation, and so on. This process is continued until all the periodic windows with periods up to P are characterized.

The kneading sequence is checked when computing each of C^*, $C_{SadNode}$ and $C_{PerDoub}$ to ensure accuracy while computing the windows.

Appendix B

Supplement for Chapter 3: Determining the next periodic window

Basics of kneading sequences. Here we describe a method for determining the sequence of all periodic windows, bounded by a maximum period P, that occurs in the map as the parameter C is increased beyond C_{odd}. This is based on kneading theory [49]. The critical point of the map is $x = 0$. The x-domain is divided into interval I_1 to the left of the critical point, the critical point itself, and interval I_2 to the right of the critical point. For a given point x, $A(x)$ corresponds to the 'address' of point x, where $A(x)$ denotes an interval defined as follows,

$$A(x) = \begin{cases} I_1, & \text{if } x < 0 \\ C', & \text{if } x = 0 \\ I_2, & \text{if } x > 0 \end{cases}$$

The function $\epsilon(A(x))$ is defined as follows,

$$\epsilon(A(x)) = \begin{cases} -1, & \text{if x lies on an interval with negative slope} \\ 0, & \text{if x=0} \\ +1, & \text{if x lies on an interval with positive slope} \end{cases}$$

Now, for given integer n, ϵ_n is defined such that $\epsilon_n = \epsilon(A(f^n(0^+)))$. The kneading determinant for the given map is given by [49],

$$D(t) = 1 + \epsilon_1 t + \epsilon_1\epsilon_2 t^2 + \cdots$$

where t is an infinitesimally small positive number. Thus $D(t)$ can be expressed as a series of the form

$$D(t) = 1 + D_1 t + D_2 t^2 + \cdots$$

where $D_m = \epsilon_1\epsilon_2\cdots\epsilon_m$ for all positive integers m. In general, a power series $D(t) = 1 + D_1 t + D_2 t^2 + \cdots$ where $D_i = \pm 1$ is said to be admissible [49] if

$$D(t) \leq |D_n + D_{n+1} t + D_{n+2} t^2 \cdots | \tag{1}$$

for every $n \geq 1$. A given power series $D(t) = 1 \pm t \pm t^2 \pm \cdots$ occurs as the kneading determinant of the quadratic map for some value of parameter C, if and only if this series is admissible. The kneading determinant is periodic with period k, for C values lying between the saddle-node bifurcation value and the superstable value of a period-k window. Then the kneading determinant takes the form

$$D(t) = \frac{\phi(t)}{1 - t^k} \tag{2}$$

for some polynomial $\phi(t) = 1 + D_1 t + \cdots + D_{k-1} t^{k-1}$ of degree k-1.

Determining window sequence. We start from $C = C_{odd}$ and go on increasing C. We look at the kneading determinant for $C = C_{odd}$, and then predict sequentially, the periods of the windows, not exceeding P, that occur as C is increased. Given a kneading sequence, a change in the sequence occurs as C crosses

the superstable parameter value of a periodic window, such that period k of this window does not exceed P. This occurs due to the crossing over of the k^{th} iterate of the critical point 0 from one side of the critical point to the other, at the superstable parameter value of the periodic window. This leads to a reversal of sign of terms from the k^{th} term onwards of the kneading sequence. The kneading sequence of the quadratic map monotonically decreases as the parameter is increased [49]. At the superstable parameter value of the period-k window, D_k changes from 1 to -1 resulting in the decrease in the kneading sequence. This is due to the change in the sign of ϵ_k. Before the superstable crossing, $D_k = 1$, which occurs either when $\epsilon_1\epsilon_2\cdots\epsilon_{k-1} = -1, \epsilon_k = -1$ or $\epsilon_1\epsilon_2\cdots\epsilon_{k-1} = 1, \epsilon_k = 1$.

The P-kneading sequence. Since, we compute the windows of periods not exceeding P, to understand the changes in the kneading sequence at superstable parameter values, we consider only the first P terms of the kneading sequence. We call this restricted kneading sequence as the P-kneading sequence, which is given as $D^P(t) = 1 + D_1t + D_2t^2 + \cdots + D_Pt^P$. Given a P-kneading sequence, the goal is to compute the next admissible P-kneading sequence.

Note that for a period-k window to occur, the kneading sequence is as Eq. 2. Hence, to find the next periodic window, successive values of k from 3 to P are considered and the k values corresponding to $D_k = -1$ are automatically eliminated. For k values corresponding to $D_k = 1$, it is checked as to whether the kneading sequence can be represented as Eq. 2.

If say, a window of period k_0 occurs where $P \geq 2k_0$, then the next few changes

in the P-kneading sequence occur due to the bifurcations and higher order windows inside the period-k_0 window. The next primary window occurs only at that subsequent value of period k, which is such that k_0 does not divide k.

Degeneracy case. In general, if there are multiple values of k that meet the criterion as per (2), it is claimed that a periodic window corresponding to the lowest of these values occurs. To show this, it is enough to show that if there are multiple such values of k, say $k_1, k_2, \cdots, k_n$, where $k_1 < k_2 < \cdots < k_n$, then the kneading sequences corresponding to $k_2, k_3, \cdots, k_n$ are not admissible. Say, k_1 and k_m meet the criterion as per Eq. 2, where m is such that $k_2 \leq k_m \leq k_n$, then we want to show that the kneading sequence corresponding to k_m is inadmissible, and hence a window of period k_1 occurs. Let us assume that the window corresponding to period k_m occurs. As the superstable parameter value of this window is crossed, there is a reversal in the signs of the terms of the kneading sequence, starting from the k_m^{th} digit. To show that this new sequence does not meet the admissibility criterion, let us compare this kneading sequence $D^P(t)$ with the sequence $|D_{k_1} + D_{k_1+1}t + \cdots + D_P t^{P-k_1}|$. Note that before the superstable parameter value, $D_{k_m} = 1$ which equals $D_{k_m-k_1}$ based on Eq. 2. The sequences $D^P(t)$ and $D_{k_1} + D_{k_1+1}t + \cdots + D_P t^{P-k_1}$ are identical up to the first $(k_m - k_1 + 1)$ terms. However, after the superstable parameter value, D_{k_m} changes to -1, but $D_{k_m-k_1} = 1$, hence $D^P(t) > |D_{k_1} + D_{k_1+1}t + \cdots + D_P t^{P-k_1}|$, proving the inadmissibility of the kneading sequence. Thus, the window corresponding to period k_m cannot occur. Hence, if there are multiple values of k satisfying Eq. 2 when the P-kneading sequence is considered, the period

corresponding to the lowest value must occur.

An example. Consider $C = 1.6284, P = 8$. Then

$$D(t) = 1 - t - t^2 + t^3 - t^4 + t^5 - t^6 - t^7 + t^8.$$

In this case, both $p_1 = 5$ and $p_2 = 8$ satisfy the criterion as per (2). However, a period-5 window occurs next. Thus, the P-kneading sequence following the superstable crossing is

$$D(t) = 1 - t - t^2 + t^3 - t^4 - t^5 + t^6 + t^7 - t^8.$$

The P-kneading sequence decreases (is non-increasing) as C is increased, until it reaches $D(t) = 1 - t - t^2 - \cdots - t^P$ when $C = 2$.

Appendix C

Supplement for Chapter 4: Details on self-similarity

A. Justification of Eq. (7).

In Chapter 3, we considered three parameter values $C, C+\epsilon$ and $C-\epsilon$. However, for our argument to follow, it is convenient to consider two parameter values, C and $C+\epsilon$, with C defined to be ϵ-uncertain, e. g., with respect to chaos, for $A(C)$ chaotic and $A(C+\epsilon)$ periodic. Since we are only interested in power-law scalings with ϵ, the results will be unchanged. In addition, it is also convenient to single out the part of the period-p window, henceforth referred to as the "basic part", corresponding to the parameter range between the beginning of the period-p window at the tangent bifurcation to a period-p periodic attractor and the parameter value corresponding to the Feigenbaum point at which there is an accumulation of an infinite number of period-doublings of orbits of period $2^m p$. By the approximate self-similarity of windows, the basic part of a window constitutes an approximately fixed fraction of the total window width.

Because a C value that is ϵ-uncertain with respect to the occurence of large chaotic attractors does not lie in any window, $(C+\epsilon)$ lies in a primary window. Because most of the periodic range of a primary window corresponds to its basic part,

which constitutes a fixed fraction of the whole window, for our scaling considerations it suffices, to assume that $(C+\epsilon)$ lies in the basic part of a primary window.

We classify the primary windows as those with the basic part having width exceeding ϵ and those with the basic part having width less than ϵ.

The primary windows with the basic part having width exceeding ϵ each contribute a length of ϵ to the set of C values that are ϵ-uncertain with respect to large chaotic attractors. Thus the net contribution to the set of C values that are ϵ-uncertain with respect to a large chaotic attractor, resulting from these windows is proportional to $\epsilon N_1(\epsilon)$. The primary windows with the basic part having width less than ϵ contribute a length proportional to the primary window width (assuming self-similarity of windows) to the set of C values that are ϵ-uncertain with respect to a large chaotic attractor. Assuming $N_1(\epsilon) \sim \epsilon^{-\alpha'}$, the net contribution to the set of C values that are ϵ-uncertain with respect to a large chaotic attractor is,

$$\begin{aligned} F_1(\epsilon) &\sim \int_0^\epsilon x\, dN_1(x) + \epsilon N_1(\epsilon) \\ &\sim -\alpha' \int_0^\epsilon x \cdot x^{-\alpha'-1}\, dx + \epsilon \cdot \epsilon^{-\alpha'} \\ &\sim -\alpha' \int_0^\epsilon x^{-\alpha'}\, dx + \epsilon \cdot \epsilon^{-\alpha'} \\ &\sim \epsilon^{1-\alpha'}. \end{aligned}$$

Thus, $F_1(\epsilon) \sim \epsilon^{1-\alpha'}$. But since $F_1(\epsilon) \sim \epsilon^{\alpha}, \alpha' = 1-\alpha$, and, $N_1(\Delta) \sim \Delta^{-\alpha'} \sim \Delta^{-(1-\alpha)}$ which is the second part of Eq. (7).

To obtain the first part of Eq. (7), as before, we assume that given a value of C that is ϵ-uncertain with respect to chaos, $(C+\epsilon)$ lies in the basic part of some periodic window. Then we classify the windows of all orders as those with the basic

part having width exceeding ϵ and those with the basic part having width less than ϵ. The windows with the basic part having width exceeding ϵ each contribute a length of ϵ to the set of C values that are ϵ-uncertain with respect to chaos. Then the net contribution to the set of C values that are ϵ-uncertain with respect to chaos resulting from these windows is proportional to $\epsilon\bar{N}(\epsilon)$. The periodic windows with the basic part having width less than ϵ contribute a length proportional to the window width to the set of C values that are ϵ-uncertain with respect to chaos. Then the net contribution to the set of C values that are ϵ-uncertain with respect to chaos is proportional to

$$\begin{aligned}
\bar{F}(\epsilon) &\sim \int_0^\epsilon x\, d\bar{N}(x) + \epsilon\bar{N}(\epsilon) \\
&\sim -\beta' \int_\epsilon^0 x \cdot x^{-\beta'-1}\, dx + \epsilon \cdot \epsilon^{-\beta'} \\
&\sim \epsilon^{1-\beta'}.
\end{aligned}$$

Thus, $\bar{F}(\epsilon) \sim \epsilon^{1-\beta'}$. But since $\bar{F}(\epsilon) \sim \epsilon^{\beta}, \beta' = 1-\beta$, and, $\bar{N}(\Delta) \sim \Delta^{-\beta'} \sim \Delta^{-(1-\beta)}$ which is the first part of Eq. (7).

B. Self-similarity of windows.

Here we briefly review results from Ref. [11] on the self-similarity of windows. For the quadratic map, Eq. (1), let C_*, C_d and C_x denote the C values at the start of a period-p window (tangent bifurcation creating a period-p orbit attractor), at the first period-doubling (bifurcation from a period-p attractor to a period-2p attractor), and at the end of the window (where a p-piece chaotic attractor is destroyed through

Window size	Period	C_*	m_C	Relative deviation of m_C from 9/4
0.04032749	3	1.750000	2.176	0.033
0.00896172	5	1.624397	2.219	0.014
0.00221143	4	1.940551	2.241	0.0042
0.00174414	5	1.860587	2.241	0.0038
0.00100269	7	1.673954	2.242	0.0036
0.00038901	8	1.711036	2.247	0.0013
0.00028460	9	1.595649	2.248	0.00088
0.00026443	6	1.907251	2.249	0.00064
0.000233746	9	1.555257	2.249	0.00029

Table .1: Results for all the primary windows with $C_x - C_* > 2.3 \times 10^{-4}$ in $1.54 < C < 2.00$ for the map $x_{n+1} = C - {x_n}^2$. The last column gives the relative error $\frac{|m_C - (9/4)|}{(9/4)}$.

a crisis). Let

$$m = \frac{C_x - C_*}{C_d - C_*}.$$

For the entire range of the quadratic map, $C_* = -1/4$ (creation of the period-1 orbit), $C_d = 3/4$ (beginning of the period-2 orbit), $C_x = 2$ (final crisis), corresponding to

$$m_C = \frac{2 + (1/4)}{(3/4) + (1/4)} = \frac{9}{4}.$$

According to the self-similarity claim, m for any window should be close to $m_C = 9/4$. As shown in Table I (reproduced from Ref. [11]), the period p of a window does not have to be very large for this to be true. For example, even for the period 3 window the deviation of of m from 9/4 is only 3.3%.

C. The effect of deviation from self-similarity. We now provide heuristic evidence for our statement in Ref. [13] that the small deviations from exact scaling, as reflected by the last column of Table I, should result in negligible change in β (i.e., substantially below the uncertainty level of ± 0.037 in Eq. (2)). To address this in a crude way, we first note that the deviations of m from $m_C = 9/4$ for periods greater than 3 are all substantially less than the 0.033, the value for the period 3 window. A worst case scenario that should greatly overestimate the error is to assume that self-similarity still applies, but all primary window widths are off by 0.033. Replacing all the δ_i in Eq. (12) by $(1.033\ \delta_i)$ and recalculating the prediction for β (as in Fig. 3), we obtain a value of 0.385. The difference between this value and the value 0.392 given in Eq. (2) is 0.007 which is well-within the uncertainty

± 0.037 for the value in Eq. (2).

Bibliography

[1] J. Moehlis, H. Faisst, and B. Eckhardt. Periodic orbits and chaotic sets in a low-dimensional model for shear flows. *SIAM J. Appl. Dyn. Syst.*, 4(2):352, 2005.

[2] P. G. Drazin and W. H. Reid. *Hydrodynamic Stability.* Cambridge University Press, Cambridge. 1981.

[3] J. Moehlis, H. Faisst, and B. Eckhardt. A low-dimensional model for turbulent shear flows. *New J. Phys.*, 6:56, 2004.

[4] B. Eckhardt and A. Mersmann. Transition to turbulence in a shear flow. *Phys. Rev. E*, 60:509–517, 1999.

[5] A. Schmiegel. *Transition to turbulence in linearly stable shear flows.* PhD dissertation, Philipps-Universitat Marburg, Marburg, Germany, 1999.

[6] J. Moehlis, T. Smith, P. Holmes, and H. Faisst. Models for turbulent plane couette flow using the proper orthogonal decomposition. *Phys Fluids*, 14 (7):2493–2507, 2002.

[7] O. Dauchot and N. Vioujard. Phase space analysis of a dynamical model for the subcritical transition to turbulence in plane couette flow. *Eur. Phys. J. B*, 14:377–381, 2000.

[8] J. D. Skufca. *Understanding the chaotic saddle with focus on a 9-variable model of planar couette flow.* PhD dissertation, University of Maryland College Park, 2005.

[9] B. Eckhardt and H. Faisst. *Dynamical systems and transition to turbulence*, volume 77 of *Fluid Mechanics and its Applications*, pages 35–50. 2005.

[10] H. Faisst and B. Eckhardt. Sensitive dependence on initial conditions in transition to turbulence in pipe flow. *J. Fluid. Mech.*, 504:343–352, 2004.

[11] S. Bottin and H. Chate. Statistical analysis of the transition to turbulence in plane couette flow. *Eur. Phys J. B.*, 6:143–155, 1998.

[12] S. Bottin, F. Daviaud, P. Manneville, and O. Dauchot. Discontinuous transition to spatiotemporal intermittency in plane couette flow. *Europhys. Lett.*, 43 (2):171–176, 1998.

[13] T. Mullin and J. Peixinho. Transition to turbulence in pipe flow. *J. Low Temp. Phys.*, 145:75–88, 2006.

[14] J. Peixinho and T. Mullin. Decay of turbulence in pipe flow. *Phys. Rev. Lett.*, 96:094501, 2006.

[15] A. P. Willis and R. R. Kerswell. Critical behavior in the relaminarization of localized turbulence in pipe flow. *Phys. Rev. Lett.*, 98:014501, 2007.

[16] B. Eckhardt, T. M. Schneider, B. Hof, and J. Westerweel. Turbulence transition in pipe flow. *Annual Review of Fluid Mechanics*, 39:447–468, 2007.

[17] T. Mullin and J. Peixinho. *Recent observations in the transition to turbulence in a pipe*, pages 45–55. Bangalore: Springer. 2006.

[18] C. Grebogi, E. Ott, and J. A. Yorke. Crises, sudden changes in chaotic attractors, and transient chaos. *Physica D*, 7(1):181–200, 1983.

[19] B. Hof, J. Westerweel, T. M. Schneider, and B. Eckhardt. Finite lifetime of turbulence in shear flows. *Nature*, 443:59–62, 2006.

[20] T. M. Schneider. *State space properties of transitional pipe flow.* PhD dissertation, Philipps University at Marburg, 2007.

[21] B. Hof, A. de Lozar, D. J. Kuik, and J. Westerwee. Repeller or attractor? selecting the dynamical model for the onset of turbulence in pipe flow. *Phys. Rev. Lett.*, 101:214501, 2008.

[22] M. Avila, A. P. Willis, and B. Hof. On the transient nature of localized pipe flow turbulence. *J. Fluid Mech.*, 646:127–136, 2010.

[23] K. Avila, D. Moxey, A. de Lozar, M. Avila, D. Barkley, and B. Hof. The onset of turbulence in pipe flow. *Science*, 333:192–196, 2011.

[24] L. Kim and J. Moehlis. Characterizing the edge of chaos for a shear flow model. *Phys. Rev. E*, 78:036315, 2008.

[25] J.D. Skufca, J.A.Yorke, and B. Eckhardt. Edge of chaos in a parallel shear flow. *Phys. Rev. Lett.*, 96:174101, 2006.

[26] T.M. Schneider, B. Eckardt, and J.A. Yorke. Turbulence transition and the edge of chaos in pipe flow. *Phys. Rev. Lett.*, 99:034502, 2007.

[27] C.C.T. Pringle and R.R. Kerswell. Using nonlinear transient growth to construct the minimal seed for shear flow turbulence. *Phys. Rev. Lett.*, 105:154502, 2010.

[28] Y. Duguet, L. Brandt, and B. R. J. Larsson. Towards minimal perturbations in transitional plane couette flow. *Phys. Rev. E*, 82:026316, 2010.

[29] C.C. Pringle, A.P. Willis, and R.R. Kerswell. Minimal seeds for shear flow turbulence: using nonlinear transient growth to touch the edge of chaos. *J. Fluid Mech.*, 702:415–443, 2012.

[30] Y. Duguet, A. Monokrousos, L. Brandt, and D.S. Henningson. Minimal transition thresholds in plane couette flow. *Phys. Fluids*, 25:084103, 2013.

[31] A. P. Willis and R. R. Kerswell. Turbulent dynamics of pipe flow captured in a reduced model: puff relaminarisation and localised 'edge' states. *J. Fluid Mech.*, 619:213–233, 2009.

[32] F. Mellibovsky and A. Meseguer. The role of streamwise perturbations in pipe flow transition. *Phys. Fluids*, 18:074104, 2006.

[33] H. Shan, Z. Zhang, and F. T. M. Nieuwstadt. Direct numerical simulation of transition in pipe flow under the influence of wall disturbances. *Int. J. Heat Fluid Flow*, 19:320–325, 1998.

[34] B. Hof, A. Juel, and T. Mullin. Scaling of the turbulence transition threshold in a pipe. *Phys. Rev. Lett.*, 91:244502, 2003.

[35] B. Hof. *Transition to turbulence in pipe flow*, pages 221–231. Springer. 2004.

[36] A. A. Draad, G. D. C. Kuiken, and F. T. M. Nieuwstadt. Laminar-turbulent transition in pipe flow for newtonian and non-newtonian fluids. *J. Fluid Mech.*, 377:267–312, 1998.

[37] J. Peixinho and T. Mullin. Finite-amplitude thresholds for transition in pipe flow. *J. Fluid Mech.*, 582:169–178, 2007.

[38] F. Mellibovsky and A. Meseguer. Critical threshold in pipe flow transition. *Philos. Trans. A. Math. Phys. Eng. Sci.*, 367(1888):545–560, 2009.

[39] F. Mellibovsky and A. Meseguer. Pipe flow transition threshold following localized impulsive perturbations. *Phys. Fluids*, 19:044102, 2007.

[40] A. Meseguer. Streak breakdown instability in pipe poiseuille flow. *Phys. Fluids*, 15:1203–1213, 2003.

[41] J. Philip, A. Svizher, and J. Cohen. Scaling law for a subcritical transition in plane poiseuille flow. *Phys. Rev. Lett.*, 98:154502, 2007.

[42] F. Waleffe. On a self-sustaining process in shear flows. *Phys. Fluids*, 9:883, 1997.

[43] H. E. Nusse and J. A. Yorke. A procedure for finding numerical trajectories on chaotic saddles. *Physica D*, 36:137–156, 1989.

[44] J. Vollmer, T.M. Schneider, and B. Eckhardt. Basin boundary, edge of chaos and edge state in a two-dimensional model. *New Journal of Physics*, 11:013040, 2009.

[45] K. T. Alligood, T. Sauer, and J. A. Yorke. *CHAOS: An Introduction to Dynamical Systems*. Springer-Verlag, 1996.

[46] B. R. Hunt and E. Ott. Structure in the parameter dependence of order and chaos for the quadratic map. *J. Phys. A*, 30:7067–7076, 1997.

[47] C. Grebogi, S. W. McDonald, E. Ott, and J. A. Yorke. Exterior dimension of fat fractals. *Phys. Lett. A*, 110:1–4, 1985.

[48] J. D. Farmer. Sensitive dependence on parameters in nonlinear dynamics. *Phys. Rev. Lett.*, 55:351–354, 1985.

[49] *On iterated maps of the interval Dynamical systems*, Lecture Notes in Math., Berlin, 1988. Springer.

[50] J. Graczyk and G. Swiatek. Generic hyperbolicity in the logistic family. *Ann. of Math*, 146:1–52, 1997.

[51] http://yorke.umd.edu/windows/.

[52] J. A. Yorke, C. Grebogi, E. Ott, and L. Tedeschini-Lalli. Scaling behavior of windows in dissipative dynamical systems. *Phys. Rev. Lett.*, 54:1095–1098, 1985. See Sec. B of Appendix C.

[53] That is, given a system parameter value C for which there is a chaotic attractor and a small value of $\tilde{\epsilon} > 0$, one can find a parameter perturbation $C \to C + \delta C$ with $|\delta C| < \tilde{\epsilon}$ such that the attractor is no longer chaotic, and this can *always* be done *no matter how small* $\tilde{\epsilon}$ is.

[54] J. M. Wersinger, J. M. Finn, and E. Ott. Bifurcation and 'strange' behavior in instability saturation by nonlinear three wave mode coupling. *Phys. Fluids*, 23:1142, 1980.

[55] B. A. Huberman, J. P. Crutchfield, and N. H. Packard. Noise phenomena in josephson junctions. *Appl. Phys. Lett.*, 37:750, 1980.

[56] F. Argoul, A. Arneodo, P. Richetti, J. C. Roux, and Harry L. Swinney. Chemical chaos: from hints to confirmation. *Acc. Chem. Res.*, 20:436, 1987.

[57] M. V. Jacobson. Absolutely continuous measures for one-parameter families of one-dimensional maps. *Comm. Math. Phys.*, 81:39–88, 1981. has shown that C values for which $A(C)$ is chaotic form a positive Lebesgue measure set, while J. Graczyk and G. Swiatek [Ann. of Math. 146, 1 (1997)] demonstrate that intervals of C values with periodic attractors are dense in the region, $C_F < C < 2$, where chaos can occur (here C_F denotes the 'Feigenbaum point' at which period doublings of periods 2^m accumulate).

[58] We comment that this is a consequence of Lebesgue's density theorem which states that, for a Lebesgue measurable set Q (in this case the set of C values that yield chaotic attractors), for almost every point x in Q, the limit of $\epsilon \to 0$ of $\mu(Q \cap [x-\epsilon, x+\epsilon])/(2\epsilon)$ is one, where μ denotes the Lebesgue measure.

[59] In taking the Laplace transform $\int_0^\infty M(u)\exp(-su)du$ and the inverse Laplace transform $(2\pi i)^{-1}\int_p \hat{M}(s)\exp(su)ds$, where the contour P runs from $-i\infty+\sigma$ to $+i\infty+\sigma$, we take $Re(s) > \gamma$ and $\sigma > \gamma$, respectively.

[60] E. Ott. *Chaos in Dynamical Systems*. Cambridge University Press New York, 2002.

[61] M. R. Joglekar, E. Sander, and J. A. Yorke. Fixed points indices and period-doubling cascades. *J. Fixed Point Theory Appl.*, 8:151–176, 2010.

[62] http://shoup.net/ntl/.